ISSN 0038-531X

Russian Original Vol. 57, No. 1, July, 1984

January, 1985

SATEAZ 57(1) 429–506 (1984)

SOVIET ATOMIC ENERGY

АТОМНАЯ ЭНЕРГИЯ
(ATOMNAYA ÉNERGIYA)

TRANSLATED FROM RUSSIAN

CONSULTANTS BUREAU, NEW YORK

SOVIET ATOMIC ENERGY

Soviet Atomic Energy is abstracted or indexed in *Chemical Abstracts, Chemical Titles, Pollution Abstracts, Science Research Abstracts, Parts A and B, Safety Science Abstracts Journal, Current Contents, Energy Research Abstracts,* and *Engineering Index.*

Mailed in the USA by Publications Expediting, Inc., 200 Meacham Avenue, Elmont, NY 11003.

POSTMASTER: Send address changes to *Soviet Atomic Energy,* Plenum Publishing Corporation, 233 Spring Street, New York, NY 10013.

Soviet Atomic Energy is a translation of *Atomnaya Énergiya,* a publication of the Academy of Sciences of the USSR.

An agreement with the Copyright Agency of the USSR (VAAP) makes available both advance copies of the Russian journal and original glossy photographs and artwork. This serves to decrease the necessary time lag between publication of the original and publication of the translation and helps to improve the quality of the latter. The translation began with the first issue of the Russian journal.

Consultants Bureau journals appear about six months after the publication of the original Russian issue. For bibliographic accuracy, the English issue published by Consultants Bureau carries the same number and date as the original Russian from which it was translated. For example, a Russian issue published in December will appear in a Consultants Bureau English translation about the following June, but the translation issue will carry the December date. When ordering any volume or particular issue of a Consultants Bureau journal, please specify the date and, where applicable, the volume and issue numbers of the original Russian. The material you will receive will be a translation of that Russian volume or issue.

Subscription (2 volumes per year)
Vols. 56 & 57: $560 (domestic), $621 (foreign)
Vols. 58 & 59: $645 (domestic), $715 (foreign)
Single Issue: $100
Single Article: $8.50

CONSULTANTS BUREAU, NEW YORK AND LONDON

c/b
233 Spring Street
New York, New York 10013

Published monthly. Second-class postage paid at Jamaica, New York 11431.

SOVIET ATOMIC ENERGY

A translation of *Atomnaya Énergiya*

January, 1985

Volume 57, Number 1 **July, 1984**

CONTENTS

CONTENTS

(continued)

Engl./Russ.

The Russian press date (podpisano k pechati) of this issue was 6/26/1984. Publication therefore did not occur prior to this date, but must be assumed to have taken place reasonably soon thereafter.

ARTICLES

AN ESTIMATE OF THE ERRORS OF A METHOD FOR DETERMINING THE DEPLETION OF SPENT MIXED URANIUM–PLUTONIUM FUEL OF FAST REACTORS

V. Ya. Gabeskiriya, V. I. Borisenkov,
V. V. Kalygin, M. N. Maslennikova,
V. S. Prokopenko, V. M. Prokop'ev,
V. L. Chernyshev, and A. P. Chetverikov

UDC 621.039.626:621.039.54

The necessity arises for a precision determination of the depletion of spent nuclear fuel in the investigation of the breeding of secondary fuel, carrying out the guarantees of MAGATÉ, optimization of the fuel cycle, studying the durability of fuel elements, and solving a number of other scientific and technical problems.

Serious difficulties appear in the measurement of the depletion of the fuel of a fast reactor. In thermal reactors the effective cross sections of absorption of neutrons by nuclides which enter into the chain of nuclear transmutations differ by two to three orders of magnitude, which leads to an abrupt change in the isotopic composition of the uranium and plutonium in the course of irradiation. Therefore by using the method of heavy atoms [1], one can determine the depletion with an error of 5-7% from the change in the isotopic composition. However, this method cannot be used in measuring the depletion of the fuel of a fast reactor, since due to the absence of a sharp difference in the absorption cross sections of neutrons by nuclides the dependence of isotopic composition of the elements on depletion is weakly expressed.

It is difficult to determine the depletion of the fuel of fast reactors from the fission products, since the yield of fission products depends strongly on the neutron spectrum of the fast reactor [2]. The most complicated problem is to determine the depletion of spent mixed uranium-plutonium fuel, especially in connection with the use of plutonium having a high content of the heavy isotopes. The yield of fission products depends on the fissionable nuclei. For a mixed fuel it is necessary to calculate the effective yield of the fission products [1] used as monitors of depletion and to know the effective fission and radiative capture cross sections of neutrons for the heavy nuclei contained in the fuel. These cross sections are known with significant errors. Therefore the need has arisen to analyze the contribution of random and uneliminated systematic errors to the overall error of determination of the depletion of fast reactor fuel and to find ways to increase the measurement accuracy.

Measurement Procedure. The sample of spent fuel being investigated was dissolved, and a complex marker containing ^{238}U, ^{242}Pu, and ^{142}Nd was introduced into an aliquot of the solution obtained. The extraction of elements for mass spectrometric analysis was performed by the method of [3]. The isotopic composition of the elements was measured with a reconstructed MI-1305 mass spectrometer. A three-ribbon source was used as the ion source. The construction of a detachable evaporator has been carried out in such a way that one can charge the samples through a vacuum lock without breaking the high vacuum in the source region and without examination of its ion-optical system. In order to raise the sensitivity when measuring ion currents, a type VÉU-1A secondary electron multiplier was used. The mass spectra were recorded in digital form with the help of an Shch 1513 voltmeter and the information obtained was processed on a computer, which eliminated subjective errors. The ratio of the content of heavy elements and the depletion monitor to the content of uranium or one of its isotopes was determined with the use of the complex marker.

The depletion of fuel in percentage was calculated from the formula

$$F = \frac{100 N_M}{N_U Y_{eff}} \Big/ \left(1 + \frac{N_{Pu}}{N_U} + \frac{N_M}{N_U Y_{eff}}\right),$$

where N_M, N_U, and N_{Pu} are the molar concentrations of the depletion monitor, uranium, and plutonium in the initial solution and Y_{eff} is the effective yield of the fission products

Translated from Atomnaya Énergiya, Vol. 57, No. 1, pp. 8-10, July, 1984. Original article submitted November 18, 1983.

0038-531X/84/5701-0429$08.50

which are used as depletion monitors calculated from the formula $Y_{eff} = \sum g_j Y_i$ (g_j is the fraction of fissions of nuclei j in the total number of fissions, and Y_j is the yield of the depletion monitor upon fission of a nucleus).

Experimental and computed values of the ratios of the reaction rates for BOR-60 neutron spectra [4-6] were used in the calculation of the fraction of fissions of ^{235}U, ^{236}U, ^{238}U, ^{239}Pu, ^{240}Pu, ^{241}Pu, and ^{242}Pu. The total ^{145}Nd and ^{146}Nd content was used as the depletion monitor. The choice of the monitor stems from the fact that the total yield of the indicated neodymium isotopes is practically independent of the neutron spectrum of a fast reactor [2]. Thus one of the main difficulties in measurement of depletion of the fuel of a fast reactor is overcome. The selected monitor adequately satisfies all the other requirements imposed on depletion monitors [1]. The data given in [7] were used in the calculation of the effective yield of fission products.

A series of parallel measurements of depletion in a single sample of mixed uranium–plutonium fuel used up in a BOR-60 fast reactor were performed to determine the convergence of the results (Table 1). Analysis of the data, carried out in accordance with GOST 8.207–76, has shown that the results of parallel measurements satisfy the normal distribution law. In accordance with the rules for estimating the abnormality of observational results (GOST 11.002-73), it was established that the result of measurement No. 17 has a coarse error, and it is necessary to exclude it.

The relative mean square deviation of the result of a single measurement calculated in accordance with GOST 11.004–74 was found to be equal to 0.008. Thus, the confidence level of the random relative error of a single measurement at a confidence level of P = 0.95 is $\varepsilon = 1.6\%$. With n parallel measurements the random component of the total error is reduced accordingly by a factor of $\sqrt{n}$.

The error of determination of the isotope content of the actinide elements and the fission products includes an uneliminated systematic error caused by an error in the calibration solutions used and by an uneliminated systematic error of the mass spectrum method of measuring the molar fractions of isotopes of the elements being investigated. The indeterminacy of the nuclear constants used to calculate the effective yield of the depletion monitor makes an important contribution to the uneliminated error of depletion measurement.

In order to analyze the effect of the different sources of error on the accuracy of the method of depletion determination, the uneliminated systematic error of the method was calculated, and the effect of the individual components on it was discussed. The calculations have been made for mixed fuel with U/Pu = 4. The content of heavy isotopes of plutonium ($^{240-242}Pu$) was 40%, which corresponds to the composition of plutonium accumulated in thermal reactors. The calculations are given for different ratios of molar fractions of the uranium isotopes N_8/N_5.

The limit of the uneliminated systematic error Θ of the result of the depletion measurement (in %) was calculated from the formula $\Theta = 100\sqrt{\Sigma(\Delta F_i/F)^2}$, where ΔF_i is the change in the depletion upon a change in the value of the i-th parameter entering into the calculation by its uneliminated systematic error.

The computational results are given in Table 2. Analysis of Table 2 shows that even with a systematic error of determination of the uranium and plutonium isotope content of ~1% this component makes no noticeable contribution to the total uneliminated systematic measurement error. However, the accuracy of determination of the relative content of the depletion monitor N_M/N_U is important.

The total error is produced mainly by the indeterminacy of the yield of fission products. The contribution of the error in the effective neutron absorption cross sections of ^{238}U and ^{239}Pu (σ_{a_8}, σ_{a_9}) and α_8 (the ratio of the capture and fission cross sections of ^{238}U) is also appreciable. The total error depends significantly on the composition of the fuel, since as the ^{235}U in the original fuel decreases the contribution of the fraction of fissions of the plutonium isotopes, for which the yield of fission products is known with poorer accuracy than for ^{235}U to the total depletion, increases.

When two parallel measurements are performed, the confidence limits of the error in the depletion determination result calculated from the formula $\Delta = \sqrt{\theta^2 + \varepsilon^2}$, are equal to 2.7, 2.9, 3.4, 4.2, and 4.9% for fuel with a ratio of molar fractions of ^{238}U and ^{235}U of 0.1, 1, 3, 10, and 100, respectively.

TABLE 1. Experimental Results of Parallel Measurements of Depletion of the Fuel of a Fast Reactor

Meas. No.	$\frac{N_{Pu}}{N_U}$	$\frac{N_M}{N_U} \cdot 10^2$	Depletion, %
1	0,2458	0,6973	7,91
2	0,2479	0,7148	8,08
3	0,2404	0,7038	8,00
4	0,2464	0,7121	8,06
5	0,2458	0,7061	8,00
6	0,2389	0,6961	7,94
7	0,2435	0,6962	7,91
8	0,2354	0,6928	7,92
9	0,2434	0,6986	7,94
10	0,2446	0,6962	7,90
11	0,2476	0,7023	7,95
12	0,2434	0,6943	7,89
13	0,2467	0,7066	8,00
14	0,2374	0,6922	7,90
15	0,2486	0,6970	7,89
16	0,2404	0,6942	7,91
17	0,2467	0,7305	8,25
18	0,2404	0,6984	7,95
19	0,2469	0,7082	8,02
20	0,2381	0,6932	7,91
21	0,2440	0,7108	8,06

TABLE 2. Contribution of the Separate Components to the Total Error of Measurement of the Fuel Depletion of a Fast Reactor, %

Parameters	θ_i	$\frac{N_8}{N_5}=0,1$	$\frac{N_8}{N_5}=1$	$\frac{N_8}{N_5}=3$	$\frac{N_8}{N_5}=10$	$\frac{N_8}{N_5}=100$
N_5	1	0,6	0,4	0,19	0,7	0,008
N_8	1	0,11	0,3	0,5	0,6	0,6
N_9	1	0,14	0,11	0,10	0,10	0,09
N_0	1	0,08	0,06	0,06	0,06	0,06
N_1	1	0,04	0,03	0,03	0,03	0,03
N_2	1	0,01	0,01	0,01	0,01	0,01
$\bar{\sigma}_{a_6}$	25	$>0,001$	$>0,001$	$>0,001$	$>0,001$	$>0,001$
$\bar{\sigma}_{a_7}$	25	$>0,001$	$>0,001$	$>0,001$	$>0,001$	$>0,001$
$\bar{\sigma}_{a_8}$	15	0,02	0,17	0,4	0,6	0,8
$\bar{\sigma}_{a_9}$	10	0,3	0,4	0,5	0,6	0,6
$\bar{\sigma}_{a_0}$	25	0,04	0,04	0,03	0,009	0,002
$\bar{\sigma}_{a_1}$	25	0,007	0,026	0,07	0,13	0,2
$\bar{\sigma}_{a_2}$	50	0,07	0,10	0,12	0,15	0,2
α_5	15	0,08	0,08	0,07	0,04	0,006
α_6	40	$>0,001$	$>0,001$	$>0,001$	$>0,001$	$>0,001$
α_7	40	$>0,001$	$>0,001$	$>0,001$	$>0,001$	$>0,001$
α_8	20	0,02	0,13	0,3	0,4	0,6
α_9	15	0,04	0,05	0,06	0,07	0,07
α_0	25	0,011	0,011	0,007	0,003	0,002
α_1	40	$>0,001$	0,002	0,006	0,012	0,02
α_2	50	0,003	0,05	0,06	0,08	0,09
Y_5	2,8	1,9	1,4	1,0	0,5	0,06
Y_6	30	0,04	0,03	0,026	0,016	0,002
Y_7	30	$>0,001$	$>0,001$	$>0,001$	$>0,001$	$>0,001$
Y_8	14	0,1	0,7	1,3	2,1	2,6
Y_9	4,2	0,7	1,1	1,5	1,9	2,2
Y_0	20	0,6	0,8	1,1	1,5	1,7
Y_1	20	0,7	1,1	1,5	1,9	2,3
Y_2	20	0,04	0,06	0,09	0,1	0,1
N_M/N_U	1	0,9	0,9	0,9	0,9	0,9
Total unelimi-nated systemat-ic error		2,5	2,7	3,2	4,02	4,8

Conclusions. The indeterminacy in the yield of fission products of plutonium isotopes makes the main contribution to the total measurement error of depletion. Therefore the error increases as the fraction of plutonium, especially its heavy isotopes, in the original fuel increases. The contribution of the random component to the total error is inappreciable, and there is no need to carry out a large number of parallel measurements. It is advisable to make two measurements to eliminate the coarse error. The depletion can be determined with an error no worse than 5% when the total ^{145}Nd and ^{146}Nd content is selected as the depletion monitor, depending on the composition of the mixed uranium–plutonium fuel.

LITERATURE CITED

1. Yu. B. Novikov, At. Énerg., 43, No. 4, 240 (1977).
2. W. Maeck, in: Proc. Panel Meeting on Fission Product Nuclear Data, JCP-1040, Bologna, Nov. 26-30, 1973.
3. V. Ya. Gabeskiriya et al., At. Énerg., 44, No. 5, 446 (1978).
4. V. Ya. Gabeskiriya et al., Preprint NINAR P-24 (290), Dimitrovgrad (1976).
5. V. M. Gryazev et al., Preprint NINAR P-25 (359), Dimitrovgrad (1978).
6. V. S. Prokopenko et al., At. Énerg., 45, No. 3, 230 (1978).
7. E. Crouch, AERE-R 7785, Harwell, Oxfordshire (1975).

NUCLEAR-PHYSICAL INVESTIGATION OF MASS TRANSPORT OF CARBON AND NITROGEN BY SODIUM COOLANT

O. V. Starkov, I. V. Istomin,
V. A. Karabash, M. Kh. Kononyuk,
A. N. Sosnin, and V. S. Shorin

UDC 539.1.08:620.193:621.039

The durability of structural materials (steels) in liquid sodium, used as a coolant, remains an urgent problem for fast reactors. In order to make a correct prediction of the behavior of steels and the change in their mechanical properties during the operation of power equipment for $(2-3)\cdot10^5$ h one must have an understanding of the processes of mass transport and corrosion. Laboratory investigations [1-5] showed that the transport of the main elements (Fe, Cr, Ni) does not appreciably limit the operating life of steels in liquid sodium of reactor purity. The corrosion rate is low, amounting to less than 5 μm/yr for austenitic chromium-nickel steels at 700°C. The principal corrosion effect is the transport of interstitial impurities, carbon and nitrogen. The transport rate depends in a fairly involved way on the temperature as well as on the composition of the steels, the heat treatment conditions, and geometric and other factors. Processes of absorption of the carbon and nitrogen by the material (austenitic steels) are possible and so are processes of denitration and decarburization (for unstabilized 10Kh2M pearlitic steel); all of this has a different effect on the mechanical properties of the steels.

Transport of carbon through liquid sodium between steels of different composition can be described by the diffusion equation. In order to solve the equation it is necessary to know the boundary conditions, in particular the relation between the areas of the surface of the steel that is the source of carbon (S_s) and the steel that is the receiver (S_r) of the carbon and the value of the thermodynamic activity of the carbon. The solution of the diffusion equation shows that the thermodynamic activity is proportional to the surface concentration C_0 of carbon. Thus, in order to study the thermodynamic properties of complex systems one must have experimental data about the functions $C(x)$ of the distribution of the gaseous impurities over depth in the range >50-100 μm, which is characteristic of the width of the corrosion zone. Existing methods of chemical analysis to determine the nitrogen and carbon content with a layered mechanism of removing material of the specimen have a poor depth resolution ($\Delta x \geqslant 50$ μm), which does not allow C_0 to be measured with the necessary accuracy for large gradients of impurity distribution.

Translated from Atomnaya Énergiya, Vol. 57, No. 1, pp. 10-14, July, 1984. Original article submitted November 4, 1983.

0038-531X/84/5701-0432$08.50

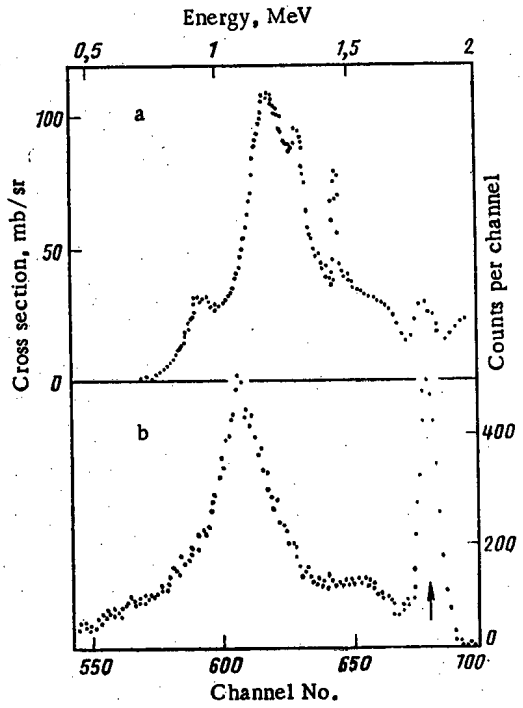

Fig. 1. Differential cross section of the $^{12}C(d, p_0)$ reaction for the angle $\theta_L = 165°$ (a) and amplitude spectrum of protons in the region of carbon impurities in a 10Kh2M steel specimen for $E_1 = 1.76$ MeV (b). The arrow points to the peak of surface contaminants.

In the work reported here the nuclear-physical method of microanalysis from the instantaneous radiation was used to study the distribution of nitrogen and carbon in specimens of unstabilized 10Kh2M pearlitic steel in contact with liquid sodium under different conditions. The method is based on the spectrometry of protons from the (d, p_0) reactions which occur on impurity nuclei when the surface of the specimen is probed with a deuteron beam having an energy of 1-2 MeV [6]. The protons were detected by two semiconductor detectors of the DKPs type, set up at angles of 150 and 165° to the beam in a scattering chamber connected to the ion guide of an EG-2.5 electrostatic accelerator. The electronics of the experiment permitted simultaneous accumulation of amplitude spectra from two detectors, one of which was adjusted to detect the carbon impurity and the other, to detect nitrogen. The details of the method and the experimental technique were described in [7, 8]. The method has a depth resolution $\Delta x \leqslant 1$ μm at a probing depth $R_0 \leqslant 10$ μm. In order to obtain information at a greater depth the method was employed in conjunction with the sectioning technique.

In order to simplify the analytical procedure, we assumed that the desired distribution $C(x)$ in the region $x \leqslant R_0$ has the form

$$C(x) = C_0 + (C_p a)\,\delta(x), \tag{1}$$

where the distribution function of surface contaminants in the specimen is approximated by a δ function and C_p is the average impurity concentration in a surface film of average thickness a. The assumption (1) permits the method to be made a rapid method since the procedure of analyzing the measured spectra can be replaced by one of comparing the reaction yields $Y(E_1)$ for several values of the incident deuteron energy E_1. The yield $Y(E_1)$

$$Y(E_1) = A\int_0^{R(E_1)} \sigma(x)\,C(x)\,dx = A\sigma_0\Phi(E_1)\,S_0^{-1}\,[C_0 + C_p a z(E_1)], \tag{2}$$

where the functions $\Phi(E_1)$ and $z(E_1)$ have the form

$$\Phi(E_1) = \int_0^{E_1} [\sigma(E)/\sigma_0]\,[S_0/S_1(E)]\,dE;$$

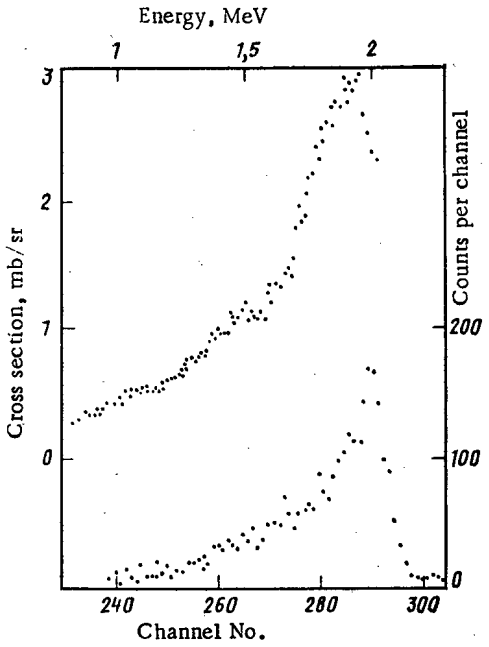

Fig. 2. Differential cross section of the $^{14}N(d, p_0)$ reaction for the angle $\theta_L = 150°$ [a) points at top] and amplitude spectrum of protons in the region of nitrogen impurities in a 10Kh2M steel specimen for $E_1 = 2.02$ MeV [b) points at bottom].

TABLE 1. Content of Carbon ($\times 10^2$) and Nitrogen ($\times 10^3$) in Surface Layers of 10Kh2M Steel after Tests, mass %

Conditions of tests				Carbon				Nitrogen		
				distance from surface, mm				distance from surface, mm		
T, °C	t*, h	carbon receiver	S_s/S_r	0	0,05	0,1	0–0,1 †	0	0,05	0,1
400	$5{,}6\cdot10^4$	10Kh18N10	1 : 1	130±10	12,5±0,6	10,8±0,3	12±1	100±10	25±1	18±0,7
510	10^3	10Kh18N10T	1 : 200	0,99±0,11	2,88±0,26	3,46±0,10	2,5±0,5	1,5±0,15	5,03±0,42	7,8±1,5
550	$5\cdot10^2$	10Kh13	1 : 1	2,0±0,32	4,30±0,10	4,69±0,37	5±1	2,05±0,3	1,0±0,3	8,98±0,32
650	$5\cdot10^2$	10Kh13	1 : 1	1,01±0,07	1,07±0,04	2,17±0,10	5±1	2,17±0,10	1,69±0,10	4,27±0,2

*t denotes the duration of the tests.
†Data from chemical analysis.

$$z(E_1) = S_0\sigma(E_1)\,[\sigma_0 S_1(E_1)\,\Phi(E_1)]^{-1}.$$

Here $\sigma[E(x)]$ is the cross section of the reaction at a depth x, R(E) is the range of deuterons of energy E, $S_1(E)$ is the stopping power of the substance, $\sigma_0 \equiv \sigma(E_0)$, $S_0 \equiv S_1(E_0)$, and E_0 is a certain "base" energy. The constants A and σ_0 were determined in an experiment with a standard, i.e., a specimen of known stoichiometry, for which we used specimens of reactor graphite, natural diamond (carbon), and aluminum nitride (nitrogen). The S(E) data were taken from [9], making it possible to determine the relative value of $S(E)/S_0$ with an error of 1-1.5%. The energy dependence of the reaction cross section $\sigma(E)/\sigma_0$ was measured in experiments with thin carbon and nitrogen (adenine $C_5H_5N_5$) films with an error of no more than 2%.

The results of cross-sectional measurements are given in Figs. 1-2. The figures show that a broad resonance at $E_d = 1.2$ MeV dominates in the $^{12}C(d, p_0)$ reaction cross section while the cross section for the $^{14}N(d, p_0)$ reaction grows smoothly by a $\sim E^{3.1}$ law to a resonance at 1.9 MeV. The shape of the cross section essentially determines the shape of the spectra measured (see Figs. 1b and 2b) and the effective depth <x> of analysis; calculation for $R_1 = 1.8$ MeV gave a value of <x> = 4.9 μm in an analysis for carbon and 2.8 μm in an analysis for nitrogen in steel.

This method of isolating the surface film is easily realized in the case of nitrogen microanalysis. Measurements showed that the nitrogen film on steel specimens is fairly stable

and has a thickness of approximately 1 monolayer (0.1-0.2 μg/cm² for C_p = 1). The thickness of the surface carbon film is substantially greater (0.4-3μg/cm²) and C_p increases with time [scattering-chamber pressure ~$3 \cdot 10^{-5}$ torr (1 torr = 133.322 Pa)]. Thus, C_p for the carbon film was determined by a simpler method, exploiting the fact that the surface film is explicitly isolated in the measured proton spectrum at a deuteron energy $E_1 > 1.7$ MeV and a detector resolution $\delta E \sim 50$ keV (see Fig. 1b). For carbon analysis, therefore, it was sufficient to carry out measurements for one value of deuteron energy, viz., $E_1 = 1.76$ MeV. This value is optimum since interference with oxygen [the contribution of the $^{16}O(d, p_0)$ to the measured spectrum] is minimal at the energy indicated [8]. For nitrogen the interference of the $^{14}N(d, p_0)$ and $^{14}N(d, \alpha_0)$ reactions is easily eliminated by placing a polyethylene filter (~17 mg/cm²) in front of the detector; the filter removes other impurities from the spectrum of detected protons (see Fig. 2b) [7].

The specimens, in the form of disks 14 mm in diameter, were sections made at a particular depth in the material in contact with liquid sodium. They were prepared from the wall of an operating tube of a BN-350 steam generator as well as test-stand specimens and their surface was polished. The beam diameter on the specimen was ~1.5 mm. The system for moving the specimen permitted simultaneous scanning of the beam over the surface of the target. The final data were obtained by averaging the results of measurements at 3-5 points of the surface in order to eliminate the influence of local inhomogeneities which in some cases served as the main source of errors. The dose of an individual irradiation was 50-130 μCi at a beam current of 0.1-0.3 μA and the statistical error of measurement of the yields $Y(E_1)$ for the specimens was 1-5%, depending on the impurity content and the value of E_1, for a measuring time of 10-25 min. The estimated inherent (systematic) error of the method in the case of one-parameter analysis (of carbon) is 3%.

The results and characteristics of the conditions of the testing of specimens of 10Kh2M steel are given in Table 1. The investigations were carried out at 400-650°C for 500-56,000 h. High-alloy steels of different compositions (10Kh13, 10Kh18N10, 10Kh1810T) were the carbon receivers. The presence, in the austenitic chromium-nickel steel, of titanium which is strongly carbide-forming substantially affected the surface concentration of carbon in the 10Kh2M steel. When the testing apparatus was made of 10Kh18N10T steel, then according to chemical analysis data the average carbon content in the surface layer 50-100 μm thick of 10Kh2M steel was 0.03 and 0.02 mass % after being kept in sodium at 500 and 550°C, respectively. When 10Kh18N10 steel served as the carbon receiver, C_0 increased to 0.075-0.09 mass %. Data from nuclear microanalysis show (see Table 1) that when 10Kh2M steel is decarburized, the value of C_0 is smaller than the data from chemical analysis by a factor of 2-2.5. Such a low carbon content near the surface can be explained not only by equalization of the thermodynamic activity of carbon in the system 10Kh2M–Na–10Kh18N10T, tending to equilibrium, but also by a change in the stoichiometric equilibrium of the surface layers of the steels with respect to the main elements (Cr, Fe, Ni) because of their dissolution and deposition in the sodium. This, in turn, causes a change in the thermodynamic activity of the nitrogen and carbon. Consequently, when the surface is depleted of chromium the content of carbides and nitrides decreases.

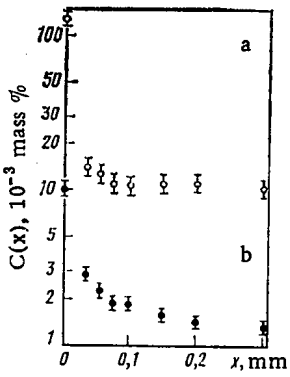

Fig. 3. Distribution of concentration C(x) of carbon impurity (a) and nitrogen impurity (b) over the depth x for the wall of the steam generator made of 10Kh2M steel in the BN-350 plant.

TABLE 2. Average Carbon Content in a 0.1-mm Surface Layer of 10Kh2M Steel after 500 h in Sodium, mass %

Carbon receiver	550°C	650°C
10Kh18N10	0,075	0,05
10Kh13	0,045	0,020
10Kh18N10T	0,025	—

The hypothesis put forward here can be illustrated by the data for the wall of a BN-350 steam generator operated for 56,000 h (Fig. 3, Table 1) at 390-400°C. At such a temperature a change in the stoichiometry of the surface layers can be observed only after long tests, owing to the slow rate of mass transport of the main elements. The results of mass-spectrometric analysis of specimens of 10Kh2M steel reveal that near the surface the chromium content increases from 2.25% to 3-4%, as is confirmed by the existence of a process of transport of the main elements in a nonisothermal loop through the sodium between the 10Kh18N10 and 10Kh2M steels. This process leads to carburization of the 10Kh2M steel, which is not entirely usual for a low-alloy pearlitic steel. Nevertheless, this tendency is indicated by chemical analysis data which attest to a carbon concentration of up to 0.12 ± 0.01 mass % in the surface layer (~100 μm) of the 10Kh2M steel. The results of nuclear microanalysis (see Fig. 3) support this with great reliability for carbon as well as for nitrogen, for which no other data were obtained. The results of microanalysis show that carburization and nitration processes are noticeable at a depth <40 μm even at a low temperature.

Table 1 also presents the results of nuclear-physical analysis of the transport of nitrogen and carbon between 10Kh2M and 10Kh13 steels; this analysis stemmed from interest in ferritic chromium steels as possible structural materials for sodium-cooled reactors. The data presented indicate decarburization of 10Kh2M steel after it has been held in sodium at 550-650°C and that the decarburization rate almost doubles when the temperature is increased by 100°C. These data can be compared with the results of chemical analysis for carbon in the surface layer of 10Kh2M steel (thickness 100 μm) with 10Kh18N10 and 10Kh18N10T steels as the carbon receivers (Table 2). It turns out that the results for 10Kh13 steel are intermediate between the values of the concentration for 10Kh18N10 and 10Kh18N10T steels. It thus follows that the thermodynamic activity of carbon in chromium ferritic steel occupies a position intermediate between the corresponding values for titanium-stabilized and unstabilized chromium-nickel steel.

The simultaneous measurement of the distribution of nitrogen and carbon impurities in surface layers of 10Kh2M steel by means of nuclear microanalysis permits an unambiguous conclusion as to the correlation in the variations in the carbon and nitrogen concentrations (see Fig. 3, Table 1), viz.: The decarburization process takes place simultaneously with the nitration process. This correlation is in accordance with the values and signs of the thermodynamic parameters of the reaction of nitrogen and carbon with the alloying elements in the steel [1]. Quantitative estimation of such parameters is an urgent and interesting problem. The application of the methods of nuclear microanalysis, which have a high sensitivity and resolution over depth, are very promising for the solution of this problem. The results of this paper also indicate a necessity of more detailed investigations of the surface zone to a depth $\leqslant$10 μm, in which a particularly pronounced change occurs in the concentration of both the interstitial impurities and the main elements. In this region (of the order of the grain size of the material) the nuclear method of analysis on the basis of instantaneous radiation in practice has no competition from other nuclear and atomic methods.

In conclusion, the authors express their gratitude to B. D. Kuz'min for taking a constant interest in the work, V. G. Balin, A. F. Gurbich, Yu. M. Nikitin, and M. P. Filin for participation and assistance in the individual stages of the work, as well as to the members of the ÉG-2.5 group for reliable operation of the accelerator in the desired regime.

LITERATURE CITED

1. B. A. Nevzorov et al., Corrosion of Structural Materials in Liquid Alkali Metals [in Russian], Atomizdat, Moscow (1977).

2. O. V. Starkov, B. A. Nevzorov, and I. N. Luk'yanova, Zashch. Met., 7, No. 6, 674 (1971).
3. O. V. Starkov and I. N. Luk'yanova, Zashch. Met., 10, No. 3, 255 (1974).
4. O. V. Starkov and E. S. Kononov, Zashch. Met., 11, No. 1, 63 (1975).
5. O. V. Starkov and M. Kh. Kononyuk, Zashch. Met., 14, No. 6, 540 (1978).
6. J. Bird, B. Campbell, and P. Price, Atomic Energy Rev., 12, 275 (1974).
7. A. F. Gurbich et al., Preprint FEI-1122, Physics and Power Engineering Institute, Obninsk (1980).
8. V. G. Balin et al., Preprint FEI-1341, Physics and Power Engineering Institute, Obninsk (1982).
9. J. Janni, Atomic Data Nucl. Data Tables, 27, 150 (1982).

CRITICAL TRANSPORTATION VELOCITY OF SUSPENSIONS IN HEAT-CARRIER FLOWS

V. V. Alekseev, F. A. Kozlov, and Yu. I. Zagorul'ko

UDC 621.039.534.63

Studying the transportation of suspensions in heat-carrier flows is associated with the need to obtain theoretical dependences for estimating the transfer and accumulation of impurities in the loops.

The critical velocity of transportation of particles suspended in a turbulent flow, defined as the smallest velocity of the suspension-bearing flow (at which no accumulation of a deposit on the floor of the horizontal channel occurs), depends on a series of parameters: the dimensions, density, form, and concentration of the parameters; the viscosity and density of the liquid; the dimensions, form, and roughness of the channel surface; the adhesional-interaction force and the friction of the particles with the surface.

In the known empirical dependences used to calculate the critical velocity [1-3], the influence of only some of these parameters is taken into account; the region of definition of the individual characteristics is significantly restricted. There is a considerable discrepancy in the numerical estimates of the critical velocity obtained from the data of different authors.

In the calculation method described here, the forces which act on particles at the surface of a circular channel are considered, and the influence of all significant determining parameters is taken into account. The following basic hypotheses are employed.

When $u \geqslant u_c$, the particle flux deposited on the channel surface is equal to the particle flux removed from the wall and entrained in the layer of liquid at the wall. When $u < u_c$, the individual particles incident on the channel surface are retained there, as a result of which deposit accumulation occurs. In the case of deposition of a single particle (which occurs at a sufficiently small particle concentration in the liquid flow), the critical velocity is identically equal to the velocity of particle breakaway. To determine the breakaway velocity, the balance of all the forces acting on the particle at the channel surface is considered. The dependence of the critical velocity on the particle concentration is specified on the basis of the breakaway condition for a group of particles.

Estimation of the Forces Acting on a Particle at the Channel Wall

Using the data of [4], the force exerted by the liquid flow on a particle remaining within the limits of a laminar sublayer of the boundary layer may be estimated:

$$F_{F+} = 10.5 l_+^2 \quad (0 < l_+ \leqslant 5). \tag{1}$$

If the particle dimension exceeds the thickness of the buffer sublayer of the boundary layer ($l_+ > 30$), the velocity of flow around the particle is taken to be equal to the flow velocity at a distance of $l/2$ from the wall. A Karmanovskii velocity distribution over the

Translated from Atomnaya Énergiya, Vol. 57, No. 1, pp. 14-18, July, 1984. Original article submitted October 28, 1983.

0038-531X/84/5701-0437$08.50

channel cross section is assumed. In this case, taking account of the dependence of the frontal force on the velocity of flow around the particle [5], it is found that

$$F_{F+} = 69.15\ |l_+ \ln (l_+/3.68)|^{1.4} \quad (30 \leqslant l_+ \leqslant 41.4); \tag{2}$$

$$F_{F+} = 4.32\ |l_+ \ln (l_+/3.68)|^2 \quad (41.4 \leqslant l_+ \leqslant 60); \tag{3}$$

$$F_{F+} = 1.12\ |l_+ \ln (4.51 l_+)|^2 \quad (l_+ > 60). \tag{4}$$

The dependence of F_{F+} on l_+ taken in a linear approximation in logarithmic coordinates between the points $l_+ = 5$ and $l_+ = 30$ is described by the equation

$$F_{F+} = 4.7 l_+^{2.49} \quad (5 \leqslant l_+ \leqslant 30). \tag{5}$$

With an approximation to a few percent, Eqs. (2)-(5) may be written in the less accurate form

$$F_{F+} = 5.18 l_+^{2.44} \quad (5 \leqslant l_+ \leqslant 300). \tag{6}$$

The lift force is estimated using the dependence

$$F_{L+} = 0.076 l_+^3. \tag{7}$$

The simplest form of the dependence of the adhesion force on the particle dimension was proposed in [7]

$$F_a = k_a l. \tag{8}$$

The particle weight, taking account of the expulsion force, is

$$F_w = \pi g l^3 (\rho_p - \rho)/6. \tag{9}$$

Calculation of the Critical Velocity of Suspension-Bearing Flows with Small Particle Concentrations in the Liquid

A small concentration of the suspension here is understood to be such that the mutual influence of the particles at the channel wall when $u \geqslant u_c$ may be neglected. In this case, the critical velocity is taken to be equal to the breakaway velocity.

The breakaway condition for a particle at the wall of a horizontal channel (in its lower part) is [8]

$$F_F \geqslant k_T (F_a + F_w - F_L). \tag{10}$$

If the particle is nonspherical, Eqs. (1) and (6) take the form

$$F_{F+} = 10.5 (k_s l_+)^2; \tag{11}$$

$$F_{F+} = 5.18 (k_s l_+)^{2.44}, \tag{12}$$

where $k_s = l_M/l$, $l = (6V/\pi)^{1/3}$.

Substituting F_F, F_a, F_w, and F_L into Eq. (10) from Eqs. (1) and (6)-(9), an expression is obtained for the dynamic flow velocity corresponding to particle breakaway

$$u^* \geqslant \{k_T [k_a/l + \pi g (\rho_p - \rho) l/6]\ 10.5\rho\}^{0.5}/k_s \quad (l_+ \leqslant 5); \tag{13}$$

$$u^* \geqslant \left\{\frac{k_T [k_a + \pi g (\rho_p - \rho) l^2/6}{\rho (5.18 k_s^{2.44} + 0.076 k_1 l_+^{0.56}}\right\}^{0.41} \frac{\nu^{0.18}}{l^{0.591}} \tag{14}$$

$$(5 \leqslant l_+ \leqslant 300).$$

The critical velocity is determined from the solution of the equation establishing a relation between the dynamic and mean-mass flow velocity [9]:

$$u^* = u_c/[5.15 \lg (u_c D_c/\nu) - 4.64]. \tag{15}$$

For a channel with a rough surface, when the particle is on the side of a projection, the breakaway condition may be written in the form

$$F_F \cos\alpha - F_W \sin\alpha + F_L \sin\alpha \geqslant k_T (F_a + F_W \cos\alpha + F_F \sin\alpha - F_L \cos\alpha). \quad (16)$$

The angle α is estimated approximately from the relation (Fig. 1)

$$\cos\alpha \approx (R_r - h_r/2)/R_r. \quad (17)$$

Using Eq. (16), the following expressions are obtained for a rough surface

$$u^* \geqslant \left[\frac{k_T k_a l + \pi g (\rho_p - \rho)(\sin\alpha + k_T \cos\alpha) l/6}{10{,}5\rho(\cos\alpha - k_T \sin\alpha)}\right]^{0.5} / k_s \quad (18)$$

$$(l_+ \leqslant 5);$$

$$u^* \geqslant \left[\frac{k_T k_a + \pi g (\rho_p - \rho)(\sin\alpha + k_T \cos\alpha) l^2/6}{\rho(5{,}18 k_s^{2.44}(\cos\alpha - k_T \sin\alpha) + 0{,}076(\sin\alpha + k_T \cos\alpha) l_+^{0.56})}\right]^{0.41} \frac{\nu^{0.18}}{l^{0.591}} \quad (19)$$

$$(5 \leqslant l_+ \leqslant 300).$$

Equations (18) and (19) are valid if $h_{r+} \leqslant 5$. For cases when the particle touches a few projections of the rough surface, the breakaway velocity is determined using Eqs. (13) and (14).

Dependence of the Critical Velocity on the Concentration of the Suspension

At velocities of the suspension-bearing liquid flow exceeding the critical value, there is an equilibrium dynamic layer of particles at the channel surface; the density of the layer depends on the concentration of the suspended phase. If particles at the channel wall are sufficiently far apart, their mutual influence in the boundary layer of liquid may be neglected. In this case, the critical velocity is equal to the breakaway velocity. The limiting concentration of the suspension at which this condition is still satisfied may be determined as follows. On average, the number of particles on unit surface at the face of an isolated element of suspension volume is

$$n = \varphi (6c/\pi l^3)^{2/3}, \quad (20)$$

where φ is a coefficient.

The mean distance between the centers of spherical particles at the face surface is

$$s = (\pi l^3/6c)^{1/3} (1/\varphi)^{1/2}. \quad (21)$$

It may be assumed that coincidence of the face planes and the channel surface has little influence on s when $u \geqslant u_c$. There evidently always exists a line $s = s_1$, on crossing which the mutual influence of particles at the channel wall may be neglected. The value of s_1 corresponds to a suspension concentration

$$c_1 = (\pi/6)(s_1/l)^3 (1/\varphi)^{3/2}. \quad (22)$$

The ratio s_1/l depends on the conditions of liquid flow around the particle. If the particle size considerably exceeds the thickness of the laminar sublayer, the ratio may be estimated on the basis of the data of [10], and is ~15-20.

When $c > c_1$, the critical velocity is determined on the basis of the breakaway condition for a group of particles. For a group of particles at the wall, the adhesion force and the weight increase in proportion to the surface density of particles n in comparison with the same forces acting on a single particle. At the same time, as a result of the mutual influence of the particles, the frontal and lift forces increase considerably less than the adhesion force and the weight. For a group of particles, Eqs. (10) and (16) may be written in the form

$$F_F + k_T F_L \geqslant k_T (F_a + F_W) kn; \quad (23)$$

$$F_F (\cos\alpha - k_T \sin\alpha) + F_L (\sin\alpha + k_T \cos\alpha) \geqslant (k_T F_a + F_W (\sin\alpha + k_T \cos\alpha)) kn. \quad (24)$$

The value of k is determined from the condition that, when $c = c_1$, the critical velocity is equal to the breakaway velocity, or $kn = 1$; hence, $k = s_1^2$.

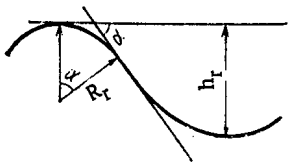

Fig. 1. Determining the angle of slope of a rough surface.

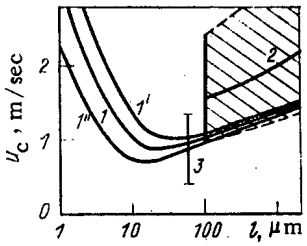

Fig. 2

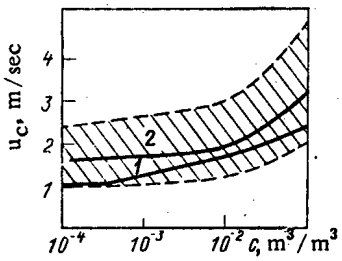

Fig. 3

Fig. 2. Dependence of the critical velocity on the dimensions of the suspension particles: 1, 1', 1") calculation by the method here described; 2) calculation from the data of [3]; 3) experimental values.

Fig. 3. Concentration dependence of the critical velocity: 1) by the method here described; 2) calculation from the data of [3].

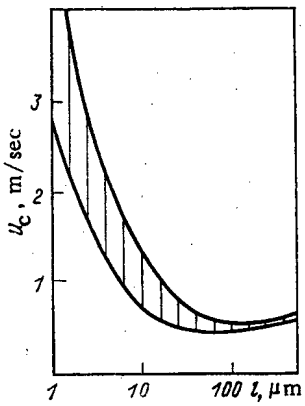

Fig. 4. Dependence of the critical velocity for iron particles in sodium.

It follows from the solution of Eqs. (23) and (24) that Eqs. (13), (14), (18), and (19) are used to determine the critical velocity; when $l_+ \leqslant 5$, the right-hand side of the inequality is multiplied by $(kn)^{0.5}$, and when $5 \leqslant l_+ \leqslant 300$ by $(kn)^{0.41}$. When $c \leqslant c_1$, kn = 1. If $c > c_1$ the product kn is found on the basis of the estimate of s_1. When $l_+ < 2$, the particles are immersed in laminar flow, and their mutual influence is small even at a distance of $2l$, i.e., $s_1 = 2l$. When $l_+ > 15$, $s_1 = 15l$. In the range $2l \leqslant l_+ \leqslant 15$, s_1 varies from $2l$ to $15l$. In final form (taking account of the simplifications adopted), data for the calculation of kn are given in Table 1.

The coefficient φ may be regraded as a parameter taking account of the influence of mutual collisions of particles on their deposition. As the distance between particles decreases, so φ differs more strongly from unity. Taking a linear dependence of φ on s, $\varphi = A/c^{1/3}$ may be written, where A is a proportionality factor. Calculation of A is based on the condition that, when $c \approx 10^{-4}$, the particle collisions are practically nonexistent, i.e., $\varphi = 1$.

Finally

$$\varphi = 1/(21.4c^{1/3}). \tag{25}$$

Experimental Determination of the Adhesion and Friction Coefficients

To confirm the possibility of using Eq. (8) to calculate the adhesion force of particles in sodium and to determine the coefficients k_a and k_T, the following procedure is used. From the balance of forces acting on a particle, at an inclined surface, it follows that the limiting particle dimension at which breakaway sets in under the action of the gravitational force is

$$l_L = \left[\frac{6k_a}{\pi g(\rho_p - \rho)(\cos\beta + \sin\beta/k_T)}\right]^{1/2}. \tag{26}$$

Equation (26) is intended for the calculation of the coefficients k_a and k_T from the experimental value of l_L at different angles of slope of the surface. With this aim, the functional dependence $l_L^2(k_a, k_T)$ is analyzed by the least-squares method.

To determine l_L in liquid, a stand was set up in an empty vessel, with Kh18N10T steel supports fixed at the same level, having a polished surface on one side. The polished support surfaces were inclined to the horizontal at angles of 0, 30, 60, and 90°. A carefully mixed suspension of particles of the chosen material was poured into the vessel. Particles of the suspension of dimension less than l_L were retained on the supports after deposition. After evaporation of liquid from the vessel at a rate at which the velocity of level drop is no more than 1 μm/sec, the substrate is transferred to the field of view of the microscope. Since the adhesion force in the gas medium is several orders of magnitude higher than in the liquid [4], transfer of the supports and their rotation does not lead to particle breakaway.

Using the ocular scale of the microscope, the longitudinal and transverse dimensions of the largest particles were estimated with an accuracy of up to 2.5 μm. The vertical dimension of the particles was determined by scanning. The particles considered were oval in form; the deviation from the mean dimension was by no more than a factor of 1.5 for each of the three measurements. For each support, the mean dimensions of the three or four largest particles were averaged. The value obtained was taken to be equal to the limiting particle dimension l_{Li} in the calculations.

To estimate the accuracy with which the coefficients k_a and k_T are determined, the standard deviation of the values measured for l_L from the results given by Eq. (26) was calculated. Experimental and theoretical values of the parameters for particles of different materials obtained in water, alcohol, and sodium are shown in Table 2. Taking into account that the adhesion force is probabilistic in character, the value of k_a corresponding to the maximum adhesion force is determined by the given method.

Theoretical Estimates of the Critical Velocity. Comparison with Experimental Data

The dependence of the critical velocity on the dimension of tungsten particles in sodium, calculated in accordance with the data in [3] and the method here proposed, is shown in Fig. 2. The following initial parameter values are adopted: $k_a = 5.7 \cdot 10^{-5}$ N/m, $k_T = 1.25$, $k_s = 0.7$, $\alpha = \pi/12$, $D_c = 0.02$ m, $c \simeq 0$, and a sodium temperature of 300°C. Curve 2 is a generalization of a large number of experimental points (shaded region) for suspended particles with dimensions of more than 100 μm. The segment of straight line 3 denotes the limits of experimentally measured values of the critical velocity. Theoretical values are enclosed between curves 1' and 1'', which correspond to the limiting deviation of the adhesion and friction coefficients from the mean.

Curves of the concentration dependence of the critical velocity for a tungsten suspension in sodium with l = 100 μm are shown in Fig. 3. The shaded region and curve 2 correspond to calculation by the data of [3].

On the basis of the results obtained, the critical flow velocity of sodium with suspended iron particles is estimated, in conditions close to those for flow in the active-zone channels of the BN-600 reactor. The sodium temperature is taken to be 600°C, D_c = 2.42 mm, k_s = 0.7, $\alpha = \pi/12$. The results of calculation are shown in Fig. 4. Hence it follows that, for the given case, with a mean-mass flow velocity of 4.75 m/sec, all particles of size >1 μm are transported.

TABLE 1. Dependence for Determining the Product kn

l_+	c_1	kn
$l_+ < 2$	$(\pi/48)/\varphi^{3/2}$	$(48c/\pi)^{2/3}\varphi$
$2 \leqslant l_+ \leqslant 15$	$[\pi/(6l_+^3)]/\varphi^{3/2}$	$(6c/\pi)^{2/3}l_+^2\varphi$
$l_+ > 15$	$1{,}55\cdot10^{-4}/\varphi^{3/2}$	$346c^{2/3}\varphi$

TABLE 2. Results of Experimental Determination of Adhesion and Friction Coefficients of Particles in Liquids

Medium	Particle material	k_a, 10^{-5} N/m (maximum value)	k_T
Water	Tungsten	6,0±1,8	0,87±0,20
Ethyl alcohol	Stainless steel	3,2±0,9	0,75±0,20
Sodium	The same	9,7±3,2	1,17±0,11
Sodium	Graphite	6,3±2,7	1,10±0,16
Sodium	Tungsten	5,7±2,5	1,25±0,13
Sodium	Nickel	8,7±2,8	1,22±0,11

The given relations allow the critical velocity of suspension-bearing flows to be calculated over a broad range of initial parameters. Using the data of Table 2, the transportability of suspensions of particle size up to 1 μm may be estimated, the most dangerous points may be determined from the viewpoint of clogging of the cross section, and the propagation of some active and inactive impurities in loops with a sodium heat carrier may be estimated.

NOTATION

l, particle dimension, m; l_M, minimum particle dimension, m; l_L, limiting particle dimension, m; D_c, channel diameter, m; h_r, microprojection height of surface roughness, m; R_r, radius of roughness projection, m; s, distance between particle centers; s_1, limiting value of the distance between particles, m; V, particle volume, m^3; F_F, frontal force, N; F_a, adhesion force, N; F_w, weight, N; F_L, lift force, N; u_c, critical velocity, m/sec; u^*, dynamic velocity, m/sec; c, bulk concentration of suspension, m^3/m^3; c_1, maximum concentration at which the critical velocity is equal to the particle breakaway velocity, m^3/m^3; ρ, liquid density, kg/m^3; ρ_p, particle density, kg/m^3; n, number of particles per unit channel surface, m^{-2}; ν, kinematic viscosity, m^2/sec; k_T, sliding friction; k_a, adhesion coefficient, N/m; $l_+ = l_{u*}/\nu$, $F_{F+} = F_F/\rho\nu^2$, $F_{L+} = F_L/\rho\nu^2$, dimensionless parameters; k_s, sphericity coefficient; k, proportionality factor; g, acceleration due to gravity, m/sec^2; α, angle of slope of surface of a roughness projection; β, angle of inclination of the support to the horizontal; Re, Reynolds number.

LITERATURE CITED

1. R. Brown, Trans. Am. Nucl. Soc., 30, 471 (1978).
2. V. S. Knoroz, in: Izv. Vses. Nauk.-Issl. Inst. Gidrotekh., 40, 37 (1949).
3. D. Thomas, AIChE J., 8, No. 3, 373 (1962).
4. J. Happel and G. Brenner, Hydrodynamics at Small Reynolds Number [Russian translation], Mir, Moscow (1976).
5. P. G. Romankov and M. I. Kurochkina, Hydromechanical Processes of Chemical Technology [in Russian], Khimiya, Moscow (1974).
6. J. Cleaver and B. Yates, J. Coll. Interf. Sci., 44, 464 (1973).
7. A. D. Zimon, Adhesion of Dust and Powders [Russian translation], Khimiya, Moscow (1976).
8. A. D. Zimon and G. A. Serebryakov, in: Abstracts of a Conference on Aerosol Adhesion [in Russian], Frunze (1974).
9. L. G. Loitsyanskii, Mechanics of Liquids and Gases [in Russian], Fizmatgiz, Moscow (1970).
10. V. I. Subbotin et al., Preprint No. 672, FEI, Obninsk (1976).

USE OF DETECTORS EXTERNAL TO REACTOR TO DETERMINE THE REACTOR POWER AND THE MEAN ENERGY DISTRIBUTION OVER THE HEIGHT OF THE ACTIVE ZONE

A. N. Kamyshan, A. M. Luzhnov,
A. S. Makhon'kov, V. V. Morozov,
N. S. Orekhova, and S. G. Tsypin

UDC 621.039.512.44

Systems based on detectors positioned outside the reactor have been successfully used to monitor the power and mean energy distribution over the height of the active zone in non-Soviet atomic power stations with PWR [1-3]. The development of systems with monitoring from outside the reactor is also of great importancd in the USSR [4]. As a rule, these systems, permitting continuous take-up of information characterized by inertialessness and high reliability, are associated with emergency-protection systems of the reactor.

A typical setup of detectors external to the reactor (DER) is shown in Fig. 1. Three or four detector units are positioned around the reactor, each with two to four detectors at different heights [1, 3, 5]. Since the neutron field outside the reactor depends on the energy distribution over the volume of the active zone, the form of the energy distribution over the height may be recovered using the appropriate method of analysis of the detector readings. The integral of this distribution will be proportional to the reactor power.

In the present work, an attempt is made to determine some characteristics of systems of DER optimal from the viewpoint of a reasonable compromise between the error of the results and complexity of construction. One of the basic characteristics of this system is the number of detectors in each unit. Usually, it oscillates from two to four, but there is no sound basis for the choice of any specific number [1, 3, 5]. For a specified class of functions, including a set of possible forms of height distributions, how may the minimum number of detectors sufficient for recovering any function from this class with satisfactory accuracy be found? To estimate the accuracy of recovery, the following criteria may be used

$$\delta_s = \int_0^H |F(z) - f(z)|\, dz \Big/ \int_0^H F(z)\, dz; \tag{1}$$

$$\delta_F = |\max_{z\in[0,\,H]} F(z) - \max_{z\in[0,\,H]} f(z)| \Big/ \max_{z\in[0,\,H]} F(z). \tag{2}$$

Here F(z) is the true energy distribution over the height; f(z) is the energy distribution recovered; H is the active-zone height.

The reading of detector number k in the unit is related to the energy distribution over the volume of the active zone $F_V(r)$ through the space-dependent weighting function of this detector $S_k^V(r)$

$$D_k = \int_V F_V(\mathbf{r})\, S_k^V(\mathbf{r})\, d\mathbf{r}, \tag{3}$$

where V is the volume of the active zone; $S_k^V(r)$ is the space-dependent weighting function, which specifies the response of detector k to a point fission source of unit power at point r.*

It is assumed that $F_V(r)$ may be written in the form

$$F_V(\mathbf{r}) = F(z)\, F_1(r, \varphi), \tag{4}$$

where the function $F_1(r, \varphi)$ is normalized to unity

*Methods of determining the weighting functions were considered in detail in [6-8].

Translated from Atomnaya Énergiya, Vol. 57, No. 1, pp. 18-21, July, 1984. Original article submitted August 22, 1983.

0038-531X/84/5701-0443$08.50

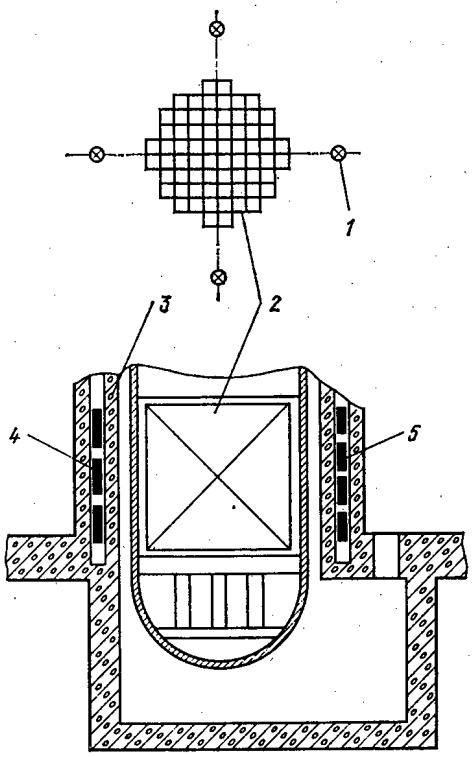

Fig. 1. Positioning of detectors: 1) detector units; 2) active zone; 3) shield; 4) channel and three-detector unit; 5) channel and four-detector unit.

$$\int_0^{2\pi} d\varphi \int_0^R rF_1(r, \varphi)\, dr = 1,$$

and R is the radius of the active zone.

Combining Eqs. (3) and (4) gives

$$D_k = \int_0^H F(z)\, S_k(z)\, dz, \tag{5}$$

where

$$S_k(z) = \int_0^{2\pi} d\varphi \int_0^R r\, dr S_k^V(z, r, \varphi)\, F_1(r, \varphi).$$

Below, $S_k(z)$ will be simply called the weighting functions. The height of the active zone is divided into N equal sections, and Eq. (5) is written in the form

$$D_k = W_1 \int_{z_1}^{z_2} \varphi_1(z)\, S_k(z)\, dz + \ldots + W_N \int_{z_N}^{z_{N+1}} \varphi_N(z)\, S_k(z)\, dz,$$

where the sequence $\{z_n;\ n = \overline{1, N}\}$ specifies the division of the active-zone height; and

$$\varphi_n(z) = F(z) \Big/ \int_{z_n}^{z_{n+1}} F(z)\, dz; \tag{6}$$

$$W_n = \int_{z_n}^{z_{n+1}} F(z)\, dz,$$

or

$$D_k = W_1 S_{k1} + W_2 S_{k2} + \ldots + W_N S_{kN}, \tag{7}$$

where

$$S_{kn} = \int_{z_n}^{z_{n+1}} \varphi_n(z)\, S_k(z)\, dz.$$

If the number of detectors in the unit is N, and the reading of each detector is written in the form in Eq. (7), the following system of equations is obtained:

$$\begin{pmatrix} S_{11} & S_{12} & \ldots & S_{1N} \\ S_{21} & S_{22} & \ldots & S_{2N} \\ \cdot & \cdot & \cdot & \cdot \\ S_{N1} & S_{N2} & \ldots & S_{NN} \end{pmatrix} \begin{pmatrix} W_1 \\ W_2 \\ \cdot \\ W_N \end{pmatrix} = \begin{pmatrix} D_1 \\ D_2 \\ \cdot \\ D_N \end{pmatrix}, \tag{8}$$

solution of which yields $\{W_n;\ n = \overline{1, N}\}$. From the values of $\{W_n\}$ (called the incomplete integrals of the distribution), the integrand function F(z) may be recovered.

One method of recovery was described in [5]. The function F(z) is written in the form of a series of sines with as many terms as there are detectors in the unit

$$F(z) = C_1 \sin\left(\frac{\pi z}{H}\right) + C_2 \sin\left(\frac{2\pi z}{H}\right) + \ldots + C_N \sin\left(\frac{N\pi z}{H}\right). \tag{9}$$

In this case, recovery of F(z) reduces to finding the coefficients $\{C_n;\ n = \overline{1, N}\}$. These coefficients are related to $\{W_n;\ n = \overline{1, N}\}$.

$$\begin{pmatrix} A_{11} & A_{12} & \ldots & A_{1N} \\ A_{21} & A_{22} & \ldots & A_{2N} \\ \cdot & \cdot & \cdot & \cdot \\ A_{N1} & A_{N2} & \ldots & A_{NN} \end{pmatrix} \begin{pmatrix} C_1 \\ C_2 \\ \cdot \\ C_N \end{pmatrix} = \begin{pmatrix} W_1 \\ W_2 \\ \cdot \\ W_N \end{pmatrix}. \tag{10}$$

Here A is a matrix of constant coefficients, which may be obtained by substituting Eq. (9) into Eq. (10) successively for all n from 1 to N.

Since the number of incomplete integrals from which F(z) is recovered is equal to the number of detectors in the unit, determining the optimal number of detectors entails finding the minimum number of incomplete integrals sufficient for the recovery of any distribution from the specified set of possible forms with the required accuracy.

As an example, the results of recovery for two, three, and four incomplete integrals of the distribution given in [9] are shown in Fig. 2. It is evident that the recovery of the initial distribution from two integrals (i.e., from the readings of two detectors) may lead to considerable distortions in form of the distribution, while increase in the number of integrals from three to four does not facilitate significant decrease in error according to the estimates in Eqs. (1) and (2). On the basis of an analysis of the distributions in [1] for PWR, it may be concluded that a construction with three detectors in a unit is acceptable. Two detectors allow the form of the distribution to be approximately estimated only in the case when the function which describes it is unimodal.

Determining the number of detectors in the unit, it is natural to pose the question of how to position these detectors in order to have minimum error in recovering the distribution by the method in Eqs. (8)-(10). Change in configuration and physical properties of the protection and the position of the detectors appearing in the unit only influence their weighting functions. Therefore, the initial problem reduces to finding the form of the weighting functions ensuring minimum error of recovery. The weighting functions of the detectors are used in calculating the elements of the weighting matrix S, which specifies the coefficients of the system of linear equations in Eq. (8). The relative error of the incomplete integrals which are the solution of this system depends on the conditionality of the matrix S and may exceed by a factor of m (m is the conditionality number of the matrix) the relative error of the elements of the matrix S and the detector readings $\{D_k;\ k = \overline{1, N}\}$.

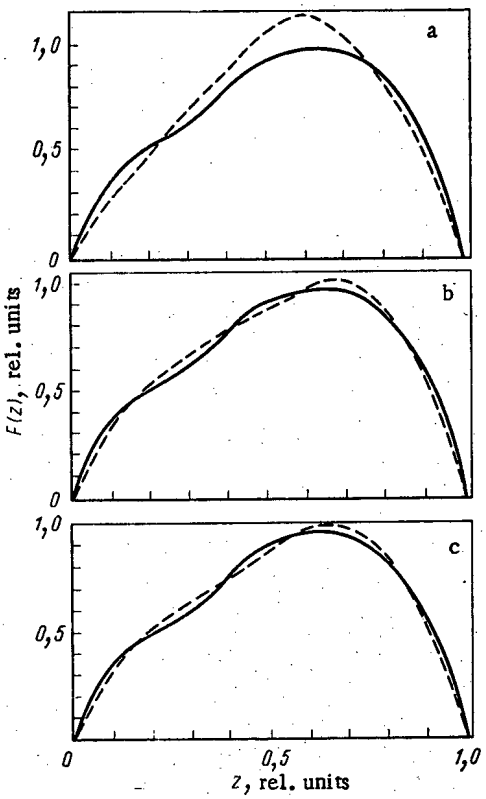

Fig. 2. Results of recovery of the distribution from two (a), three (b), and four (c) values of the incomplete integrals with δ_F = 11, 3.5%, 2.4% and δ_s = 19%, 4.8%, 2.7%, respectively — see Eqs. (1) and (2): the continuous curves correspond to the initial distribution and the dashed curves to the distribution recovered.

One form of matrix with the minimum possible conditionality number, equal to unity, is a diagonal matrix with identical elements on the diagonal

$$\| S_{ij} \| = \begin{pmatrix} S & 0 & \dots & 0 \\ 0 & S & \dots & 0 \\ 0 & 0 & \dots & S \end{pmatrix}.$$

A weighting matrix of this form corresponds to the "ideal" weighting functions shown in Fig. 3. In this case, each of the detectors of the unit records only the radiation of the section of the active zone opposite it (called "its section"), and does not react to the radiation of other sections. In existing systems, the detector units are most often positioned in vertical channels in hydrogen-containing protection. The weighting functions for one such construction with four detectors per unit are shown in Fig. 3 [6]. The conditionality number corresponding to the weighting matrix is three, which may lead to threefold elevation of the error in the partial integrals in comparison with the error for a construction with an "ideal" form of the detector weighting functions with the same accuracy of the initial data. Therefore, in developing systems of DER it is expedient to choose a construction in which the weighting function has the form closest to ideal. The development of such a construction is a separate problem, and will not be considered here.

Systems of DER are also used in monitoring reactor power [1, 5]. To measure the power W, it is sufficient to have one detector, if its weighting function is equal to a nonzero constant when $z \in [0, H]$. However, the creation of a construction in which the detector would have such a weighting function is a complex scientific and engineering problem. It is obvious that it is better to use a construction with several detectors in a unit, since in this case such rigorous requirements need not be imposed on their weighting functions.

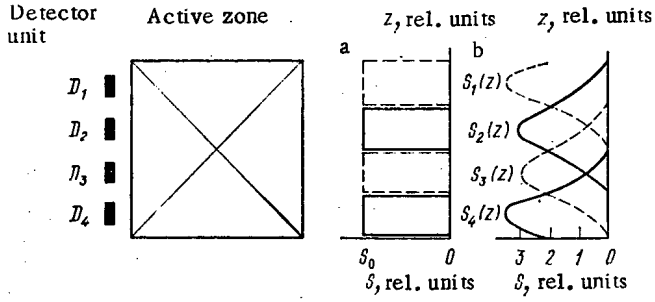

Fig. 3. Weighting functions of detectors: a) "ideal"; b) in a real system [6].

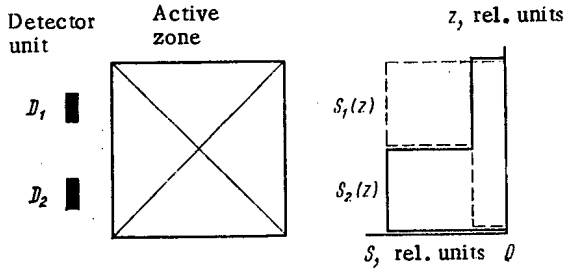

Fig. 4. Weighting functions ensuring that α_1 and α_2 are equal in Eq. (11).

The relation between the power and the readings of the detectors in each unit is now determined. Suppose that a two-detector unit is used to measure the power. The power W is proportional to the sum of the incomplete integrals W_1 and W_2, which are written in accordance with Eq. (8), with N = 2

$$W = W_1 + W_2 = \alpha_1 D_1 + \alpha_2 D_2. \tag{11}$$

Here $\alpha_1 = (S_{22} - S_{21})/(S_{11}S_{22} - S_{12}S_{21})$; $\alpha_2 = (S_{11} - S_{12})/(S_{11}S_{22} - S_{12}S_{21})$.

It follows from Eq. (11) that the power is proportional to a linear combination of the detector readings; the coefficients α_1 and α_2 are not equal, in the general case, and depend on the weighting functions of the detectors. In practice, it is expedient for the coefficients to be equal, since in this case the power is proportional to the sum of the detector readings. With the weighting functions shown in Fig. 4, α_1 and α_2 are equal. It is obvious that such weighting functions of the detectors may only be present in complete symmetry (relative to the central plane) of the geometry and physical properties of the space separating the detectors and the active zone of the reactor. If there is no such symmetry, the condition of proportionality of the reactor power to the sum of detector readings of the unit is observed only with considerable error.

Thus, it is expedient to use units with no less than three detectors for the correct determination of the power and mean energy distribution over the height of the active zone. The position of the detectors is chosen for a specific construction of the reactor and shielding in accordance with the given requirements on the weighting functions.

LITERATURE CITED

1. P. Sipush et al., Nucl. Technol., 31, 12 (1976).
2. J. Humpfries and R. Knapp, in: Proceedings of an IAEA Symposium on Nuclear Power Plant Control, France (1978).
3. H. Neuschafer and J. Humpfries, Trans. Am. Nucl. Soc., 27, 856 (1977).
4. I. S. Krasheninnikov and V. V. Matveev, At. Energ., 50, No. 2, 110 (1981).
5. US Patent No. 4,079,236 (1978).
6. C. Mildrum and J. Easter, Trans. Am. Nucl. Soc., 27, 676 (1977).

7. M. Crump and J. Lee, Nucl. Technol., 41, 87 (1978).
8. H. Tochihara et al., Nucl. Technol., 58, 310 (1982).
9. V. A. Sidorenko, Problems of Safe Operation of Water-Cooled–Water-Moderated Reactors [in Russian], Atomizdat, Moscow (1977).

BUILDUP OF GASEOUS NUCLEAR REACTION PRODUCTS IN CHROMIUM AND NICKEL CAUSED BY HIGH-ENERGY ELECTRON IRRADIATION

A. G. Zaluzhnyi, O. M. Storozhuk,
M. V. Cherednichenko-Alchevskii,
N. L. Emets, L. Z. Ozhigov,
Yu. N. Ranyuk, and V. A. Yamnitskii

UDC 539.18.188:621.039:581.3

In performing experiments involving irradiation of materials with accelerated particle beams for the purpose of simulating and investigating the phenomena occurring during irradiation in reactors, it is necessary to maintain the similarity numbers with respect to certain factors, such as the total number of primary defects, the spectrum of primary knocked-out atoms (PKA), the amount and mass distribution of nuclear reaction products, the damage profile, etc.

While the required similarities pertaining to the numbers of primary defects, their distribution profiles, and the PKA spectra can readily be secured for simulation of neutron damage in heavy-ion or proton irradiation of materials [1], certain difficulties are encountered with regard to the amount and mass distribution of nuclear reaction products. The problem of helium buildup in simulator experiments is especially critical, since helium actually causes many radiation phenomena, for instance, high-temperature embrittlement.

Simulator experiments on helium buildup involve alpha-particle irradiation in cyclotrons, where the so-called tritium trick [2] or the (p, α) reaction [3] is used. However, irradiation with a beam of high-energy electrons and photons [4] also makes it possible to study the helium buildup in materials for different ratios of the number of helium atoms to the number of primary radiation defects. We shall present here the results of theoretical and experimental determinations of the buildup of gaseous nuclear reaction products, primarily helium and hydrogen, resulting from irradiating various materials with 200-MeV electrons.

The following basic processes occur as a material is irradiated with a high-energy electron beam: development of electron–photon showers; formation of PKA by the shower electrons; interaction between shower photons and nuclei of the target material along with the formation of PKA due to photons, light nuclear reaction products (up to helium inclusively), and residual nuclei; decay of radioactive residual nuclei. The simultaneous occurrence of many mutually related processes makes it difficult to obtain numerical results, and, therefore, we used mathematical simulation of the interaction between radiation and the material, utilizing the IMITATOR program system [5] and BÉSM-6 and ES-1040 computers.

Several simplifications are presently used in simulating the electromagnetic shower: We neglect the angular divergence of the electron and photon beams as well as the Compton scattering, due to which the results obtained hold only for targets with a thickness of up to two radiation lengths. The spectra of PKA produced as a result of electron scattering on the target nuclei are calculated by using the total electron spectrum (primary and secondary electrons resulting from the development of the electron–photon shower) and considering the Fermi form factor. The number of primary point defects is determined by means of the TRN-standard cascade function. The formation of nuclear reactor products in the material is calculated on the basis of the photon spectrum at a given depth in the target without considering the electronuclear processes.

Translated from Atomnaya Énergiya, Vol. 57, No. 1, pp. 21-25, July, 1984. Original article submitted May 30, 1983.

 0038-531X/84/5701-0448$08.50

The multistage process of interaction between a photon and a nucleus has been divided conventionally into two stages. At the first stage, the nucleus is considered as an assembly of free nucleons and quasi-deuterons. while the energy pulse is transmitted to the nucleus by the oncoming photon during collisions with nucleons; forced absorption is simulated first, and then the cascade stage of nuclear interaction proper [6]. At the time when the energy of individual nucleons is lower than the emission threshold, the second simulation stage is initiated: the vaporization–fission model, which accounts for the process of "cooling" of residual nuclei as competition between the emission of individual particles and the fission process [7].

The calculations are performed by using the Monte Carlo method for a set of fixed photon energies. The items determined in calculations are the number and the space–energy distribution of the following particles emerging from the nucleus: π^+-; π^0-, π^--mesons, neutrons, protons, deuterons, tritons, and ^{3}He and ^{4}He nuclei. The fission events, the charge, the mass, and the residual nucleus energy are recorded separately.

If we know the photon energy spectrum at a certain given depth in the material dN_γ/dE_γ and the probability of development of the i-th nuclear reaction products $p_i(E_\gamma)$ during the photonuclear process for photons with the energy E_γ, the yield of the product in question from a thin target layer at the assigned depth is calculated from the equation

$$\sigma_i = \int_{E_n}^{E_{\gamma\max}} p_i(E_\gamma)\,\sigma_{\gamma\,\mathrm{tot}}(E_\gamma)\left\langle \frac{dN_\gamma(E_\gamma)}{dE_\gamma}\right\rangle dE_\gamma, \qquad (1)$$

where $\sigma_{\gamma tot}$ (E_γ) is the total cross section of absorption of a photon with the energy E_γ by the target material, determined by means of the semiempirical expressions interpolating the experimental data from [8]. Integration is performed from the neutron emission energy E_n (approximately 8 MeV) to the maximum bremsstrahlung photon energy $E_{\gamma max}$. The energy spectra and the charge and mass distributions of residual nuclei are calculated by means of equations similar to (1). In connection with the fact that a considerable part of the residual nuclei are unstable, the experimentally obtained radioactive decay chains [9] are considered in simulation.

The described simulation method [10] was used for calculating the distribution of primary radiation damage and the buildup of hydrogen and helium resulting from chromium and nickel irradiation with 225-MeV electrons (Fig. 1). The buildup of helium and hydrogen is determined almost entirely by photonuclear processes, whose contribution to the development of primary defects does not exceed 15%, since the predominant role is played by secondary electrons of the electron–photon shower. The mass distribution of residual nuclei resulting from electron irradiation that has been found by simulation differs fundamentally from such a distribution resulting from fast neutron irradiation.

Figure 2 shows the histograms of the yields of light nuclear reaction products and residual nuclei for chromium and nickel at a depth of 2 cm in the case of irradiation with 225-MeV electrons and irradiation with neutrons from a BOR-60 reactor. This figure also shows the fission cross section of the nucleus in question (denoted by f). In accordance with Fig. 2, electron irradiation produces, besides ^{4}He, other gaseous nuclear reaction products: ^{3}He, hydrogen isotopes (up to tritium, inclusively), argon, chlorine, and possibly, nitrogen and oxygen, which are generated as a result of fission of the residual nuclei from the photonuclear reaction (the fission barrier after Nix is used in calculations).

It should be mentioned that a considerably greater buildup of helium is produced by electron irradiation than by irradiation with neutrons from the BOR-60 spectrum (the yield of nuclear reaction products in the latter case has been calculated by using the ALICE statistical nucleus model, which has also been included in the IMITATOR system [11]). It is also remarkable that, during electron irradiation of chromium, the buildup of argon exceeds the helium buildup resulting from neutron irradiation.

Simultaneously with simulation of the buildup of gaseous nuclear reaction products caused by electron irradiation, we performed an experiment on direct determination of the amounts of helium formed in chromium and nickel under the action of an electron beam. For this, we irradiated in a KhFTI LUÉ-300 linear electron accelerator a package of consecutively arranged targets with an electron fluence of 10^{19} cm^{-2} at 225 MeV.

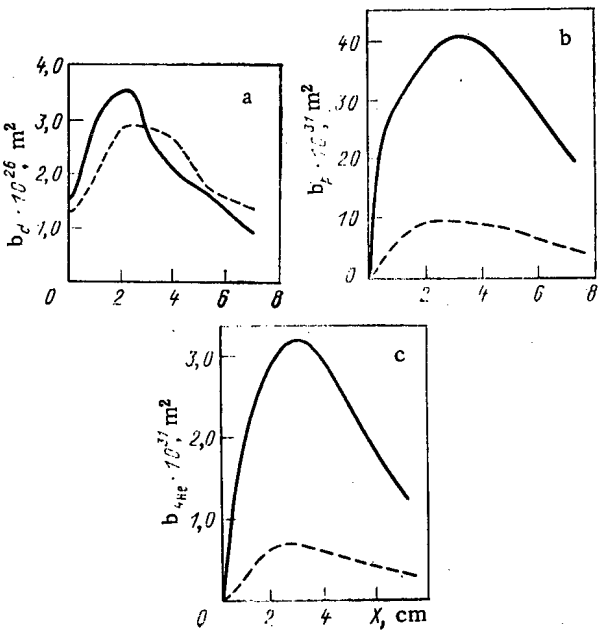

Fig. 1. Theoretical distributions of defects (a), hydrogen (b), and helium (c) in chromium (-----) and nickel (———) developing under the action of a 225-MeV electron beam.

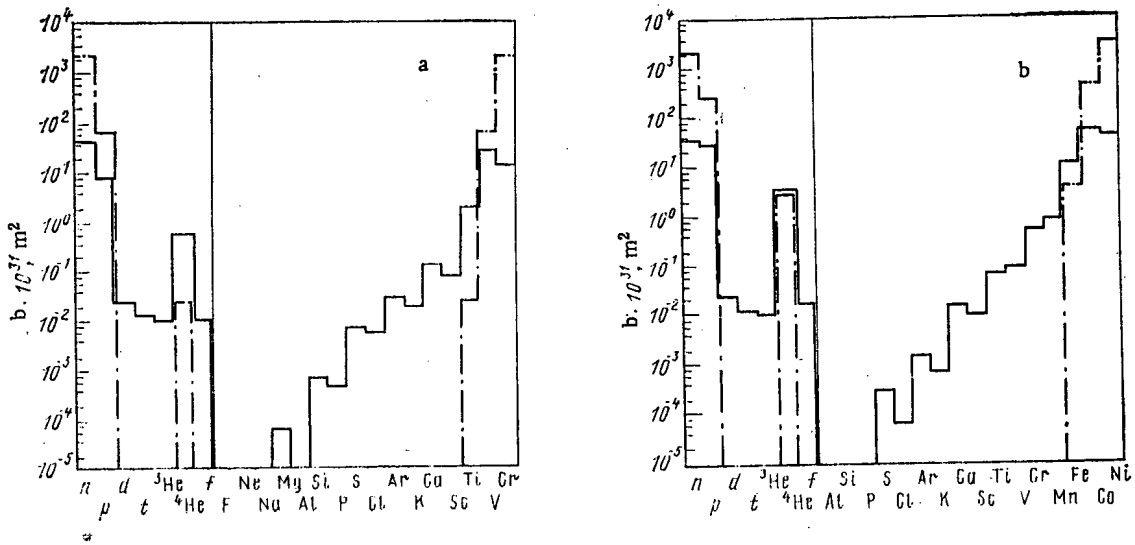

Fig. 2. Theoretical histograms of the yields of light nuclear reaction products and residual nuclei at a depth of 2 cm, produced by irradiating chromium (a) and nickel (b) with a 225-MeV electron beam (———) and neutrons from BOR-60 (-•-•-•-).

The helium percentage in the irradiated specimen, which has a thickness of 0.2 mm, is determined by vaporization in vacuum with direct determination of the amount of helium by means of an IPDO-2A partial-pressure gauge. The specimen is placed in a molybdenum glass flask with a tungsten heater, which ensures temperatures of up to 2300°K. The flask walls are intensively cooled during the vaporization process. A forevacuum is created in the volume by means of a TsVN-1 adsorption pump, while an NORD-100 magnetic discharge pump is used both for preparation for the experiment (when all the units of the degassing device are heated to 600-700°K) and for creating the high vacuum immediately before the experiment. During the vaporization process, the atomization volume is evacuated by means of a GIN-05M1 ion-getter pump, which pumps out only chemically active gases under sorption conditions. An RMO-4S omegatron data unit is connected directly to the branch pipe of the ion-getter pump.

The sensitivity of the device with respect to the partial pressure of gases is equal to $4 \cdot 10^{-8}$ Pa, which corresponds to 10^{11} helium atoms in the volume of the device, i.e., the atomic fraction of the helium percentage in the vaporized specimen (~5 mg) is approximately equal to 10^{-6}%.

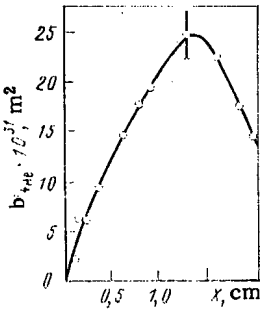

Fig. 3. Experimental helium distribution, determined by irradiating a package of nickel targets with 225-MeV electrons at 90°C, using a fluence of 10^{19} cm^{-2}.

The maximum helium percentage is observed at a depth of roughly one radiation length, while its atomic fraction amounts to ~$3 \cdot 10^{-6}$% for chromium and ~$2.5 \cdot 10^{-5}$% for nickel. According to calculations, for an electron fluence of 10^{19} cm^{-2}, the atomic fraction of the percentage amounts to $0.6 \cdot 10^{-6}$ and $3.2 \cdot 10^{-6}$% for chromium and nickel, respectively. Moreover, the theoretical position of the maximum helium percentage is located at a distance of 1.5 radiation lengths for chromium, and 2 radiation lengths for nickel. The experimentally determined helium distribution in the package of nickel targets is shown in Fig. 3. The discrepancy between the calculated and the experimental positions of the maximum can readily be explained by the fact that the angular divergence of the electron–photon shower leading to a shift of the maximum toward the surface of the target package has been neglected. It is much more difficult to explain the discrepancies between the absolute values of the maximum (amounting to factors of 5 and 8 for chromium and nickel, respectively).

First of all, it should be mentioned that the maximum recorded for chromium when using an electron fluence of 10^{19} cm^{-2} is commensurable with the experimental error of the IPDO-2A instrument. In connection with this, the chromium specimens were additionally irradiated with 275-MeV electrons to a fluence of 10^{21} cm^{-2}. The atomic fraction of the maximum helium percentage in this experiment amounted to $\sim 6.7 \cdot 10^{-5}$%. With linear extrapolation of this value to the electron fluence of 10^{19} cm^{-2}, the atomic fraction of the helium percentage amounts to $0.67 \cdot 10^{-6}$%, which is in good agreement with the theoretical value ($0.6 \cdot 10^{-6}$% for electrons with an energy of 225 MeV).

The discrepancies between the theoretical and experimental data on the helium buildup in nickel may be caused by the following factors:

accumulation of additional amounts of helium due to the yield of ^3He, produced directly by photonuclear reactions as well as by the decay of the tritium formed in these reactions;

buildup of helium due to photonuclear reactions on small amounts of impurities (commercially pure nickel containing certain amounts of carbon and oxygen was used in the experiment);

formation of helium due to secondary (n, α) reactions on neutrons occurring as a result of photonuclear processes;

helium yield in the α decay of certain unstable nuclear reaction products (radioactive residual nuclei);

possible inadequacy of the simulator description of the helium buildup process.

Allowance for the additional amount of ^3He yields a correction of not more than 10% (see Fig. 2) and cannot explain the discrepancy between the theoretical and the experimental data. In addition, in the range of low mass values (up to 29 inclusive), the RMO-4S omegatron tube has maximum resolving power.

A considerable helium yield is observed in photonuclear reactions on carbon and oxygen in connection with the high probability of the photodisintegration processes (γ, 3α) and (γ,

4α), respectively. Thus, the theoretical helium yield from ^{12}C with a photon spectrum characteristic for the development of electromagnetic showers in nickel at a depth of 2 cm corresponds to a cross section of $20 \cdot 10^{-31}$ m^2. Hence, for a 0.1% mass concentration of carbon in nickel, the additional helium buildup amounts to approximately 10%, which cannot explain the discrepancy between the theoretical and experimental data either.

The largest correction – up to 30% with respect to the amount of stored helium – is provided by an allowance for the secondary (n, α) reactions on photonuclear neutrons. The spectrum of photonuclear neutrons that are formed in nickel at a depth of 2 cm as a result of irradiation with 225-MeV electrons lies in the range from 0.1 to 100 MeV, while the mean cross section of the (n, γ) reaction for such a spectrum amounts to $35 \cdot 10^{-31}$ m^2. Considering that the dimensions of the target package are much smaller than the mean free path of neutrons in nickel, we can calculate the additional helium yield by means of the expression

$$\sigma_{He} = \Phi t N_0 \int_V \frac{dV}{4\pi |\bar{r}|^2} \int_{E_{n\,min}}^{E_{n\,max}} \sigma(n, \alpha)(E_n) \left\langle \frac{dN_n(E_n)}{dE_n} \right\rangle dE_n. \quad (2)$$

where Φt is the electron fluence, N_0 is the atomic density of the target package, V is the total target volume, r is the distance between the point at which the helium yield is calculated and some other point in the volume V, dN_n/dE_n is the differential energy distribution of photoneutrons, $\sigma(n, \alpha)(E_n)$ is the excitation function for the (n, α) reaction, and E_n is the neutron energy. Expression (2) has been derived on the assumption of an isotropic three-dimensional photoneutron distribution. Consideration of the effect of α decay results in an increase of not more than 1% in the overall amount of stored helium.

Thus, additional helium sources may increase the buildup of helium by 40-50%, however, even then, there is a discrepancy between the theoretical and experimental data amounting to a factor of 4-5. Therefore, it would be advisable to perform further investigations in order to refine the mathematical models and discover other sources of helium buildup. It should be mentioned that anomalies in the buildup of helium are also observed when nickel is irradiated with fast and slow neutrons.

The threshold of the $^{58}Ni(n, \alpha)^{55}Fe$ reaction on fast neutrons amounts to approximately 2 MeV (it is equal to ~4 MeV for the $^{56}Fe(n, \alpha)^{53}Cr$ reaction), in connection with which, for a typical neutron flux spectrun in a fast reactor, the (n, α) reaction cross section is much larger for nickel than for iron, especially if we take into account the competing (n, 2n) and (n, p) reactions, the thresholds of which are higher for nickel than for iron. For a neutron energy of 8 MeV, the cross section of the $^{58}Ni(n, \alpha)^{55}Fe$ reaction is equal to $57 \cdot 10^{-31}$ m^2, while the cross section of the $^{56}Fe(n, \alpha)^{53}Cr$ reaction amounts to only $10 \cdot 10^{-31}$ m^2.

Helium buildup in nickel due to thermal neutron irradiation occurs as a result of the two-stage reaction $^{58}Ni(n, \gamma)^{59}Ni(n, \alpha)^{56}Fe$ [1]. However, the half-life of ^{59}Ni is equal to ~5000 years, so that it can be neglected. Using the equation for determining the isotope percentage in radioactive decay chains [9], we obtain the relationship

$$N_{He}/N_{Ni} = 1 - \frac{1}{\sigma_2 - \sigma_1} [\sigma_2 e^{-\sigma_1 \Phi t} - \sigma_1 e^{-\sigma_2 \Phi t}], \quad (3)$$

where σ_1 is the cross section of the $^{58}Ni(n, \alpha)^{59}Ni$ reaction, σ_2 is the cross section of the $^{59}Ni(n, \alpha)^{56}Fe$ reaction, Φt is the neutron fluence, and N_{He} and N_{Ni} are the atomic percentages of helium and nickel, respectively. The value of σ_1 in the thermal region of the spectrum is well known ($4.2 \cdot 10^{-28}$ m^2), while the value of σ_2 varies in the $(12\text{-}14) \cdot 10^{-28}$ m^2 range. The large cross section of the $^{59}Ni(n, \alpha)^{56}Fe$ reaction is due to its exoergic nature. For the above values of σ_1 and σ_2, relationship (3) yields a quadratic dependence of helium buildup on the neutron fluence in the range up to 10^{22} cm^{-2}, while, for higher fluence values, the dependence becomes linear. The atomic fraction of helium buildup in nickel reaches 0.1% for a thermal neutron fluence of 10^{22} cm^{-2}.

In conclusion, it would be useful to indicate the possible scope of application of the simulation experiments on irradiation with an electron beam. A highly characteristic parameter of radiation damage is the ratio of the helium percentage to the number of primary radiation defects (atomic fraction of the helium concentration in percentages to the number of displacements per atom). Figure 4 shows the behavior of this ratio along the target thick-

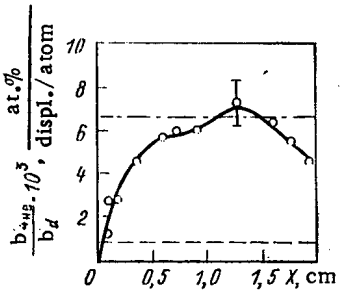

Fig. 4. Behavior of the ratio of the number of stored helium atoms to the number of primary defects during irradiation of a package of nickel targets with 225-MeV electrons in a BOR-60 reactor (-----) and in a thermonuclear reactor (-•-•-•-).

ness and provides its characteristic values for a thermonuclear reactor and a BOR-60 fast reactor. The curve was plotted on the basis of experimental data on the helium buildup and calculations of the number of the defects generated. It is evident from Fig. 4 that the same package of targets can be used for simulating the effect of different neutron flux spectra. In conclusion, it should be emphasized that irradiation with high-energy electrons and photons produces a larger buildup of gaseous nuclear reaction products than irradiation of the targets by charged particles of any other type.

LITERATURE CITED

1. V. V. Gann, V. V. Rozhkov, and O. V. Yudin, Problems of Atomic Science and Engineering, Physics of Radiation Damage and Radiation Metallography Series [in Russian], Vol. 3(11), (1979), p. 10.
2. R. Blackburn, Met Rev., 11, 163 (1966).
3. V. A. Kuz'menko, B. A. Shilyaev, and V. A. Yamnitskii, Problems of Atomic Science and Technology, Physics of Radiation Damage and Radiation Metallography Series [in Russian], Vol. 1(12) (1980), p. 18.
4. V. F. Zelenskii et al., Problems of Atomic Science and Technology, Physics of Radiation Damage and Radiation Metallography Series [in Russian], Vol. 1(2) (1975), p. 8.
5. V. V. Gann, V. A. Yamnitskii, and A. M. Vaisfel'd, Problems of Atomic Science and Technology, Physics of Radiation Damage and Radiation Metallography Series [in Russian], Vol. 1(5) (1980), p. 39.
6. N. L. Emets et al., KhFTI AN USSR Preprint 72-37, Kharkov (1972).
7. N. L. Emets and Yu. N. Ranyuk, Problems of Atomic Science and Technology, Physics of Radiation Damage and Radiation Metallography Series [in Russian], Vol. 1(9) (1979), p. 31.
8. B. Bülow and B. Forkmen, Rep. from Technical Reports, Series N 156, Handbook on Nuclear Activation Cross Section, Vienna (1974).
9. N. G. Gusev and P. P. Dmitriev, Radioactive Chains (Manual) [in Russian], Atomizdat, Moscow (1978).
10. V. V. Gann et al., Problems of Atomic Science and Technology, Physics of Radiation Damage and Radiation Metallography Series [in Russian], Vol. 2(16) (1981), p. 14.
11. V. A. Kuz'menko, B. A. Shilyaev, and V. A. Yamnitskii, Problems of Atomic Science and Technology, Physics of Radiation Damage and Radiation Metallography Series [in Russian], Vol. 2(10) (1979), p. 43.

CORROSION-TEST METHODS FOR ZIRCONIUM ALLOYS IN A RESEARCH REACTOR

G. V. Samsonov, S. V. Seredkin, and V. N. Shulimov

UDC 669.296:669.018.2:620.172.251.296

Increased importance attaches to research on the corrosion resistance of zirconium alloys in superheated steam on account of the increasing use of RBMK reactors in nuclear power, which make extensive use of these alloys [1].

The numerous data obtained under laboratory conditions cannot finally determine the viability in reactors, since it has been found [2] that radiation substantially affects the oxidation. A major requirement in the tests is that the medium should be constant. However, the composition of the medium in a closed autoclave alters continuously because corrosion products accumulate, which means that the number of specimens tested simultaneously is restricted by the relation

$$m/S \geqslant 0.4, \quad (1)$$

where m is the mass of a specimen in g and S is the total surface in cm^2. This condition is even more difficult to meet when there is radiolysis.

Therefore, the medium must be constantly changed in order to obtain reliable results, and this is usually feasible in full-scale reactor loops, but it involves considerable expense. Also, it is difficult to carry out experiments at elevated coolant parameters because of the restricted viability of the constructional materials. The safety of the entire reactor system is also adversely affected.

Ampul devices are more widely used in routine tests at certain stages in radiation-induced corrosion [3]. The main advantages are that there is good measuring equipment, together with reliability and economy. The safety of the entire installation is also not reduced [4]. Conditions (1) are met in such experiments by means of devices for pumping the corrosion medium continuously through an ampul at a low speed, which is justified by the low corrosion-product accumulation rate.

The Nuclear Reactor Research Institute has devised a suite of ampul devices of this type for use with swimming-pool-type research reactors RBT, and here we consider some of them.

Open Stem Loop [5]. There are two major components: the ampul containing the specimens, which is located in a channel in the core, and a system for supplying superheated steam, which usually lies outside the core.

As the steam flow is small, the device can be built as an open circuit without adverse effect on the radiation environment in the reactor, which receives the medium after passage through the ampul. This eliminates the complicated equipment characteristic of a full-scale reactor loop.

The apparatus (Fig. 1) consists of two steam generators (SG), a superheater SH, a condenser, a line supplying a distillate to the SG, a sampling device, and means of flushing the ampul with inert gas (helium) before the reactor is run up. All the pipelines are thermally insulated and electrically heated.

The working conditions in the heaters in the SG are determined by the pressure and temperature and are controlled automatically. In the SH (autoclave), one can place reference specimens for testing under identical conditions but without irradiation. The flowrate is estimated from the rate at which the measuring vessel at the exit from the circuit fills up and from the change in liquid level in the SG, which is monitored by a level gauge.

The steam is supplied to the ampul when the reactor has been run up and the temperature in the circuit is higher than the condensation temperature at the working pressure. When the

Translated from Atomnaya Énergiya, Vol. 57, No. 1, pp. 25-28, July, 1984. Original article submitted October 31, 1983.

 0038-531X/84/5701-0454$08.50

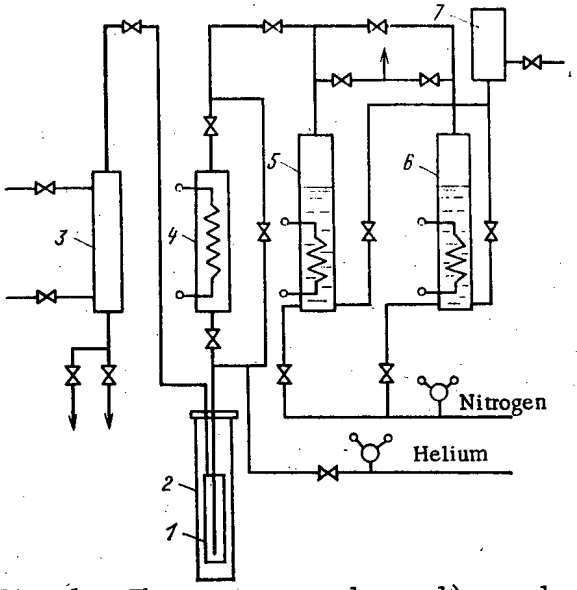

Fig. 1. The open steam loop: 1) ampul, 2) reactor channel, 3) condenser, 4) steam superheater; 5, 6) reserve and working steam generators; 7) vessel.

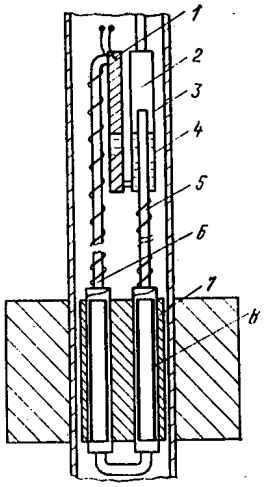

Fig. 2. Natural-circulation steam loop: 1) evaporator; 2) TET; 3) condenser; 4) liquid; 5) riser tube; 6) descent tube; 7) ampul; 8) specimens.

distillate has been used up in the working SG, the reserve one is switched on. The apparatus has been operated for some years with the RBT-6 reactor.

Compact Natural-Circulation Loop. The device is completely contained in a reactor channel and does not require additional equipment in the reactor bay. The loop provides for continuous change in the medium in the ampul, so the composition remains constant. The specimens are tested at a normal steam pressure.

Figure 2 shows the design. The evaporator and condenser are partially filled with liquid and are at some distance from the ampul. The descending and rising parts of the circuit and the evaporator are equipped with electric heaters. Under working conditions, natural circulation occurs in the two-phase medium, with the ampul receiving only superheated steam. The condenser is a vessel connected to a tube brought out from the reactor via the upper flange. The tube is cooled by natural circulation of helium in the channel. After condensation, the liquid trickles into the evaporator. The passage of steam through the ampul can be judged from the readings of the thermoelectric transducer TET: The temperature at this point should

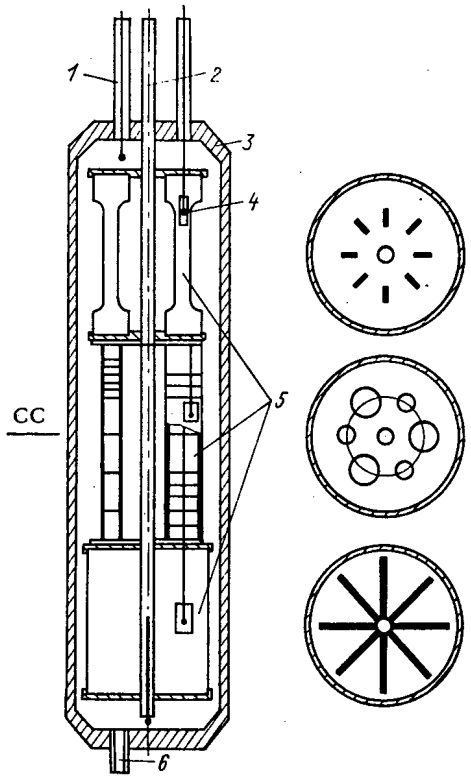

Fig. 3

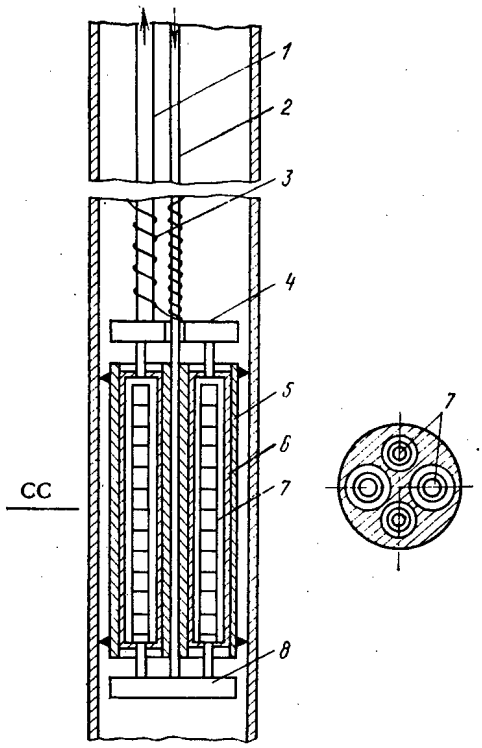

Fig. 4

Fig. 3. Ampul with free specimen setting: 1) heat input tube; 2) central tube; 3) ampul; 4) TET; 5) specimen; 6) filling tube (CC is core center).

Fig. 4. Special ampul with ring specimens; 1) steam outlet tube; 2) steam supply tube; 3) heater; 4) upper collector; 5) aluminum block; 6) container; 7) specimen; 8) lower collector.

rise to 100°C. The radiolysis products are vented via the tube into the reactor bay. The loss of water by radiolysis or leakage is made good via a capillary tube.

In tests with the RBT-6, it was found that the system was highly reliable and that the circulation was stable. Topping up was not required during the experiment. The instability in the specimen temperature was not more than ±5°C. The amount of corrosion medium in the circuit (70-100 cm^3) was 10-20 times the amount of medium in a sealed tube, which ensures that (1) is obeyed with an unaltered number of specimens.

Design Features of Ampuls for Corrosion Tests in a Flowing Medium. Ampules for irradiating specimens in a corrosion medium can be divided into two types: universal (Fig. 3), in which specimens of various shapes can be accommodated (rings, tubes, flat corrosion-test specimens, and flat tensile-test ones), and special ampuls, which are adapted only to specimens of a particular type, e.g., ring or flat ones. A universal ampul does not provide identical temperatures for all the specimens. The temperature pattern is set up mainly by the natural circulation of the steam, with its low thermal conductivity (one cannot control the specimen temperature within wide limits by varying the conductivity of the thermal gap filled with helium). Such an ampul is best used in high-temperature tests (T > 500°C) when it is not necessary to have the entire volume isothermal. One way of reducing the temperature nonuniformity is to use a device with specimens of the same type. In such an ampul (Fig. 4), there is a small gap between the specimens and the walls, and the heat is transmitted mainly by conduction. To equalize the temperatures, the ampul is placed in an aluminum block separated from the walls of the channel by an exactly set gas space. In this design, the temperature difference between a specimen and the wall of the ampul is small (~50°C), so there is improved scope for adjusting the specimen temperatures by altering the thermal impedance between the block and the channel (range up to 300°C). These special ampuls can accommodate specimens of various sizes, for example, rings of two different diameters but at the same temperature. For this purpose one chooses appropriate widths for the gas and steam gaps. A similar ampul has been devised for testing flat specimens (Fig. 5). The specimens are placed in a rect-

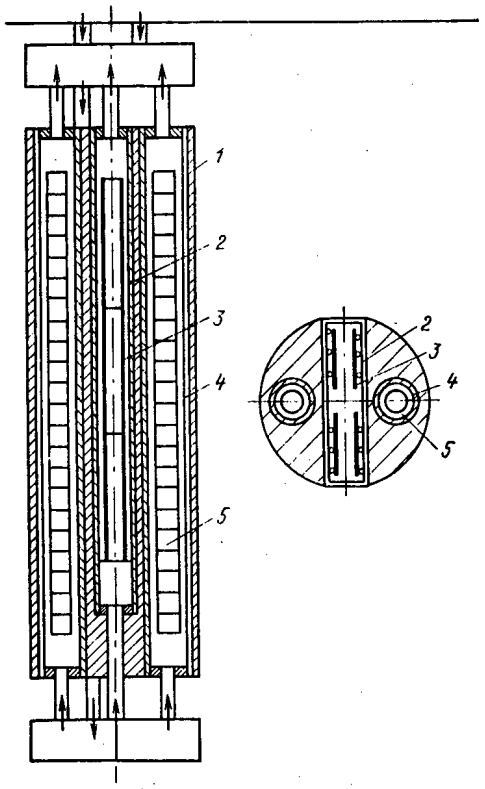

Fig. 5

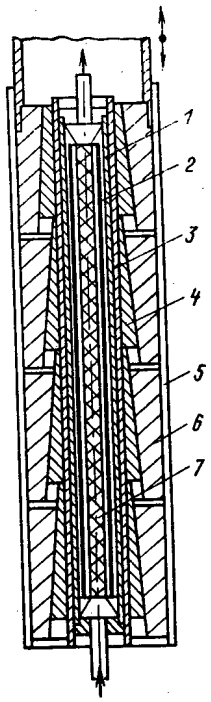

Fig. 6

Fig. 5. Special ampul for flat and ring specimens: 1) aluminum block; 2) rectangular container; 3) flat specimens; 4) cylindrical container; 5) ring specimens.

Fig. 6. Ampul for examining corrosions under variable temperature conditions: 1) ampul; 2) specimen; 3) copper leak; 4) conical 12Kh18N10T steel sleeves; 5) reactor channel; 6) conical aluminum sleeves; 7) radiant heater.

angular 12Kh18N10T steel container inserted in a longitudinal slot in the aluminum block. An advantage of this design is that one can equalize the temperature over the height, which is done by profiling the steam gap in accordance with the power distribution over the height of the core.

In addition to the ampuls for use in flowing media at constant temperatures, we also devised a special ampul providing specimen temperature regulation in the range 400-1000°C. This ampul can be used in examining the corrosion resistance of zirconium alloys under conditions approximating those of emergencies leading to overheating of the fuel-pin cladding.

The device (Fig. 6) consists of an ampul containing ring specimens, a copper leak, and conical 12Kh18N10T steel sleeves fitted on the leak. The gas gap contains conical aluminum sleeves whose internal surfaces are matched to the outer surfaces of the sleeves, while the outer surfaces match the inner surface of the channel. The specimen temperature is controlled by varying the gas gap between the sleeves by displacing the aluminum sleeves along the vertical axis. The ampul has been tested in the RBT-6. The temperature control range was 300-1000°C with a rate of change of 2-4°C/sec.

This suite of equipment for use with swimming-pool research reactors for examining corrosion in zirconium alloys in superheated steam has been operated for several years. It is planned to use the system also with other reactors.

LITERATURE CITED

1. A. S. Zaimovskii, A. V. Nikulina, and N. G. Reshetnikov, Zirconium Alloys in Nuclear Power [in Russian], Énergoizdat, Moscow (1981).
2. A. V. Byalobzheskii, Radiation-Induced Corrosion [in Russian], Nauka, Moscow (1967).

3. P. G. Aver'yanov et al., in: Proceedings of the All-Union School on Research Methods within Reactors [in Russian], Dmitrovgrad (1978), p. 419.
4. B. V. Samsonov, S. V. Seredkin, and V. N. Shulimov, NIIAR Preprint No. 20(428), Dmitrovgrad (1980).
5. P. G. Aver'yanov et al., NIIAR Preprint No. 56(509), Dmitrovgrad (1981).

PURIFICATION OF THE FIRST CIRCUIT OF NUCLEAR POWER SYSTEMS WITH A TWO-COMPONENT COOLANT-GAS FLOW

A. V. Beznosov, P. N. Martynov,
S. Yu. Orlov, and V. E. Serov

UDC 621.039

During prolonged use, deposits of contaminants develop on the inner surfaces of the first circuit of reactor systems and in stagnant zones thereof. In general, the contaminants result from soiled equiment undergoing repair work, contamination by repair work, impurities contained in the gas and the coolant of the first filling or introduced in refilling of the circuit by these media, erosion products of the construction materials of the circuit, products originating from wear of the circuit components by erosion, cavitation, or mechanical effects, fission products of the nuclear fuel and other fuel-element materials (when their shells leak), and impurities introduced in the circuit in the recharging of the core or in repair work. The quantity, the physicochemical composition, the thickness, and the properties of the contaminant deposits on a particular circuit section depend upon the corrosion of the construction material at the surface of contact between the solid wall and the coolant, the crystallization of the impurities from a saturated solution onto the surface, the adsorption of impurities by the deposits from the coolant flow, the separation of dispersed impurity particles from the flow toward the walls, the solution of precipitates, and the destruction of deposits and the subsequent removal of dispersed contaminant particles by hydrodynamic forces. In the general case, several zones which can be treated in different ways can be distinguished in the distribution of the contaminants at a wall (Fig. 1).

As a consequence of these processes, the surface of the circuit can be considered a filter removing impurities from the coolant toward the walls; the absolute mass ratio of the impurities retained by the circuit surfaces and the system of coolant treatment deserves the greatest attention. It has been observed in the operation of reactor circuits of the primary coolant of nuclear power systems [1, 2] that contaminant deposits develop on the inner surfaces in continuous operation of the coolant-treatment system. This negatively influences the operational features of such circuits. The surfaces can be purified from the deposits (including precipitates weakly adhering to the walls) by mechanical means, i.e., by washing the surfaces with a large quantity of coolant or with chemical agents, but these methods are either little efficient or technologically complicated. It is therefore interesting to search for and to investigate other techniques of cleaning the circuit surfaces from deposits, to simplify the cleaning of the circuits, to reduce the cost of the cleaning process, and to reduce the volume of the liquid radioactive waste material obtained. One of the techniques is based on cleaning the circuit by introducing a small amount of a gaseous component into the coolant flow, which gaseous component is neutral or chemically active vis-a-vis the deposits. Subsequently, the two-component mixture enriched with the impurities is discharged onto a filter. Techniques of flotation cleaning of liquids from dispersed impurities are being used. In these techniques, gas is bubbled through a large volume of the mixture [3] or gas flows with a high gas concentration (up to 50% by volume) are employed in special cleaning operations with total or partial shutoff of the equipment (e.g., in maintenance work). The introduction and dispersion of a small amount (up to 3% by volume) of the gas into the coolant flow, the destruction of deposits more or less strongly adhering to the walls, the attachment of particles to the bubble surface (wetting and adhesion on the particle–liquid interface and the particle–liquid–gas boundary), and the transport of the contaminant to filters are the important stages of the proposed process.

Translated from Atomnaya Énergiya, Vol. 57, No. 1, pp. 29-31, July, 1984. Original article submitted January 24, 1983.

 0038-531X/84/5701-0458$08.50

The proposed introduction of a gas component into the coolant flow can be obtained via an external gas supply, with subsequent release of the gas into a special gas-treatment system (for this purpose one can use compressors—gas blowers), with circulation of the gas within the circuit (without release of the gas), or with ejectors introducing the gas into the flow with the energy provided by a jet of the flow proper and gas circulation within the coolant circuit. It is not desirable to introduce the gas from an external supply (tank, compressor) because the amount of radioactive products discharged from the circuit is increased, the required flow of the gas to be introduced is technologically hard to maintain, and the dispersion of the gas in the case of real, admissible pressure fluctuations in the circuit is difficult owing to difficulties in monitoring the development of the purification process. Some of the above shortcomings can be eliminated by introducing into the circuit a compressor which makes the gas separated from the flow (e.g., on the free surfaces) return into the coolant flow. But such compressors still have to be built and the problem of dispersing the gas introduced still must be solved. The ejection of the gas by the coolant flow offers itself as a better solution (Fig. 2). In this technique basically all systems connected to the circuit (air vents, treatment of the coolant) are involved; an ejection device, a filter on the manifold of the air vents, and lines connecting these two components are introduced in addition. The surfaces can be cleaned intermittently or continuously. The coolant which is gathered in the coolant-purification system is partially directed into the ejector, whereupon the two-component flow is returned into the main circulation circuit. In this fashion the gas concentration is substantially reduced by dilution with the main current. The gas component interacts with the deposits, destroys the deposits, and tears them off and into the coolant flow by purely physical processes (gas cavitation, etc.) in the ejection of a neutral gas, or by physicochemical effects in the case of an added chemical agent. Part of the deposit particles gets close to the gas bubbles and adhesion of the particles to bubbles takes place in the gas current, whereby the specific surface energy at the interphase boundary decreases. Another part of the dispersed contaminant particles is caught by the coolant flow proper. The coolant flow is purified from the contaminants by filters mounted in the manifold of the air vents and in the coolant-treatment system. The gas (or the vapor—gas mixture) which was separated on the free level of the coolant in, say, the volume compensator is returned into the circulation circuit by the ejector. If necessary, a chemical agent which can interact with the deposits is introduced into the gas (or vapor—gas) volume of the circuit or into the gas supply line to the ejector.

The introduction of a small amount of gas (up to 3% of the flow volume) does not noticeably influence the performance of the main equipment. Even a slight improvement of the performance is possible: The anticavitation resistance of the materials of the pump components through which the flow runs is increased, the heat dissipation coefficient is slightly increased by additional swirling of the flow [4, 5], and the pressure pulsations in the circuit (and its vibration characteristics) assume a higher frequency with a reduced amplitude.

An analysis of the changes in the coolant level in the compensator volume is important for determining the performance of the circuit. The increased coolant level after putting the system into operation can be determined with the formula

$$G_g d\tau = dv + \frac{J_{vc}}{V_c} v\, d\tau, \tag{1}$$

when we assume that the bubbles are homogeneously mixed within the coolant volume and that the gas is fully separated; the notation is interpreted as follows: G_g denotes the gas supplied (m^2/h) to the circuit by ejection, with the supply reduced to the conditions in the circuit; v (m^3) denotes the volume of the gas component in the circuit, with the volume reduced to the conditions in the circuit; J_{vc} (m^3/h) denotes the release of two-phase coolant through the volume compensator; and V_c denotes the volume of the coolant in the circuit. When we solve this equation, we obtain

$$\Delta H S = \frac{G_g V_c}{J_{vc}} + v_0 \exp\left(-\frac{J_{vc}}{V_c}\tau\right) - \frac{G_g V_c}{J_{vc}} \exp\left(-\frac{J_{vc}}{V_c}\tau\right), \tag{2}$$

where S denotes the free surface area (m^2) in the volume compensator, and v_0 denotes the volume (m^3) of the homogeneously mixed gas in the circuit at the time at which the system is put into operation.

The possible gas filling V_n in the upper volumes of the circuit, which are not ventilated by the air vents, was disregarded in Eq. (2).

It follows from an analysis of Eq. (2) that after sufficiently long time intervals (which are given by the ratio of the coolant flow through the volume compensator to the coolant flow through the circuit), the increase in the coolant level is

$$\Delta HS = G_g V_c / J_{vc} \ ; \tag{2a}$$

when the gas ejection is terminated, the time required for reducing the coolant level and for the practically complete degassing of the circuit (with V_n being disregarded) can be determined with the formula

$$T = 5V_c / J_{vc} \ . \tag{2b}$$

The hydraulic characteristics of the tube duct and the equipment change only insignificantly when the gas concentration is as high as 5% and, as expeiments made by the authors on models of circuit components have shown [6], the changes do not exceed 3%.

The equation for the balance of contaminants in the circuit after putting the system shown in Fig. 2 into operation can be stated in the following form

$$dA/d\tau = w_e + \Sigma w_i - (A\chi_f / V_c - k_2) J_{vc} - (A/V_c - k_1) J_{ps}, \tag{3}$$

where w_e denotes the amount of contaminants entering as a result of the ejection treatment; Σw_i, total output rate of the contaminant sources in the circuit; J_{ps}, flow of the coolant through the treatment system; k_1, concentration of contaminants in the treated coolant behind the treatment system; χ_f, flotation coefficient, with the attachment of contaminants to the gas bubbles taken into account; k_2, contaminant concentration in the coolant behind the filter on the air-vent manifold; and J_{vc}, coolant flow through the air-vent system. The solution of this equation (wherein the output rate of the sources of contaminants is assumed to be constant in time) can be stated in the form

$$A = \frac{\chi_f J_{vc} + J_{ps}}{V_c} (w_e + \Sigma w_i + k_1 J_{vc} + k_2 J_{ps} + A_0 \exp\left(- \frac{\chi_f J_{vc} + J_{ps}}{V_c} \tau \right). \tag{4}$$

When the gas concentration in the coolant is constant, we have

$$w_e / d\tau = ksn, \tag{5}$$

where k denotes the coefficient of contaminant-mass removal from a unit of surface; s denotes the area of the deposits in contact with bubbles; and n denotes the number of gas bubbles, which, on the average, is defined by the ratio of the total gas concentration to the average static bubble volume. An analysis of Eqs. (3) and (4) reveals that the removal of the contaminants towards the filters increases from the time at which the gas is admitted to the circuit, with k being constant. Obviously, during the purification process, when a certain time has elapsed, the coefficient of mass removal of contaminants from a unit surface must decrease and when a normative value of the contaminant mass in the volume of the circuit (contaminant concentration) has been reached, the purification system can be switched off.

The w_e value is given by the flow conditions of the two-component mixture and the solidity of the contaminant deposits, with the solidity depending upon the type of the coolant, the contaminant sources, and the physicochemical composition of the contaminants. Since the time of the purification process and the periodicity with which the purification system is put into operation depend upon the real form of the circuits, the materials used therein, the conditions of operation of the circuits (power rating, impurities), etc., definite rules for purification can be established only experimentally on the real circuit. The gas phase in the coolant flow is of great importance for the purification with the proposed technique.

When the authors made experiments in models with optically transparent materials and with ejection devices of different orientation, intense coagulation of the bubbles formed by the ejector was observed on the section of hydrodynamic stabilization [6]. But with bubble dimensions for which the rate of bubble surfacing is equal to the speed of the pulsating components of turbulent flow, a release of the gas to the lower points of the horizontal channels in the models of the circuit components was observed:

$$v_{x,y,z} \approx \frac{2(\rho' - \rho'')}{3\mu''} g R_{cr}^2 \frac{\mu' + \mu''}{3\mu' - 2\mu''}, \tag{6}$$

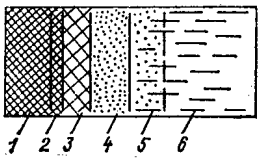

Fig. 1. Scheme of the qualitative distribution of impurities near a wall: 1) construction material; 2) oxide film; 3) dense layer of deposits adhering to the wall; 4) porous impurity layer soaked with coolant; 5) laminar sublayer enriched with contaminants; 6) core of the flow.

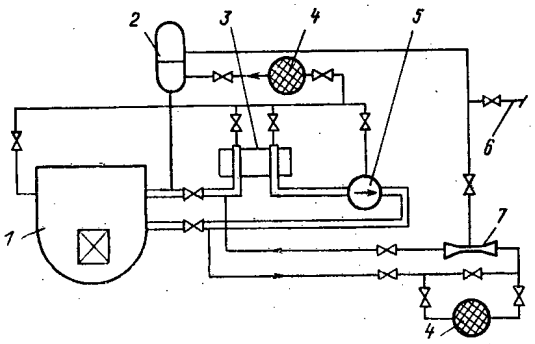

Fig. 2. Scheme of purifying surfaces with a two-component coolant-gas flow: 1) reactor; 2) volume compensator; 3) heat exchanger; 4) filter; 5) circulating pump; 6) inlet of chemical agent; 7) ejecting device.

where $v_{x,y,z}$ denotes the pulsating component of the speed; ρ', ρ'' and μ', μ'' denote the density and the kinematic viscosity of the coolant and the gas, respectively; g denotes the gravity acceleration; and R^2_{cr} denotes the critical bubble radius. When visual observations on the bubble flow in long channels and in models of the circuit components (curves, narrow passages, etc.) were compared, a greater dispersion of the gas phase was found in the latter case.

The authors made experiments in which they purified steel tubes from contaminant deposits with the aid of an ejection device developing a two-component flow [6]. The experiments were made at 15°C in an isothermal water circuit with relatively clean surfaces. An experimental tube section of steel 3 (l = 300 mm, d_{int} = 20 mm) with extensive deposits of iron oxide was fit into the circuit. In order to determine the amount of contaminants which are carried away, a retaining filter was mounted behind the monitoring section; the filter was weighed before it was inserted, after operation of the test setup without ejection, and after operation tion with ejection of a gas phase. The volume concentration of the gas in the two-component flow amounted to 5% and the water speed to 1.5 m/sec in the experiments. The difference between the contaminant particle masses carried away by the water flow without admission of gas and with admission of gas through the ejector was $(1.5\text{-}3.0)\cdot10^{-3}$ g/(m^2•h). These tests, as well as other experiments made by the authors (on test stands and on setups under conditions ruling inside reactors), have shown [6] that a rather intense purification of the circuit surfaces from contaminant deposits takes place when the circuits are treated with a two-phase flow.

LITERATURE CITED

1. I. K. Morozova et al., Removal and Deposition of the Corrosion Products of Reactor Materials [in Russian], Atomizdat, Moscow (1975).
2. P. Cohen, The Technology of the Water in Power Reactors [Russian translation], Atomizdat, Moscow (1973).
3. V. A. Glembotskii, Principles of the Physical Chemistry of Flotation Processes [in Russian], Nedra, Moscow (1980).
4. Heat Transfer in a Two-Phase Flow [in Russian], Énergiya, Moscow (1980).

5. K. Sekoguchi et al., ISME, 23, No. 184, 1625 (1980).
6. V. E. Serov et al., The Characteristics of a Two-Component Coolant-Gas Flow and Its Use for Cleaning Equipment of Atomic Power Stations and Accelerators [in Russian], Reports of the Gorki Polytechnical Institute No. 81,100,755, Gorki (1983).

CONSTRUCTION OF AUTOMATIC SYSTEMS FOR RADIATION MONITORING OF THE ENVIRONMENT OF NUCLEAR POWER STATIONS

É. P. Volkov, A. I. Glushchenko,
V. N. Durnev, V. V. Zhabo,
M. I. Saparov, and L. P. Kham'yanov

UDC 621.039.58

Providing safety for the population and protecting the environment from contamination are one of the important problems of modern power engineering, including nuclear energetics. The accident in the Three-Mile-Island Atomic Power Station (March 30, 1979) has led in many countries to a reassessment of the safety concepts and technical solutions in the planning, building, and utilizing of atomic power stations. It has been one of the conclusions of the report issued by the presidential commission on the investigation of the accident that the services for an operational evaluation of the radiation consequences of emissions for the environment and the population were insufficiently prepared.

Though the emissions from atomic power stations are usually smaller than those of thermoelectric stations, the specific form of the operation of atomic power stations necessitates a careful observation of the radiation conditions in the environment. Establishing an operational link between emissions and environmental contamination is an important aspect in a properly organized radiation-monitoring system. When the radiation conditions in the environment are determined, two conditions of operation of atomic power stations must be distinguished, namely the normal operation or the accident conditions in which the radioactive emissions are monitored by state equipment for radiation monitoring or accident conditions of an atomic power station with uncontrollable arrival of radioactive materials. In the latter case, the dose of the radiation received by the population can be determined only at previously established points in the environment, which are provided with the corresponding equipment.

Such equipment must work automatically and must be connected to a single automatic system with transfer of the entire information from the periphery to the center in order to obtain operational monitoring and fast reception of the pertinent information. Since the propagation of contaminants in the atmosphere depends upon the state of the atmosphere, a subsystem for measuring meteorological parameters which define the thermal stratification of the atmospheric layer close to ground must form part of the equipment. Besides that, a subsystem of state radiation monitoring, which checks for gaseous and aerosol emissions from an atomic power station, must be operationally connected to an automatic "accident-monitoring" system of the environment of an atomic power station.

The presently used radiation-monitoring systems, which were developed on the basis of AKRB-03 "Seival-1" and AKRB-06 "Gorbach-1" instruments, do not comprise automated subsystems for radiation monitoring of the environment. These functions have to be performed by external dosimetry services of the atomic power station; these services are autonomous as far as the territory and the technical means are concerned. The division of the functions causes difficulties in the operational monitoring of the radiation conditions outside an atomic power station.

Systems for the automatic monitoring of the environment of atomic power stations have been developed and are presently used in a number of countries. The best of the foreign systems comprise the following components:

measuring instruments mounted at various points inside and outside the atomic power station for determining radiation parameters and meteorological and hydrological parameters (the

Translated from Atomnaya Énergiya, Vol. 57, No. 1, pp. 32-34, July, 1984. Original article submitted October 31, 1983.

 0038-531X/84/5701-0462$08.50

monitoring techniques and the points of the measurements depend upon the type of the atomic power station and the requirements of the user service);

a monitoring center with a reliable system reserve; the center is computer controlled to read out the measured values, to process and store the data, and to output the required information;

a display on the control panel for representing operational information on the radiation conditions in the area close to the atomic power station; and

a spectrometer measuring emission from humans so that incorporated gamma emitters can be determined.

The authors of [2] have described an emergency system for recording and analyzing the irradiation doses in and around atomic power stations in the direction of the possible propagation of accidental emissions. The system comprises nine remote dosimeters with a measuring range of 1 μR — 10 R/h (1 R = $2.58 \cdot 10^{-4}$ C/kg); the dosimeters are mounted at distances of 8-10 km from the atomic power station. The system also comprises a remote meteorological station, a minicomputer, and a set of color displays for projecting isotope maps along the propagation path of the radioactive cloud. This system is connected to the main radiation-monitoring system of the atomic power station. A mobile radiometric laboratory with a microcomputer on board is provided for additional operational monitoring.

An automated system for monitoring the radioactivity of the environment has been developed and implemented in the atomic power station "Paksh" in the Hungarian People's Republic [3].

The experience gathered in the use of such systems has shown that in addition to current data, efficient monitoring of the operation of an atomic power station requires average data on the dose load near the station in the form of daily, monthly, and annual values. The development of a corresponding computational model is an important task in the mathematical work of emergency-monitoring systems. In normal operation, extensive calculations are made once per day and the daily dose load is determined. Computed daily, monthly, quarterly, and annual dose loads are kept in the computer memory. Curves of the isodose distribution around the atomic power station are constructed on the basis of those data for various time intervals.

From the above considerations we can formulate the following tasks of an automated environmental radiation-monitoring system of an atomic power station:

During normal operation of the atomic power station, the system must sample, record, and process information on the radiation conditions in the region of the station, determine its normal state, and, if necessary, transmit the results of the information processing to a computer; and

in the case of an accident, the system must output instantaneous data for taking operational measures, among them measures providing for the radiation protection of the population.

In addition to the tasks listed, statistical data which are accumulated in the operation of such systems make it possible to refine the calculation of the concentration of contaminants entering the environment under various conditions of operation of the atomic power station; in these calculations, the changes in the meteorological parameters and the influence of the buildings of the industrial area upon the propagation of emissions are taken into account under the condition that the ventilation tubes of the atomic power station are not very high.

The first experimental automated system which in the USSR has been taken into operation to monitor the contamination of the atmosphere by emissions from a thermoelectric power station [4] was developed by the Moscow Power Institute in collaboration with Institutes of the Academy of Sciences of the Ukrainian SSR [5] and the Board for the Protection of Nature at the Department of Energy of the USSR and other organizations. The system comprises three main subsystems: one for monitoring the emissions from the thermoelectric power station, one for monitoring the meteorological parameters, and one for monitoring the contamination of the environment. Information obtained from these subsystems is automatically transmitted with an averaging interval of 20 min to the computer of the information-processing/computing system located in the electric power station. This system performs automatic sampling of information on the gas pollution of the air by the emissions of the Zaporozhe Electric Power Station within a radius of 25 km and transmits data to a center controlling the system and monitoring both the emissions proper and the meteorological parameters in a 300-m-thick layer.

The system for external radiation monitoring of an atomic power station must be organized in analogous fashion. The subsystem for the emissions from the atomic power station must monitor radioactive rare gases, long-lived aerosols, and radioactive iodine; the subsystem monitoring the environment must measure the dose rate of the γ radiation, and the timewise integral concentration of radioactive iodine and long-lived aerosols.

The meteorological state of the atmosphere close to ground is an important factor in the operational monitoring of the radiation conditions around an atomic power station. The temperature gradient and the wind speed at various levels are important characteristics in this case. Resistive thermometers or thermocouples mounted at various heights are conveniently used to determine temperature gradients. Special meteorological towers are set up to determine the wind speed or a net of meteorological ground observations with readings of the wind speed on the level of a wind vane are employed. In the latter case, for the purpose of calculating the wind speed in high layers and for estimating the wind speed on the level of the ventilation-tube's mouth, one must assume some dependence of the wind speed upon the altitude, and this assumption reduces the accuracy of the input information. However, rather great difficulties in building automated systems for monitoring the environment can be encountered in the technical realization of continuous meteorological observations made at various altitudes in the large number of areas of atomic power stations.

The mathematical provisions of the system are based on the algorithm expounded in [6, 7] for calculating the radiation conditions around an atomic power station, because this algorithm requires only observations made by a net of ground stations for the meteorological information input. In order to increase the efficiency in the use of the data, the system monitoring the environment must include an automatic weather station relaying the meteorological information obtained directly to a peripheral device (magnetic tape or disk) of a microcomputer. Such weather stations are now serially produced. The monitoring of the meteorological parameters obtained by ground observations must include at least the wind speed and the wind direction, precipitation data, and the air temperature at two or three points at the altitude (10 m) of the wind vanes.

The serially produced "Post-1" stations are conveniently used for external radiation monitoring. Information obtained from sensors monitoring the emissions and discharges of the atomic power station and meteorological data obtained from weather stations can be transmitted over conventional cable channels, whereas the information from the external stations is transmitted through (telephone) lines or radio links to the center which samples and processes the information. But a reliable radiation monitoring of a possible contamination of the environment makes it necessary to increase both the sensitivity of the detectors and the amount of information they provide. For example, one must develop sensors for continuously monitoring the accumulation of ^{131}I in all its physicochemical forms (molecular iodine, aerosols, methyl iodide, etc.).

The construction of automatic radiation-monitoring systems and their implementation in nuclear power generation in the USSR, first of all in atomic thermoelectric centers and atomic heating stations near huge cities will help to determine within extremely short times the radiation conditions around these objects during their normal use and in possible emergency situations when radiation effects on the nearby living population may exceed the admissible levels which are laid down in valid norms.

Emergency-monitoring systems, whose development and implementation are provided within a joint special-purpose scientific-technological program of producing automatic monitoring systems for the thermal power of atomic power stations, will increase the reliability and safety of nuclear power generation. This will expand the scale on which atomic power generation can be introduced in the national economy of the USSR and of the member-nations of the COMECON.

LITERATURE CITED

1. Nuclear Power Generation, Man, and Environment [in Russian], Énergoizdat, Moscow (1981).
2. D. P. Serpa, A. M. Walker, and T. A. Jenckes, IEEE Trans. Nucl. Sci. NS-28, No. 1, 236 (1981).
3. Sh. Dehme, in: Abstracts of the Reports of the 2nd Int. Conf. of the COMECON Member-Countries on Radiation Safety of Atomic Power Stations [in Russian], Press of the Inst. of Physics of the Academy of Sciences of the Lithuanian SSR, Vilnius (1982).
4. É. P. Volkov, V. V. Zhabo, and M. I. Saparov, Teploenergetika, No. 11, 913 (1980).

5. A. N. Shcherban', A. V. Primak, and V. I. Kopeikin, Automatic Systems Monitoring the Contamination of Air [in Russian], Tekhnika, Kiev (1979).
6. N. G. Gusev and V. A. Belyaev, in: Atomic Power Stations [in Russian], No. 4, Énergoizdat, Moscow (1981), p. 137.
7. A. I. Glushchenko et al., in: Atomic Power Stations [in Russian], No. 6, Énergoizdat, Moscow (1983), p. 47.

EFFECT OF ALUMINUM, BERYLLIUM, AND TRIVALENT CHROMIUM NITRATES ON THE EXTRACTION OF URANYL NITRATE WITH A 10% SOLUTION OF TRI-n-BUTYLPHOSPHATE IN n-PARAFFINS

B. S. Zakharkin, T. A. Rumyantseva, and D. P. Adaev

UDC 541.123.4:546.791.6:546.45.621.763

The effect of salting-out in liquid–liquid extraction systems is caused by the fact that hydration of the ions of the salting-out agent leads to a reduction of the amount of free water in the aqueous phase, an increase of activity of the substance being extracted (activity coefficient), and, consequently, to an increase of the distribution coefficient D. The individuality of the salting-out agents is manifested in their effect on the activity coefficient of the distributing salt. A detailed review of the problem of salting-out was published previously [1, 2].

In the present paper, the effect is considered of nitric acid salts of beryllium, aluminum, and trivalent chromium on the extraction of uranyl nitrate with a 10% solution of tributylphosphate (TBP) in n-paraffins. According to [1, 2], the relation between the thermodynamic properties of aqueous solutions of electrolytes and the salting-out action of salts during the distribution of the substance between the organic and aqueous phases can be described quantitatively by the equation

$$D = KE_0^q (\rho_e')^3,$$

where K is the extraction constant (for uranyl nitrate in the case of extraction with TBP, $K = 1.4 \cdot 10^5$); ρ'_e, effective surface density of water molecules in the first coordination layer of all cations present in the aqueous solution; $\rho'_e = [H^+]\rho'_{HNO_3} + \Sigma\rho'_i[C_i]Z_i$; $\rho'_{HNO_3} = 0.06$; Z, cation charge; [C], salt concentration; i, Al^{3+}, Be^{2+}, Cr^{3+}; E_a, active concentration of extractant in the organic phase ($E_a = E_0/1 + E_0[H^+]_{aq}$, E_0 is the concentration of "free" extractant, for nitric acid solutions and 10% TBP calculated by the equation

$$E_0 = \frac{0.35 - 2[U]_{org}}{1 + 8.1[HNO_3]_{undiss.} + 0.8[HNO_3]^2_{undiss.}},$$

where $[U]_{org}$ is the equilibrium concentration of uranium in the organic phase).

The degree of dissociation of nitric acid α is found, according to the data of [1, p. 100], for the effective acidity:

$$[H^+]_{eff} = ([H^+]_{aq}[NO_3^-]_{aq})^{1/2}[3];$$
$$[HNO_3]_{undiss.} = \alpha[HNO_3]_{aq};$$

$[HNO_3]_{aq}$ is the equilibrium concentration of nitric acid in the aqueous phase; q is the effective solvation number, calculated by the equation $q = 2 - (0.06[H^+]_{aq}/1 + 2 \cdot 0.06[H^+]_{aq})$; $[H^+]_{aq}$ is the equilibrium concentration of $[H^+]$ ions in the aqueous phase.

In this case, when the values of ρ' of the cations present in the solution are known, the effect of salting-out on D can be described by means of the equation quoted above. In [1, 2], the value of ρ' is quoted only for Al^{3+} (0.055); values of ρ' for Be^{2+} and Cr^{3+} are absent. In order to determine ρ'_{Be} and ρ'_{Cr}, the effect of the nitrates of these elements

Translated from Atomnaya Énergiya, Vol. 57, No. 1, pp. 34-36, July, 1984. Original article submitted August 18, 1983.

0038-531X/84/5701-0465$08.50

TABLE 1. Distribution of Uranium in the System 10% TBP—HNO_3—$UO_2(NO_3)_2$—$Al(NO_3)_3$—$Be(NO_3)_2$—$Cr(NO_3)_3$—H_2O (values of D for uranium during extraction from solutions containing aluminum are taken from [5])

Aqueous phase, mole/liter					Organic phase, mole/liter	Distribution coeff.	
$[Al(NO_3)_3]$	$[Be(NO_3)_2]$	$[Cr(NO_3)_3]$	$[HNO_3]$	[U]		D_{exp}	$D_{calc.}$
1,0	—	—	0,94	$0,48 \cdot 10^{-3}$	$8,8 \cdot 10^{-2}$	18	23
1,0	—	—	0,96	$8,0 \cdot 10^{-2}$	0,15	1,9	1,5
1,0	—	—	0,96	0,12	0,16	1,3	1,5
1,0	—	—	1,9	$3,8 \cdot 10^{-3}$	$7,0 \cdot 10^{-2}$	19	23
1,0	—	—	2,0	$7,8 \cdot 10^{-2}$	$1,5 \cdot 10^{-2}$	1,9	2,2
1,0	—	—	2,8	$1,7 \cdot 10^{-3}$	$4,0 \cdot 10^{-2}$	25	25
1,0	—	—	2,8	$9,3 \cdot 10^{-3}$	$9,2 \cdot 10^{-2}$	10	10
1,0	—	—	3,0	$1,0 \cdot 10^{-1}$	$1,4 \cdot 10^{-1}$	1,4	1,5
1,0	—	—	3,0	$2,9 \cdot 10^{-1}$	$1,6 \cdot 10^{-1}$	0,55	0,5
1,4	—	—	1,7	$2,6 \cdot 10^{-4}$	$2,1 \cdot 10^{-2}$	81	81
1,4	—	—	2,0	$2,8 \cdot 10^{-2}$	$1,4 \cdot 10^{-1}$	5,0	4,8
1,4	—	—	2,0	$1,3 \cdot 10^{-1}$	$1,5 \cdot 10^{-1}$	1,2	1,6
1,4	—	—	2,8	$1,3 \cdot 10^{-3}$	$4,2 \cdot 10^{-2}$	32	35
1,4	—	—	3,0	$2,5 \cdot 10^{-1}$	$1,6 \cdot 10^{-1}$	0,6	0,6
2,0	—	—	0,87	$6,2 \cdot 10^{-4}$	$7,8 \cdot 10^{-2}$	125	122
2,0	—	—	0,9	$2,8 \cdot 10^{-3}$	$1,2 \cdot 10^{-1}$	43	45
2,0	—	—	1,1	$1,6 \cdot 10^{-2}$	$1,5 \cdot 10^{-1}$	9,3	8,2
1,0	0,2	—	—	$9,9 \cdot 10^{-3}$	$1,2 \cdot 10^{-1}$	12	14
1,0	0,5	—	—	$5 \cdot 10^{-3}$	$1,2 \cdot 10^{-1}$	24	34
1,0	0,8	—	—	$2,8 \cdot 10^{-3}$	$1,2 \cdot 10^{-1}$	43	40
—	3,0	—	0,9	$1,1 \cdot 10^{-3}$	$1,2 \cdot 10^{-1}$	109	102
0,5	0,5	—	0,8	$1,5 \cdot 10^{-2}$	$1,3 \cdot 10^{-1}$	8,6	8,0
0,5	0,5	—	1,65	$3,6 \cdot 10^{-3}$	$7,4 \cdot 10^{-2}$	21	22
0,7	1,0	—	0,9	$1,4 \cdot 10^{-2}$	$1,4 \cdot 10^{-1}$	10	13
0,7	1,0	—	1,9	$1,2 \cdot 10^{-2}$	$1,2 \cdot 10^{-1}$	10	13
1,0	1,0	—	0,95	$9,9 \cdot 10^{-3}$	$1,5 \cdot 10^{-1}$	15	14
1,2	0,7	—	—	$1,6 \cdot 10^{-2}$	$1,5 \cdot 10^{-1}$	9,4	12
—	1,8	—	0,45	$1,7 \cdot 10^{-2}$	$1,4 \cdot 10^{-1}$	8,3	9,6
0,25	1,3	—	0,45	$1,8 \cdot 10^{-2}$	$1,4 \cdot 10^{-1}$	7,7	7,5
0,5	0,83	—	0,45	$29 \cdot 10^{-2}$	$1,4 \cdot 10^{-1}$	4,8	6,1
0,75	0,33	—	0,45	$3,8 \cdot 10^{-2}$	$1,3 \cdot 10^{-1}$	3,4	4,4
0,92	—	—	0,45	$4,0 \cdot 10^{-2}$	$1,3 \cdot 10^{-1}$	3,2	3,2
—	2,0	—	1,9	$6,2 \cdot 10^{-3}$	$1,3 \cdot 10^{-1}$	21	20
0,5	1,0	—	1,9	$1,8 \cdot 10^{-2}$	$1,3 \cdot 10^{-1}$	7,2	7,3
0,75	0,5	—	1,9	$1,4 \cdot 10^{-2}$	$1,3 \cdot 10^{-1}$	9,3	12,0
1,0	—	—	1,9	$2,3 \cdot 10^{-2}$	$1,4 \cdot 10^{-1}$	6,1	6,3
—	2,7	—	1,9	$6,1 \cdot 10^{-3}$	$1,2 \cdot 10^{-1}$	20	31
0,83	1,0	—	1,9	$1,2 \cdot 10^{-2}$	$1,3 \cdot 10^{-1}$	11	12
1,0	0,66	—	1,9	$1,3 \cdot 10^{-2}$	$1,3 \cdot 10^{-1}$	10	11
1,3	—	—	1,9	$1,3 \cdot 10^{-2}$	$9,4 \cdot 10^{-2}$	7,2	5,2
—	—	0,25	0,9	$1,3 \cdot 10^{-3}$	$6,2 \cdot 10^{-3}$	4,8	4,2
—	—	0,75	0,9	$3,1 \cdot 10^{-4}$	$6,5 \cdot 10^{-3}$	21	20
—	—	1,30	0,9	$8,8 \cdot 10^{-5}$	$6,4 \cdot 10^{-3}$	73	78
—	—	0,25	0,9	$2,7 \cdot 10^{-2}$	$5,4 \cdot 10^{-2}$	2,0	2,1
—	—	0,7	0,9	$1,0 \cdot 10^{-2}$	$8,0 \cdot 10^{-2}$	8,0	8,1
—	—	1,3	0,9	$1,9 \cdot 10^{-4}$	$1,4 \cdot 10^{-2}$	73	71
—	—	0,25	1,9	$2,0 \cdot 10^{-3}$	$2,0 \cdot 10^{-2}$	10	8,8
—	—	0,25	1,9	$2,8 \cdot 10^{-2}$	$8,2 \cdot 10^{-2}$	2,9	2,8
—	—	0,7	1,9	$3,1 \cdot 10^{-4}$	$7,7 \cdot 10^{-3}$	25	24
—	—	0,7	1,9	$3,9 \cdot 10^{-3}$	$5,6 \cdot 10^{-2}$	14	14
—	—	1,3	1,9	$3,9 \cdot 10^{-4}$	$2,0 \cdot 10^{-2}$	51	50
—	—	1,3	1,9	$5,5 \cdot 10^{-3}$	$8,2 \cdot 10^{-2}$	15	16
—	—	0,25	2,8	$1,9 \cdot 10^{-3}$	$1,7 \cdot 10^{-2}$	8,9	9,5
—	—	0,25	2,9	$9,6 \cdot 10^{-3}$	$5,6 \cdot 10^{-2}$	5,8	6,3
—	—	0,5	2,8	$2,6 \cdot 10^{-3}$	$3,1 \cdot 10^{-2}$	12	12
—	—	0,5	2,9	$8 \cdot 10^{-3}$	$6,0 \cdot 10^{-2}$	7,5	8,2
—	—	0,7	2,8	$9,8 \cdot 10^{-4}$	$1,7 \cdot 10^{-2}$	17	16
—	—	1,0	2,8	$8,0 \cdot 10^{-4}$	$1,7 \cdot 10^{-2}$	21	21
—	—	1,0	2,9	$5,9 \cdot 10^{-3}$	$6,5 \cdot 10^{-2}$	11	13
—	—	1,5	2,8	$4,6 \cdot 10^{-4}$	$1,7 \cdot 10^{-2}$	37	37
—	—	1,5	2,8	$1,6 \cdot 10^{-3}$	$3,5 \cdot 10^{-2}$	22	29
—	—	0,25	3,8	$3,5 \cdot 10^{-3}$	$4,1 \cdot 10^{-2}$	11	9,5
—	—	0,5	3,9	$7,2 \cdot 10^{-3}$	$6,7 \cdot 10^{-2}$	9,3	7,9
—	—	0,5	3,9	$4,7 \cdot 10^{-2}$	$1,1 \cdot 10^{-1}$	2,4	2,8
—	—	0,7	3,9	$3,5 \cdot 10^{-2}$	$1,1 \cdot 10^{-1}$	3,1	3,5
—	—	1,0	3,8	$1,1 \cdot 10^{-3}$	$2,1 \cdot 10^{-2}$	19	21
—	—	1,0	3,9	$7 \cdot 10^{-3}$	$7 \cdot 10^{-2}$	10	11

on the extraction of uranium with a 10% solution of TBP from nitric acid solutions was studied. The experiments were conducted in separatory funnels at room temperature (20-22°C), times of contact of the phases 3-5 min and with a phase volume ratio equal to unity. After separation the organic and aqueous solutions were analyzed for the uranium content by the method of [4], and for nitric acid (potentiometric titration). It was established beforehand that beryllium and trivalent chromium are almost unextracted with tributylphosphate; for example, the distribution coefficient of Cr(III) = $(2-6)\cdot10^{-7}$ with $[HNO_3]$ = 1-4 mole/liter and $[Cr(NO_3)_3]$ = 1-1.5 mole/liter.

From the results obtained on the distribution of uranyl nitrate in the systems $UO_2(NO_3)_2$–$Be(NO_3)_2$–HNO_3–H_2O–10% TBP, and $UO_2(NO_3)_2$–$Cr(NO_3)_3$–HNO_3–H_2O–10% TBP, the values of ρ' were calculated for beryllium and chromium, equal to 0.08 and 0.048, respectively.

From a comparison of the known values of ρ' for a number of cations [1, 2], it follows that beryllium is the most powerful salting-out agent of all cations, for which the value of ρ' is known, and chromium is a less powerful salting-out agent than beryllium and aluminum (the extraction potentials of beryllium, aluminum, and chromium are 6.45, 6.0, and 4.7, respectively.

It can be seen from Table 1 that the experimental values of D for uranium and the values calculated by the equation given above, coincide satisfactorily (deviations do not exceed ±12%). This corresponds to the results obtained in [6]. Hence it follows that with the conditions of accuracy of the experimental values of D, the method of [1, 2] allows the ability of the cation toward hydration (ρ') to be determined quantitatively with sufficiently high accuracy. If the values of ρ' present in the solution of cations are known, then the distribution of uranium during extraction with TBP can be calculated over a wide range of compositions of the aqueous phase. The equation can be used for forecasting the extraction equilibria by means of a computer, during the extraction of uranium with tributylphosphate or other neutral extractants from aqueous solutions of a complex salt composition.

LITERATURE CITED

1. A. S. Solovkin, Salting-Out and the Quantitative Description of Extraction Equilibria [in Russian], Atomizdat, Moscow (1969).
2. A. S. Solovkin, Salting-Out and the Quantitative Description of Extraction Equilibria [in Russian], Results of Science and Technology. Series Inorganic Chemistry, All-Union Institute of Scientific and Technical Information, Vol. 3 (1972).
3. A. S. Solovkin, Zh. Neorg. Khim., 15, 1914 (1970).
4. V. K. Markov et al., Uranium, Methods of Determination [in Russian], Atomizdat, Moscow (1964).
5. V. V. Revyakin, V. V. Chubukov, and N. A. Korableva, Zh. Neorg. Khim., 13, 3090.
6. I. Shilin and T. Rumyantseva, in: Proceedings of the Tripartite Symposium "Reprocessing of Spent Nuclear Fuels," Held a Mol, 17-19 May, 1978, p. 1.

NEUTRON PARAMETERS WHICH CAN BE REACHED IN FAST URANIUM BLANKETS OF HYBRID FUSION REACTORS

G. E. Shatalov

UDC 621.039.677

Great possibilities can be expected from the use of a source of thermonuclear (fusion) neutrons for the fission of heavy-element nuclei and the simultaneous production of nuclear fuel. On the one hand, depleted or natural uranium and thorium can be used in the blanket of a fusion reactor so that the cost is reduced. The problems associated with the criticality of the blanket do not arise. Mainly ^{238}U or ^{232}Tn burn in the blanket and, owing to the improved neutron balance, much more nuclear fuel is produced in the blanket of hybrid fusion reactors than in nuclear reactors. On the other hand, the multiplication of the energy in the fusion reaction improves the energy balance of the reactor so that the complexity and, accordingly, the cost of the fusion part of the unit is justified.

Attempts to make use of these advantages are often based on the limit parameters of the blanket neutrons, though such parameters are not compatible with all the limitations of real units. The goal of the present article is to evaluate the neutron parameters which must be reached in real blankets and to compare the nuclear fuel under various requirements to the blanket.

In order to reduce the number of possible versions, one must immediately introduce several assumptions which do not essentially affect the conclusions but imply restrictions on the treatment of the main points. The assumptions are as follows.

1. We do not consider symbiotic systems of fusion and fission reactors in which ^{239}Pu or ^{233}U is produced in the fusion reactor while tritium is produced in the fission reactor. It follows from the considerations below that the parameters of a hybrid fusion reactor are adequately characterized by the total production of useful isotopes and that the system closure obtained through tritium breeding does not substantially change the optimal parameters and limit parameters.

2. The considerations are referred to the initial moment of time and the changes of the parameters during the operational period of the reactor are disregarded. Corresponding corrections can be made separately and can be important for certain versions (for example, in the case of a thorium fuel). The changes of the basic parameters amount to 20-30% in the majority of blankets with uranium fuel during an operational period corresponding to a neutron load of 1.5-3(MW•yr)/m^2.

3. Blankets with enriched fuel, which resemble critical blankets, are disregarded. In such blankets, the coefficient of breeding fissile material and the energy multiplication in the blanket, both referred to a single fusion neutron, can be much greater. But the breeding of fissile materials per unit of thermal power of the blanket is reduced, as will be shown through a comparison of fuel consisting of natural uranium and enriched uranium. The specific load of the fuel elements of the blanket has values close to the limit value for the presently assumed plasma parameters of fusion reactors when natural or enriched fuel is considered. An enrichment can make sense in the blankets of fusion units in which the specific neutron load on the first wall amounts to 0.3-0.5 MW/m^2 in accordance with the plasma parameters which can be reached. But few such units are possible and as far as the economic aspects are concerned, these units are inferior to units with higher specific load values.

4. We exclude from our considerations the so-called blankets with suppressed fission (see, e.g., [1]) in which the neutron multiplication takes place mainly through (n, 2n) reactions on beryllium or lead and where the breeding of the fissile isotopes takes place on a thorium salt with continuous removal of ^{233}U (or protactinium). Such blankets have a very small energy multiplication coefficient and fissile-material breeding coefficient which is

Translated from Atomnaya Énergiya, Vol. 57, No. 1, pp. 36-41, July, 1984. Original article submitted August 1, 1983.

 0038-531X/84/5701-0468$08.50

two times smaller than that of the fast uranium blankets with nonenriched fuel considered in the present article.

Geometry of the Systems under Consideration. Calculations have been made for a number of different blanket compositions in one-dimensional geometry. An infinite cylinder with a radius of 300 cm of the central zone, uniformly filled with distributed neutron sources of the D–T fusion reaction, was assumed in the calculations. The source was assumed to be isotropic and monochromatic with an energy of 14.1 MeV. This geometry rather closely describes both tokamak-type fusion reactors and linear systems.

Calculation Method. The calculations were made with the Monte Carlo method in combination with the P_1 approximation; the BLANK program [2] with a 52-group [3] or 21-group [4] system of combined constants was employed. For the majority of elements, the 52-group system which describes the interaction of the elements with neutrons at high energies was based on the ENDL-76 library of assessed data.

Calculations with the Monte Carlo method were usually made for 5000 neturon histories. The relative error of the majority of the integral parameters (total neutron source, breeding coefficients of tritium and the fissile isotope) amounted to 1-2%; the relative error was 2-4% for the rate of the (n, 2n) and (n, 3n) reactions.

As far as neutron multiplication and the increased output energy per neutron of the source are concerned, the layers of the material undergoing fission by thermonuclear neutrons (i.e., ^{238}U or ^{232}Th) are most conveniently disposed in the region adjacent the plasma. The thickness of that region must be chosen so that a neutron of the source makes at least one inelastic collision with a probability close to unity. The probabilities of the first 2-3 inelastic collisions determine the extent of the expected neutron source in mixtures of various materials. Actually, all basic characteristics of the blanket are proportional to the effective source value: the total coefficient of isotope breeding, the number of fissions, and the energy multiplication coefficient. The basic dependencies of the integral parameters of blankets with a complicated structure can therefore be established by investigating blankets of infinite thickness and a composition corresponding to the composition of the first zone of real blankets.

The goal of the present work is to analyze the integral characteristics of a blanket. The following parameters are employed: K_T, which denotes the coefficient of tritium breeding per neutron of the thermonuclear source; K_{Pu} and $K_{^{233}U}$, which denote the coefficient of breeding fissile nuclei per source neutron in media containing ^{238}U and ^{232}Th, respectively; $K_\Sigma = K_T + K_{Pu} + K_{^{233}U} - K_{depl}$, which denotes the yield of useful isotopes per thermonuclear neutron, with K_{depl} denoting the number of capture reactions (including fission) on ^{235}U, ^{239}Pu, and ^{233}U referred to a single source neutron; E denotes the energy liberated in the blanket per source neutron:

$$E = E_0 + \sum_i (n^i_{fiss} E^i_{fiss} + n^i_{capt} E^i_{capt} - n^i_{n,2n} Q^i_{n,2n} - n^i_{n,3n} Q^i_{n,3n}),$$

where $n^i_{n,2n}$, $n^i_{n,3n}$, n^i_{fiss}, and n^i_{capt} denote the number of (n, 2n), (n, 3n), fission, and capture reactions at the i-th isotope, respectively; $Q^i_{n,2n}$ and $Q^i_{n,3n}$, energy of the (n, 2n) and (n, 3n) reactions, respectively; E^i_{fiss} and E^i_{capt}, energies liberated in fission and capture reactions, respectively; $M = E/E_0$, coefficient of energy amplification in the blanket; E_0, energy of a source neutron; $y = (K_\Sigma - 1)/E$, coefficient of breeding useful isotopes, with the coefficient referred to the unit total power of the blanket and the need for breeding tritium in the same blanket and the burnup of ^{235}U in the initial fuel composition taken into consideration; and Q, total number of neutrons in the blanket, referred to a single thermonuclear neutron [$Q = 1 + n_{n,2n} + 2n_{n,3n} + (\nu - 1)n_{fiss}$].

The neutron-physics characteristics of the reactor are usually employed in the initial economic estimates. The reactor characteristics are divided into two groups on this occasion. The first group comprises K_T, K_{Pu}, and E which describe the yield of the isotopes and the energy in the normalization to unit power of the thermonuclear reaction. These quantities are of overriding importance in systems in which the cost of the thermonuclear part of the system forms a significant fraction of the total cost or in systems in which the limitations are given by obtainable specific power of the plasma string and, accordingly, by the neutron load on the first wall. In such a case, the cost of the electric energy generated by the system and of the nuclear fuel is inversely proportional to K_{Pu} and E.

The second group comprises the coefficient y of breeding useful isotopes; this coefficient characterizes the yield of nuclear fuel per unit of thermal power of the reactor. The actual meaning of this coefficient resembles that of the breeding coefficient

$$BG = \frac{K_b - 1}{E_{fiss}},$$

where K_b denotes the plutonium-breeding coefficient normalized to one fission event. The BG value is usually employed to characterize the quality of a fast breeder reactor. In blankets in which $n_{fiss} \geq 0.3$, y and BG differ by at most 15%, whereas in systems in which n_{fiss} is small (e.g., in thorium blankets), the difference reaches 100% and y should be used as the characteristic quantity. In evaluating the economic aspects of systems in which the cost of the thermonuclear part is low or the specific energy intensity of the blanket rather than the power of the plasma string is the limiting quantity, y is of prime importance. In the limit, the cost of nuclear breeders is inversely proportional to y.

Idealized Blankets. The parameters of infinite single-component blankets with a fissile material are listed in Table 1. The best characteristics in regard to the parameters K_{fiss} and E are found in a blanket containing metallic uranium fuel. In ^{238}U, 1.02 fission events take place and 4.2 neutrons are captured with subsequent transition into ^{239}Pu per source neutron. The energy amplification coefficient M is 16. In ^{238}U the maximum value of the condition $y = 1.4 \cdot 10^{-2}$ MeV^{-1} is reached among all uranium blankets; the maximum value corresponds to a ^{239}Pu breeding in the amount of 1.1 kg/(MW•yr) of the thermal power of the blanket. The coefficient y decreases during the operational period because the average number of fission neutrons decreases while the enrichment of the fuel by plutonium proceeds.

Data for infinite uranium and thorium media have been cited in [5, 6]; in the case of ^{238}U [6], the energy multiplication coefficient is 16.5 and the total neutron capture coefficient is 4.4. These coefficients are in rather good agreement with the results of our work.

One can try to improve, in a certain sense, the blanket parameters by using natural uranium in place of ^{238}U. In this case the plutonium yield is increased to 4.75 nuclei per source neutron and the total number of fissions is raised to 1.44. But a simultaneous burnup of ^{235}U takes place and K amounts to 4.4, whereas M is increased to 22.5. Thus, the use of natural uranium increases the yield of the fissile isotopes from the blanket by 5% and the energy liberated in the blanket by about 30%. At the same time the coefficient y decreases to $1.07 \cdot 10^{-2}$ MeV^{-1} which implies an isotope breeding of 0.83 kg/(MW•yr), i.e., the breeding is smaller than that in the case of ^{238}U by 17%. The question of whether uranium should be used and the question of the possible initial enrichment of the fuel in the blanket can be solved only when all other limiting factors of a specific thermonuclear system are taken into account.

The total neutron flux at the boundary with the source is 30 cm^{-2}•sec^{-1} at a neutron flux from the source amounting to 1 cm^{-2}•sec^{-1} on the inner surface of the blanket. It is interesting to note that the fraction of neutrons with more than 5 MeV amounts to ~5%, i.e., the number of displacements of atoms in the blanket materials of hybrid fusion reactors differs only slightly from the corresponding number in fast breeder reactors when the neutron flux is the same. However, 5% of the source neutrons suffice for increasing the rate of hydrogen and helium formation in the blanket by 1-2 orders of magnitude.

Uranium compounds are inferior to the metallic fuel in regard to the parameters which are referred to the neutron source. When nuclei of elements which do not undergo fission are introduced in the blanket composition, the probability of a primary collision of source neutrons with ^{238}U nuclei decreases and this, in turn, linearly reduces the number of fission events and the breeding of fissile isotopes in the blanket. The smallest gain (~10%) in all parameters is observed in the case of uranium silicide. The characteristics of uranium oxide are below those of metallic uranium by a factor of 1.7-1.8. In units in which the limitations are associated with the specific thermonuclear power, the use of uranium oxide leads to a sharp deterioration of the parameters of the fusion reactor.

The yield y of useful isotopes per unit thermal power of the blanket changes only slightly in all the uranium compounds. The maximum advantage obtained in the case of UO_2 over metallic uranium is 12% and when the specific energy intensity of the blanket is the limiting factor, the advantages of the various uranium compounds depend upon the limitations which characterize the corresponding fuel elements in regard to temperature and intensities.

TABLE 1. Neutron Balance of Infinite Single-Component Media of Fissile Materials

Reaction and output energy	U^{nat}	^{233}U	$U_3^{nat}Si$	$^{238}U_3Si$	$U^{nat}C$	^{238}UC	$U^{nat}O_2$	$^{238}UO_2$	^{232}Th
$U(n, f)$	1,44	1,02	1,37	0,93	1,07	0,80	0,78	0,60	—
$^{238}U(n, \gamma) \rightarrow ^{239}Pu = K_{Pu}$	4,75	4,20	4,44	3,87	3,96	3,57	3,05	2,77	—
$^{232}Th(n, f)$	—	—	—	—	—	—	—	—	0,20
$^{232}Th(n, \gamma) \rightarrow ^{233}U = K_{233U}$	—	—	—	—	—	—	—	—	2,46
$^{235}U(n, \gamma)$	0,06	—	0,06	—	0,05	—	0,04	—	—
Capture by nonfissile material	—	—	0,08	0,076	0,01	0,01	0,18	0,18	—
All (n, 2n) reactions	0,33	0,33	0,32	0,32	0,31	0,31	0,23	0,23	0,59
All (n, 3n) reactions	0,18	0,18	0,15	0,16	0,14	0,14	0,11	0,11	0,25
$^{238}U(n, f)$	1,16	1,02	1,07	0,93	0,89	0,80	0,64	0,60	—
$^{238}U(n, f)$ at an energy > 6 MeV	0,57	0,57	—	—	0,50	0,49	0,38	0,38	—
$^{235}U(n, f)$	0,28	—	0,30	—	0,18	—	0,14	—	—
Total energy E (MeV)	320	230	300	210	240	190	180	145	60
$^{238}U(n, \gamma)^{239}U(n, f) - ^{235}U(n, \gamma) = K_\Sigma$	4,41	4,20	4,08	3,87	3,75	3,57	2,89	2,77	2,46
$(K_{Pu} - 1)/E$, 10^2 MeV^{-1}	1,16	1,39	1,15	1,37	1,23	1,35	1,13	1,22	2,46
$(K_\Sigma - 1)/E$, 10^2 MeV^{-1}	1,07	1,39	1,03	1,37	1,15	1,35	1,05	1,22	2,46
Total source	6,24	5,21	6,00	4,88	5,08	4,39	4,04	3,54	2,66

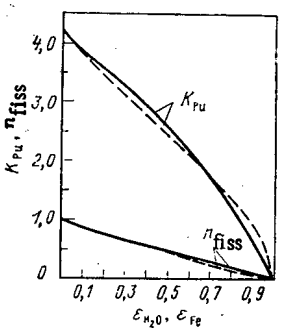

Fig. 1

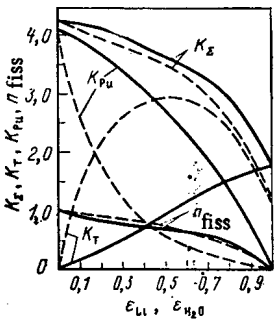

Fig. 2

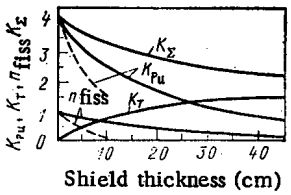

Fig. 3

Fig. 1. Parameters of infinite media of ^{238}U + Fe (-----) and of ^{238}U + H_2O (———).

Fig. 2. Parameters of an infinite medium consisting of a mixture of ^{238}U and lithium: ———) ^{238}U + natural lithium; -----) ^{238}U + ^6Li.

Fig. 3. Parameters of an infinite medium of ^{238}U with a shield of natural lithium (———) or of Fe (-----) between the medium and the source.

An even higher y value is observed in the case of thorium. In a blanket of metallic thorium, 1.9 kg/(MW•yr) ^{233}U are generated by breeding at the beginning of the operational period. But the K_Σ and E values of a thorium blanket are much lower than those of an uranium blanket and thorium cannot be used for the blankets of units in which a substantial amount of energy is spent for maintaining the fusion reaction.

Figure 1 illustrates the influence of the lithium-containing materials, construction materials and of the coolant upon the blanket parameters. Figure 1 shows the dependencies of the parameters K_{Pu} and n_{fiss} upon the fractions of the various materials in a ^{238}U mixture for a homogeneous blanket of infinite thickness. The greatest effect results from the incorporation of iron in an uranium blanket. K_{Pu} and n_{fiss} change at a rate of ∿1% per volume percent of iron in the mixture. This is a consequence of the fact that the macroscopical cross sections of the inelastic processes of uranium and iron are approximately equal at the energy of the neutron source. The blanket parameters decrease in almost the same fashion in an uranium–water mixture but in this case the mechanism of the n_{fiss} decrease depends considerably upon the decrease in the probability of the ^{238}U fission by the neutrons of the fission spectrum.

A homogeneous mixture of uranium with lithium (Fig. 2) can be used in compositions of hybrid blankets in which the maximum value of K_T must be obtained. The K_Σ and n_{fiss} values change in about the same fashion for the natural mixture of the lithium isotopes and pure ^6Li. An increase in the capture by lithium causes the maximum K_T in a mixture consisting of equal volume fractions of ^{238}U and ^6Li. The maximum K_T value is 2.93 and seems to be the absolute value for the nonenriched compositions. When lithium is introduced in an uranium blanket, K_Σ

and n_{fiss} change much more slowly than when iron is introduced. Even with a 70% volume fraction of lithium K_Σ decreases in comparison with pure uranium by 20% in the case of natural lithium and by 30% in the case of ^6Li. Thus, a homogeneous dilution of the uranium by lithium does not greatly reduce the properties of the blanket.

In order to assess real blankets, one must also know how the blanket parameters are influenced by the layers of the various materials located between the neutron source and the uranium region. Data for shields consisting of iron and lithium and inserted before an infinite uranium medium are illustrated in Fig. 3. The decrease in K_Σ amounts to 1.5%, on the average, per 1 mm thickness of an iron layer and to 0.3% per 1 mm of natural lithium. For a 10-cm-thick iron shield, the number of fission events per thermonuclear neutron is still 0.19, whereas the coefficient of breeding useful isotopes, $K_\Sigma = K_{Pu}$, amounts to 1.53; this means that it is basically possible to manufacture a breeding blanket even in the case of a thick steel shell before the uranium region. The coefficient y remains rather high ($0.88 \cdot 10^{-2}$ MeV^{-1}), and the breeding of plutonium amounts to 0.7 kg/(MW•yr) at the beginning of the operational period.

The coefficient y of a shield of natural lithium increases with increasing shield thickness up to 50 cm. This effect is caused by the formation of tritium in inelastic scattering of neutrons at ^7Li nuclei, whereby the neutron balance in the reactor is improved. In the case of a 50-cm-thick shield, y amounts to $2.8 \cdot 10^{-2}$ MeV^{-1}, which, in principle, makes it possible to reach a plutonium breeding of up to 2.0 kg/(MW•yr) in the blanket under consideration when some depletion of lithium in regard to ^6Li has taken place. The K_Σ value is two times smaller than in an uranium medium without shield. This is still acceptable, but the E value is reduced by a factor of 6. Such a blanket is obviously economically adequate in systems with a high neutron load on the first wall. The blanket can be particularly interesting for pulsed fusion reactors.

The limited thickness of the uranium region has an important influence in real blankets. The scale of the effect can be inferred from Fig. 4 which shows the dependence of the parameters of a blanket (consisting of a ^{238}U layer and an infinite ^6Li reflector) upon the thickness of the uranium layer. A ^6Li reflector for uranium blankets with a hard neutron spectrum provides the greatest K_T value which is practically equal to the outflow of neutrons from a layer of pure uranium. The highest K_T value (2.65) is obtained at a thickness of 7 cm of the uranium region. But at the maximum of K_T, the coefficient K_Σ is 3.3 and smaller than that of an infinite uranium blanket by 20%.

Limit Parameters of Real Blankets. Let us consider the changes of the parameters of idealized schemes in the transition to real blanket designs of fusion reactors. As has been explained in the preceding section, the maximum breeding of useful isotopes (4.2 nuclei per source neutron) was obtained in an infinite ^{238}U blanket. Let us observe how this quantity changes when the construction elements of the blanket are taken into account. Three basic factors reduce the K_Σ value.

1. A certain quantity of construction materials must be present in the uranium region: these materials are the shells of the fuel elements and the housings of the coolant channels. In the optimal design of fuel elements designated for a heat dissipation of 0.2-0.3 MW/liter, the fraction of the shell volume amounts to 10-15% of the fuel element volume. The housing of the cooling channels, the spacing grids, and other design elements at least double the above value and one can hardly hope for a reduction of the fraction of the design materials below 20% by volume. The effects of the various materials do not strongly differ and we will use the data for iron in our estimates (see Fig. 1). The change in K_Σ amounts to ~1% of iron in the blanket and the introduction of 20% of a construction material would reduce K_Σ to 3.4.

2. The first wall of the plasma chamber is situated between the iron zone and the uranium region in the designs of the majority of fusion reactors. It follows from Fig. 3 that the wall reduces K_Σ by 1.7% per 1 mm of wall thickness at low thickness values. In the projects of tokamak reactors which have been developed so far, the thickness of the first wall is assumed as 10-15 mm; plasma sputtering of the wall and the requirements to the rigidity of the structure have been taken into account. In fusion reactors of the open-trap type [5, 6], where the flux of particles from the plasma to the wall is smaller than in the tokamak, a thickness of 5-6 mm was assumed. When we consider this as the real lower limit, the K_Σ value which can be reached must decrease by 8-10% and amount to 3.1.

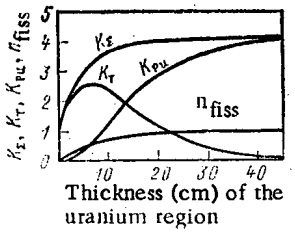

Fig. 4. Dependence of the parameters of a medium of ^{238}U with an infinite Li reflector upon the thickness of the uranium region.

TABLE 2. Parameters of Blankets in Some Fusion Reactor Projects

Unit	K_Σ	K_{Pu}	K_T	n_{fiss}
Open trap	2,9	1,8	1,4	0,7
Tokamak [4]*	2,56	1,54	1,05	0,59
Tokamak [4]†	2,76	1,54	1,22	0,83

*At the beginning of the operational period.
†At the end of an operational period of 2.25 years at a neutron load of 1 MW/m^2 on the first wall.

3. It is not advantageous to make the uranium region of the blanket very thick because the energy liberation and the plutonium breeding in this region are nonuniform and because it is hard to obtain $K_T \geqslant 1$ (see Fig. 4). When the thickness of the uranium region is reduced to the optimal value of 7-10 cm, losses of ~20% occur in the breeding of useful isotopes. The value $K_T \geq 1$ can be obtained (though this is not always desirable) in quasihomogeneous lithium-uranium mixtures (see Fig. 2), but in this case the K_Σ losses amount to 10-20%. Thus, we arrive at an effective total breeding coefficient of 2.5-2.8 which also has been assumed in the majority of promising developments of hybrid blankets of fusion reactors. The parameters of two of these reactors, in which metallic waste uranium is used in the blanket, are listed in Table 2. The expected breeding can amount to 1.4-1.8 plutonium nuclei per fusion event.

The real yield values of the fissile nuclide are reduced to 0.5-0.8 per fusion event when other uranium and thorium compounds are employed. The production of these nuclides, referred to the total thermal power, either slightly decreases (to 0.9 kg/(MW•yr)) or increases. The yield of the nuclear fuel reaches 2 kg/(MW•yr) in the case of metallic thorium fuel and certain compositions of uranium blankets.

During the operational period, K_{Pu} is almost constant and the specific breeding decreases. In the case of metallic uranium, the plutonium yield decreases by a factor of 1.3 and amounts to ~0.65 kg/(MW•yr) of thermal power by the end of an operational period of ~2 years and a neutron load of 1 MW/m^2 on the blanket surface.

Conclusions. The above considerations have shown that when the real requirements to blanket design are taken into account, a production of 1.4-1.8 tons of plutonium nuclei per fusion event can be expected in a blanket in which metallic uranium fuel is employed. Accordingly, in a reactor with a fusion power of 500 MW, 2.5-3 tons of plutonium can be produced per calendar year; when the total thermal power of the reactor is 2.5-3 GW at the beginning of the operational period, the breeding amounts to ~1 kg/(MW•yr).

LITERATURE CITED

1. J. Lee and R. Moir, Fission-Suppressed Blankets for Fissile Fuel Breeding Fusion Reactors, Preprint LLL UCRL-84104 (1980).
2. S. V. Marin, D. V. Markovskii, and G. E. Shatalov, Problems of Atomic Science and Technology, Series Physics and Technology of Nuclear Reactors [in Russian], No. 9(22) (1981), p. 26.

3. L. N. Zakharov et al., Problems of Atomic Science and Technology, Series Physics and Technology of Nuclear Reactors [in Russian], No. 8(21) (1981), p. 42.
4. S. M. Zakharova, B. N. Sivak, and G. I. Toshinskii, Byull. Inf. Tsentra Yad. Dannym. (Bull. of the Information Center for Nuclear Data), No. 3, Atomizdat, Moscow (1967) (Appendix: Constants of Nuclear Physics for Reactor Calculations).
5. R. Moir et al., Progress in the Conceptual Design of a Mirror Hybrid Fusion–Fission Reactor, Preprint LLL UCRL-51797 (1975).
6. J. Lee, Mirror Fusion-Fission Hybrids, Preprint LLL UCRL-80720 (1978).

RADIATION BACKGROUND IN LIVING ACCOMMODATIONS

É. M. Krisyuk and V. I. Parkhomenko

UDC 614.876+613.5:539.16.08+539.16

Introduction. Natural ionizing-radiation sources make the main contribution to the population dose. That contribution to the collective effective equivalent dose (EED) is 60-70%. Medical irradiation constitutes 30-40% of the collective dose. The overall contribution from all other sources, including environmental contamination from weapons tests, professional irradiation, discharges from nuclear power stations, etc., is not more than 1%.

In recent years there has been a particular increase in the interest in population irradiation research. This has occurred because the International Commission on Radiation Protection (ICRP) [1] suggested that there is a linear threshold-free effect from ionizing radiation. On that basis, the frequencies of somatic-stochastic genetic effects are proportional to the mean EED to the population. The largest doses from natural sources arise in living accommodation and working buildings, where the radiation background arises from cosmic radiation, which is partly attenuated by the material between floors, the γ rays from natural radionuclides (NRN) present in the building materials, and from radon decay products entering the air in the building from the building materials and the soil.

The γ background in a building is dependent on the specific activity of the NRN in the materials. The vast scale of building of living accommodations in the country has led to a search for new sources of traditional building materials and to the use of products made from the wastes from mining, metallurgy, and the chemical industry, as well as ash and slag from the thermal power stations. The use of these wastes has also been stimulated by the need for low-waste production technology. However, such building materials frequently have elevated NRN activities, which increases the population dose.

The elevated NRN activities in the materials also raise the concentrations of radon and its daughter decay products DDP in the air. Other reasons for elevated concentrations of radon and DDP may be that the nuclide enters the building from the soil and passes upwards between floors; low rates of air exchange are also another factor. There has been a tendency to reduce air-exchange rates in living accommodations because of the need for power economy in heating.

Until recently, there have been no standards for radioactivity in building materials, nor have there been building regulations that restrict the concentrations of radon and DDP, which has meant that in some countries (Sweden, the Federal German Republic, and the USA) there have been considerable rises in the doses to large groups of the population [2]. In recent years, there have been large-scale researches in most developed countries on the irradiation of the population from natural sources, with emphasis on the origins of the dose, and there have been discussions on restricting population irradiation.

Research Methods. The NRN contents of building materials are usually examined by γ spectroscopy, where the single measurement enables one to determine the specific activities of ^{226}Ra, ^{228}Th, and ^{40}K. If there is radioactive equilibrium in the uranium and thorium families, the activities of these nuclides completely characterize the radioactivity of the material. We have developed [3] the SGS-200 high-sensitivity γ spectrometer, where the detector is an NaI(Tl) crystal of size 150 × 150 mm containing a well (sample volume up to 212 cm^3). The minimum measurable specific activities of NRN are 23 Bq/kg for ^{40}K, 5 for ^{226}Ra, and 9 for ^{228}Th with a measurement time of 20 min and an error of 25%. A relatively small sample is used (250 g). If there are deviations from equilibrium in the uranium and thorium families (as in specimens that have undergone chemical processing), it is best to use radiochemical methods for γ spectrometry with a Ge(Li) detector, which enables one to determine the activities of several nuclides in each family, although the method is more laborious.

High-pressure chambers are mainly used to measure the γ background. The first such chamber was described in [4]. The apparatus is not readily portable, which has led to difficul-

Translated from Atomnaya Énergiya, Vol. 57, No. 1, pp. 42-48, July, 1984. Original article submitted November 14, 1983.

0038-531X/84/5701-0475$08.50

ties. This disadvantage is absent in a scintillation dosimeter as described in [5]. The detector here is an air-equivalent plastic scintillator ($C_{14}H_{10}$) covered with zinc sulfide. The instrument has a virtually constant (±10%) dose sensitivity for radiation of energy >25 keV. The photomultiplier dark current and other features give rise to a very low inherent background, which is equivalent to a dose rate of 0.04 μR/h (1 R = $2.58 \cdot 10^{-4}$ Ci/kg). The instrument has been used in large-scale research on the γ background in the Federal German Republic. In recent years, extensive use has also been made of LiF, $CaF_2(Dy)$, and $CaSO_4(Dy)$ thermoluminescent dosimeters to measure the γ background [6]. The advantages of these are that the detectors can be sent by post and the measurements made in a single laboratory, which ensures that the results are comparable.

We have calibrated geophysical exploration apparatus for irradiation from models for saturated beds containing uniformly distributed potassium with uranium and thorium in equilibrium [7], which has shown that the ratio of the dose sensitivities for these models and a point ^{226}Ra source is 1.0 ± 0.1 if one uses instruments containing gas-discharge counters. The only disadvantage of such instruments is that it is necessary to correct for the counter background.

The concentrations of radon and DDP may be determined in the air and living accommodations by means of various instruments and methods. In particular, the radon concentration can be determined with an SAS-R-2 alpha scintillation counter [8]. In determining the DDP concentrations, one usually employs the aspiration method, whose sensitivity is dependent on the throughput of the air-sampling device and the method of counting the filter. Various methods have been compared [9]. A deficiency common to them all is that one can determine the concentrations of radon and DDP only at the time of sampling; as these concentrations vary over time, one requires repeated measurements to test a single building.

In recent years, integral methods have been developed for determining the concentrations of radon and DDP averaged over large time intervals. These take passive and active forms. In the active method, the air is pumped through a filter and the α particles from the DDP deposited from it are recorded continuously [10]. This method is used to measure DDP concentrations and the sensitivity is determined by the throughput of the sampler (usually <1 liter/min), by the background in the detectors, and by the efficiency of α-particle recording. The best instruments used in that method enable one to determine DDP concentrations in the air in buildings and in the open atmosphere.

The passive method is used in measuring mean radon and DDP concentrations. The radon concentration is determined with simple devices, which usually take the form of a vessel containing a detector, with the open end closed by a membrane [11], which is made of an appropriate material, (silicone rubber, polyethylene, glass-fiber filter, etc.), which prevents the DDP and thoron penetrating into the vessel and passes only radon. The sensitivity is determined by the α-irradiation geometry, by the background, and by the phasing, as well as by the radon diffusion coefficient in the membrane. In measuring DDP concentrations, the detector is placed in a special cassette and one records the α particles from the radon and DDP deposited on the detector and present in the air [10]. The mean radon and DDP concentration is usually measured by means of thermoluminescent detectors ($CaF_2(Dy)$, $CaSO_4(Dy)$, etc.) or with track ones (cellulose nitrate, polycarbonate, etc.). The sensitivity of a passive device is usually less than that of an active one, but in the best specimens it is sufficient to measure radon and DDP concentrations in building air.

Structure of the Radiation Dose in Buildings. The floors in a building tend to reduce the cosmic-radiation dose. Values have been given [12] for the screening coefficients for buildings of various types. In particular, in a two-story wooden building the average screening coefficient is 0.94, while in a four-story building of older construction it is 0.84, and in a modern 10-story building it is 0.6. The γ-ray dose rate in the building is dependent on the specific activity of the NRN in the building materials, the size and shape of the building, the areas of the windows and doors, and the thicknesses of the walls and floors. The maximum possible dose rate can be estimated from a formula for the dose rate in an air cavity in an infinite space having uniformly distributed radionuclides:

$$P_{4\pi}\,(\mu\text{rad/h})^{*} = 0.104\,(C_{Ra} + 1.26C_{Th} + 0.086C_{K}), \quad (1)$$

*1 rad = 0.01 Gy.

where C_{Ra} C_{Th}, and C_K are the specific activities of ^{226}Ra and ^{228}Th in equilibrium with the other members of the uranium and thorium families, and of ^{40}K correspondingly in Bq/kg. The quantity in parentheses is the effective NRN specific activity C_{ef} [13].

Measurements have been made in the Fereral German Republic and Norway [14, 15] on the dependence of dose rate on wall and floor thickness, with calculations made for modern brick and concrete buildings on the basis of field studies, which has indicated [13] that the dose rate in a modern building is $\sim 0.7P_{4\pi}$. Therefore, the γ-ray dose rate in a modern stone building is determined only by the effective NRN specific activity in the walls and floors. The contribution from each component of the building material (cement, sand, ballast, etc.) is determined by its contribution to the effective NRN specific activity. If the walls and floors differ in NRN specific activity, the dose rate is determined by the mean weighted value of C_{ef}. The weighting factors are proportional to the solid angles subtended by the walls and floors at the center of the building.

A model description has been given [16] on the mechanisms whereby radon isotopes accumulate in building air. The radon concentration C_0 in the air and the specific equilibrium of the walls and floors q_i are described by the following expressions:

$$C_0 = \frac{\lambda_0}{(\lambda_0 + \lambda_V)V} \sum_{i=1}^{i=6} (C_{Ra})_i \eta_i d_i \rho_i \frac{\text{th}\,\beta_i}{\beta_i} S_i + \frac{\lambda_V}{\lambda_0 + \lambda_V} C_0^a; \tag{2}$$

$$q_i = (C_{Ra})_i \eta_i d_i \rho_i \frac{\text{th}\,\beta_i}{\beta_i} \lambda_0. \tag{3}$$

Here λ_0 is the decay constant of ^{222}Rn or ^{220}Rn; λ_V, air-exchange rate; V, volume of the building; $(C_{Ra})_i$, specific activity of ^{226}Ra or ^{224}Ra (i is the subscript for the wall or floor); η_i, radon emanation coefficient; $2d_i$, thickness of the wall or floor; ρ_i, density of the material; S_i, area of the wall or floor; C_0^a, radon concentration in atmospheric air; and β_i, ratio of the half thickness of the wall or floor to the diffusion length l_0:

$$\beta_i = d_i/(l_0)_i. \tag{4}$$

The diffusion length is determined by the diffusion coefficient b and the porosity p:

$$l_0 = \sqrt{b/p\lambda_0}. \tag{5}$$

In modern living accommodations, the air-exchange rate is usually 0.3-3 h^{-1}. Therefore, the value $\lambda_0 = 7.56 \cdot 10^{-3}$ h^{-1} for ^{222}Rn in the denominator in (2) can be neglected, which means that the ^{222}Rn concentration in the air of a building is always larger than that in atmospheric air. The value of the excess is determined by the first term in (2). For ^{220}Rn ($\lambda_0 = 45.1$ h^{-1}), one can neglect λ_V, so the concentration in building air is virtually independent of that in atmospheric air ($\lambda_V/\lambda_0 \ll 1$). The ^{222}Rn concentration in building air is inversely proportional to the air-exchange rate, whereas the ^{220}Rn concentration is almost independent of it.

Formula (2) has been derived on the assumption that the air-exchange rate is constant over time. As the ^{222}Rn concentration is inversely proportional to this rate, the mean value of C_0 with a variable air-exchange rate differs from the value obtained from (2) with $\lambda_V = \overline{\lambda_V}$. Numerical estimates show [17] that when the exchange rate varies within the usual limits, the correction factor is ~1.5.

The measured diffusion length for ^{222}Rn in building structures is 10-20 cm [18], and then the values of $\tan\beta/\beta$ for the walls and floors of modern buildings are close to one (mean value ~0.8), which means that the radon release approximates to the maximum possible value, which corresponds to all the radon atoms produced by the decay of ^{226}Ra escaping. It follows from (5) that the diffusion length for ^{220}Rn is less by a factor 77, i.e., is 1-2 mm, and then $\tan\beta/\beta \approx 1/\beta = l_0/d$, i.e., the ^{220}Rn is released only from the very superficial layers.

A basic characteristic of a building material determining the radon concentration in the air is the effective radium specific activity, which is the product of the specific activity by the emanation coefficient.

The radiation dose to lung tissue is determined not by the radon concentration but by the concentration of the short-lived decay products C_0F, where F is the equilibrium coefficient. For ^{222}Rn

$$F = 0.10485C_1/C_0 + 0.51565C_2/C_0 + 0.37950C_3/C_0, \quad (6)$$

where C_1, C_2, and C_3 are the concentrations of ^{218}Po, ^{214}Pb, and ^{214}Bi correspondingly. For ^{220}Rn

$$F = 7 \cdot 10^{-6}C_1/C_0 + 0.91326C_2/C_0 + 0.08673C_3/C_0, \quad (7)$$

where C_1, C_2, and C_3 are the concentrations of ^{216}Po, ^{212}Pb, and ^{212}Bi.

The product C_0F is called the equivalent equilibrium radon concentration. The value of the equilibrium coefficient is dependent on the air-exchange rate and on the deposition of the decay products on the walls, floor, ceiling, and other surfaces. The following formulas [19] give the dependence of the equilibrium coefficient on the exchange rate:

$$\left.\begin{aligned} C_1 &= \frac{\lambda_1}{\lambda_1 + \lambda_V} C_0 + \frac{\lambda_V}{\lambda_1 + \lambda_V} C_1^a \\ C_2 &= \frac{\lambda_2}{\lambda_2 + \lambda_V} C_1 + \frac{\lambda_V}{\lambda_2 + \lambda_V} C_2^a \\ C_3 &= \frac{\lambda_3}{\lambda_3 + \lambda_4} C_2 + \frac{\lambda_V}{\lambda_3 + \lambda_4} C_3^a \end{aligned}\right\}, \quad (8)$$

where λ_1, λ_2, and λ_3 are the decay constants of the daughter products, whose concentrations in atmospheric air are C_1^a, C_2^a, and C_3^a.

The effects of the deposition on the equilibrium coefficient have not finally been established. Numerical estimates show that the exchange rate has a not very marked effect on the equilibrium coefficient for ^{222}Rn. It is usually close to 0.5 for living accommodations. For ^{220}Rn, the value is much lower (~0.05), and it is very much dependent on the exchange rate (approximately inversely proportional to it). The rate of entry of ^{222}Rn from the soil under the building is related to the concentration in the soil there and to the permeability of the basement. It is difficult to provide theoretical estimates. On the second and higher floors, the nuclide is derived mainly from the building structures. The entry of ^{220}Rn from the soil is unlikely.

Field Studies. Studies have been made on the NRN specific activities in building materials in many countries. The foreign data have been collected in [2, 20], which has identified materials with elevated NRN activities: natural ones (granite, alum shales, bauxite, and tuffs) and industrial wastes used in building (ash, slag, phosphogypsum, red sludge, etc.). The NRN specific activities in the materials are dependent not only on the form of the latter but also on the point of extraction. For example, it has been shown [21] that the radioactivity of red brick and concrete in Denmark is lower by factors of 2-3 than that in the other Scandinavian countries.

Very thorough studies of building material activity have been made in the USSR [22, 23]. Specimens characterizing over 3000 deposits of building material and 200 forms of industrial waste have been examined. The mass character of these studies has provided a histogram of the effective NRN specific activities, where the mean value (93 Bq/kg) is appreciably less than the background levels of NRN in the earth's crust and is virtually the same as the mean NRN level for soils. The histogram is skewed when a logarithmic scale is used along the abscissa, falling more steeply on the right (Fig. 1). The extrapolated upper limit is ~370 Bq/kg (10 pCi/g). Only ~1% of materials have effective NRN activities exceeding this value. The curves for some forms of material are close to log-normal. Table 1 gives the median values for NRN activities in various materials and the 95% limits. The highest NRN levels occur in granite rubble, concrete based on it, and red brick. Most of the industrial wastes used in this country in building have NRN activities at the level of traditional building materials. Only in 5% of these wastes does the NRN effective specific activity exceed 370 Bq/kg [23].

The emanation coefficients and effective specific activities for ^{226}Ra [24] are determined by the mass proportions and contents of ^{226}Ra in the components of Soviet combined building materials (concrete, plaster work, and silicate brick), so it is possible to estimate the contribution of each component (sand, cement, aggregate, etc.) to the radioactivity of the air in the building and to the lung tissue irradiation, which is done in the same way as one estimates this contribution to the external radiation dose from the mass fractions and effective NRN specific activities of the components.

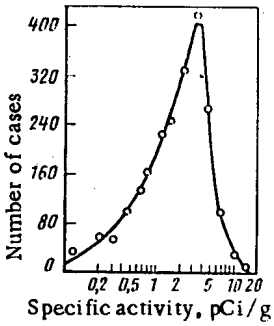

Fig. 1. Distribution of effective NRN specific activities for Soviet building materials.

TABLE 1. ERN Specific Activities in USSR Building Materials

Material	Number of specimens	Medians and 95% limits, pCi/g*											
		^{232}Th			^{226}Ra			^{40}K			effective specific activity		
		c_{min}	c_{max}	$\bar{c}$	c_{min}	c_{max}	$\bar{c}$	c_{min}	c_{max}	$\bar{c}$	c_{min}	c_{max}	$\bar{c}$
Clay	449	0,4	1,9	0,91	0,3	1,2	0,55	5,7	25,3	12,0	1,5	5,7	2,9
Sand	630	0,09	0,7	0,29	0,08	0,5	0,21	1,4	19,4	5,2	0,4	3,2	1,1
SGM†	188	0,2	1,1	0,42	0,1	0,7	0,28	1,3	32,2	6,5	0,6	3,7	1,5
Gravel	101	0,1	1,1	0,37	0,2	0,9	0,38	3,3	23,1	8,7	0,6	4,3	1,7
Limestone aggregate	403	0,06	0,3	0,13	0,1	1,1	0,34	0,2	5,2	1,1	0,2	1,8	0,7
Sandy aggregate	115	0,2	1,2	0,51	0,2	0,9	0,40	9,1	20,9	10,3	1,1	4,2	2,0
Granite aggregate	342	0,3	2,7	0,97	0,2	2,3	0,74	7,4	37,4	16,6	1,6	9,7	4,0
Cement	190	0,2	1,0	0,48	0,4	2,2	0,88	1,9	9,5	4,2	1,0	4,3	2,0
Slag	181	0,2	1,9	0,60	0,4	3,7	1,18	1,5	13,4	4,4	0,9	7,1	2,5
Clay brick	588	0,5	2,1	1,06	0,4	1,8	0,88	8,1	30,7	15,7	2,0	7,1	3,8
Silicate brick	124	0,1	0,6	0,26	0,1	0,5	0,26	1,2	10,6	3,6	0,4	2,0	0,9
Light concrete	55	0,08	2,1	0,41	0,09	3,8	0,59	1,0	25,8	5,0	0,3	7,5	1,6
Heavy concrete	121	0,09	2,3	0,45	0,20	2,0	0,64	1,4	39,7	7,5	0,6	8,2	2,2

*1 pCi/g = 37 Bq/kg;
†Sand–gravel mixture.

TABLE 2. Ratio of γ-Ray Dose Rates in Buildings P_b and Near Them P_s [14]

Building material	P_b/P_s	Building material	P_b/P_s
Pumice	1,50	Limestone	1,24
Slag	1,47	Concrete	1,24
Clinker	1,36	Foamed concrete	1,18
Brick and natural stone	1,35	Wood	0,96
Clay	1,35		

The emanation coefficients of materials treated at high temperatures (red brick, cement, ceramics, ash, and slags) are less by about an order of magnitude than those for the raw materials. For this reason, the contributions from such materials to the radon release are small even if they have elevated radium specific activities. The highest effective specific activities of ^{226}Ra occur for soil and clay, which means that the maximal air activities will be observed in buildings that can be entered by soil radon and also in homes made of unfired clay brick. The effective ^{226}Ra activity in brick is lower by a substantial factor than that in concrete, which should be responsible for a corresponding difference in the air activity for brick and concrete buildings.

The γ backgrounds in buildings and populated areas have been examined in detail in the Federal German Republic [14] within the framework of a national interdepartmental program for

researching natural radioactivity in the environment. About 30,000 measurements were made in buildings and 25,000 near them in the open air. The contributions from the cosmic radiation were subtracted. The ratio of the dose rate in a building to that outside it on average was 1.36, the exact value being dependent on the material (Table 2). The γ rays from the building make a certain contribution to the dose rate near it if the building is of stone, and for this reason the data given in Table 2 are underestimates in comparison with the ratio of the dose rate in a stone building to the γ background in the locality before it was built. There should not be this difference for wooden buildings. The ratio of the mean dose rate in stone buildings (50 mrd/yr) to the average dose rate near wooden buildings (31 mrd/yr) is 1.62, which evidently gives a better indication of the effects from building stone structures on the γ-ray dose rate.

In measurements on the γ background in Norway [15], the measurements in open areas were made in parks and gardens far from stone buildings. The following ratios were found between the dose rates in buildings and in open areas: wooden structures 0.95, concrete ones 1.42, and brick ones 1.60. These ratios are close to the corrected results found in the Federal German Republic.

Measurements have been made of the radioactivity of air in buildings in many countries, and these are summarized in an UNSCEAR [20] report. In many cases, the measurements were made in buildings in which the windows and doors had previously been closed, and therefore the values characterize the maximum radon and DDP concentrations, not the mean annual ones. There was also an effect from the time of year, since the air-exchange rates in buildings are higher in the summer than in the winter (on average by factor three) [25]). For this reason, large-scale studies made in Canada during the summer [26] give underestimates, whereas measurements made in Norway in the winter [27] give overestimates. The most accurate results in that respect have been obtained in Britain [25], where simultaneous measurements were made of the radon concentration (from the concentration of ^{218}Po or RAA) and the frequency of air exchange. The data were used to calculate the rates of entry of radon into the building air, and from that result was derived the radon concentration with the mean annual air-exchange rate of 0.93 h^{-1}. The mean annual equivalent equilibrium radon concentration was 0.31 pCi/liter (11.5 Bq/m^3), which is close to the corrected values for Canada and Norway. A similar estimate of the mean at 15 Bq/m^3 (0.4 pCi/liter) is given by UNSCEAR [20]. Recent measurements in the Federal German Republic [28] give the smaller value of 0.24 pCi/liter (9 Bq/m^3). Unfortunately, no measurement of the air-exchange rate is quoted in that paper, so it is impossible to judge whether this difference is due to a difference in the mean annual air-exchange rate or in the rate of entry of radon into the building air.

Almost all the field measurements on radioactivity in air have been made in buildings on the first floor. In [29] it has been shown that the radon and DDP concentrations on the upper floors are lower by about a factor four. Similar results were obtained in [30]. As the first floor can receive radon from the soil as well as that from the structure, whereas the upper floors receive it only from the structure, the above estimates of the equivalent concentrations characterized most likely the entry of radon from the soil under the building. Very few measurements have been made on the concentrations of decay products from ^{220}Rn in building air, and those indicate that the contributions from these isotopes to human doses are less by factors of 5-10 than those from the decay products of ^{222}Rn.

Population Radiation Doses. We have estimated the doses to the population in buildings by comparing the field studies with the calculations of [31]. The mean effective NRN specific activities in Soviet building materials were used to determine the EED for irradiation of the population by γ rays as 370 μSv/yr (1 Sv = 100 ber), which exceeds the dose in an open locality by 100 μSv/yr, with the latter determined from the mean effective specific activity of the NRN in USSR soils. The ratio of the dose rates in a stone building and in the street outside of 1.52 agrees well with the field studies. The 100 μSv/yr is the additional irradiation of the population due to the γ rays from building materials.

The following results have been obtained from calculations on the DDP concentrations in the air of living accommodations, and analysis of the field data. The EED representing the background irradiation for people in the open air throughout the year is 220 μSv/yr, while the additional irradiation due to building structures is 350 μSv/yr, and that due to emanation from the soil under buildings is 690 μSv/yr. The overall doses due to γ rays and DDP are close to the UNSCEAR estimates [20], but our estimates are more differentiated. The additional dose in buildings is 1140 μSv/yr relative to the background in an open locality, i.e.,

~30% of the total population dose from all sources of ionizing radiation [32]. Therefore, modern stone buildings are one of the main sources of irradiation, and they are comparable as regards EED with the irradiation from medical sources.

Scope for Restricting Irradiation in Buildings. The doses received in a building from γ rays and DDP are determined by different characteristics of the building materials and structure, so protective measures should be designed to restrict each of these forms of irradiation separately.

The γ-ray dose in a building is determined almost completely by the effective NRN specific activity in the building materials. A basis has been provided [33] for a standard for this for the materials used in living accommodations and civil buildings. Current approaches to standardizing population exposure are based on the argument that the restriction of irradiation should be attained not at any price but with due allowance for economic and social factors. Unfortunately, it is difficult to perform a rigorous quantitative incorporation of the use-harm relation in carrying out protective measures because of the large uncertainty with the maximum justified costs for reducing the population dose by 1 man-ber [34]. For this reason, the basis for the standard is provided by a purely qualitative incorporation of the use-harm relation. The standardized values approximated to the extrapolated upper limits for building materials as regards effective NRN specific activity ($C_{ef} \leqslant 10$ pCi/g). The purpose of the standardization is to prevent a substantial rise in the mean value of C_{ef}, and perhaps also to produce some reduction. A considerable reduction is certainly not justified on economic grounds. The standard extends to each component of a building material (sand, aggregate, cement, etc.), since the contribution to the dose and the cost of the protective measures are determined by each of the components. The characteristic is the mean value of C_{ef} for the material extracted at a given deposit (or a given part of it). Recommendations have been made on monitoring the radioactivity of building materials [35]. The value of the standard for existing buildings should be substantially higher, since the cost of protective measures is much greater. The basis for the standard should be detailed studies of the γ backgrounds in existing buildings together with estimates of the cost of protective measures (modification or transfer to other uses).

There are various ways of restricting the population exposure due to DDP. For example, the specifications could be introduced for flooring impermeability to radon in new buildings, which would gradually reduce the population dose and might eliminate the entry of radon from the soil under the building. The entry of radon from building structures can be restricted by standardizing the effective ^{226}Ra specific activities in materials [36]. It is also important to provide the necessary mean annual air-exchange rates in living accommodations. In some cases, one can use antiradon coatings on walls (for example, with oil paint). Detailed implementation of these measures should be based on large-scale research on the radioactivity of air in living accommodation and on the modes of radon entry.

LITERATURE CITED

1. Radiation Protection [Russian translation], ICRP Publ. No. 26, Atomizdat, Moscow (1978).
2. Exposure to Radiation from the Natural Radioactivity in Building Materials, Report by NEA Group of Exports, Paris, NEA OECD (1979).
3. É. M. Krisyuk et al., Prib. Tekh. Eksp., No. 5, 33 (1975).
4. R. Sievert and B. Hultquist, Acta Radiol., 37, 388 (1952).
5. W. Kolb and U. Lauterbach, in: Rapid Methods for Measuring Radioactivity in the Environment, Vienna, IAEA (1971), p. 565.
6. E. Piesch and B. Burgkhardt, in: Proceedings of the Fourth International Congress IRPA, Vol., 4, Paris (1977), p. 1245.
7. É. M. Krisyuk et al., Prib. Tekh. Eksp., No. 3, 74 (1980).
8. É. M. Krisyuk et al., in: Rapid Methods for Measuring Radioactivity in the Environment, Vienna, IAEA (1971), p. 843.
9. M. V. Terent'ev and É. M. Krisyuk, At. Énerg., 55, No. 5, 301 (1983).
10. H. Richardson, in: Proceedings of a Special Meeting on Personal Dosimetry and Area Monitoring Suitable for Radon and Daughter Products, Paris (1978), p. 45.
11. A. Frank and E. Benton, Nucl. Instrum. Methods, 109, 537 (1973).
12. R. A. Filov and É. M. Krisyuk, At. Énerg., 47, No. 6, 420 (1979).
13. V. Karpov and E. Krisiuk, Health Phys., 39, 819 (1980).
14. Die Strahlenexposition von Aussen in der Bundesrepublik Deutschland durch natürliche radioactive Stoffe im Freien und in Wohnungen, Bericht über ein vom Bundesminister des Innern. (1978).

15. E. Stranden, Health Phys., 33, 319 (1977).
16. E. Krisiuk, ibid., 38, 199 (1980).
17. É. M. Krisyuk et al., Research and Standardization for Radioactivity in Building Materials [in Russian], Atomizdat, Moscow (1974).
18. N. I. Shalak and É. M. Krisyuk, in: Radiation Hygiene [in Russian], Izd. Leningr. Nauchn.-Issled. Inst. Rad. Gigiena, Leningrad (1980), p. 32.
19. B. Hultquist, Ionizing Radiation from Natural Sources [Russian translation], Inostr. Lit., Moscow (1959).
20. Ionizing Radiation: Sources and Biological Effects. UNSCEAR Report, New York (1982).
21. K. Ulbak, in: Seminar on the Radiological Burden of Man from Natural Radioactivity in the Countries of the European Community. CEC v/2408/80 (1980), p. 237.
22. É. M. Krisyuk and V. I. Parkhomenko, in: Staatliches Amt für Atomsicherheit und Strahlenschütz. Report SAAS-250, Berlin, SAAS (1979), p. 199.
23. V. I. Parkhomenko, É. M. Krisyuk, and É. P. Lisachenko, Gig. Sanit., No. 8, 34 (1981).
24. N. A. Koroleva et al., in: Current Topics in Radiation Hygiene [in Russian], Minzdrav SSSR (1983).
25. K. Cliff, Phys. Med. Biol., 23, No. 4, 696 (1978).
26. McGregor et al., Health Phys., 39, 285 (1980).
27. E. Stranden, Phys. Med. Biol., 24, No. 5, 921 (1979).
28. G. Keller, K. Folkerts, and H. Muth, Radiat. Environ. Biophys., 20, 263 (1982).
29. J. Gemesi, D. Szy, and A. Toth, in: Proceedings of the Second International Symposium on Natural Radiation Environment, Houston (1972), p. 751.
30. F. Abu-Jarad and J. Fremlin, Health Phys., 32, 75 (1982).
31. É. M. Krisyuk et al., in: Radiation Hygiene [in Russian], Issue 10, Izd. Leningr. Nauchn.-Issled. Inst. Rad. Gigiena, Leningrad (1981), p. 47.
32. É. M. Krisyuk et al., ibid., Issue 12, p. 11.
33. É. M. Krisyuk, Gig. Sanit., No. 12, 32 (1980).
34. É. M. Krisyuk, in: Radiation Hygiene [in Russian], Issue 11, Izd. Leningr. Nauchn.-Issled. Inst. Rad. Gigiena, Leningrad (1982), p. 30.
35. É. M. Krisyuk, Health-Physics Evaluation of Building Materials: Recommendations on Methods [in Russian], Izd. Leningr. Nauchn.-Issled. Inst. Rad. Gigiena, Leningrad (1976).
36. É. M. Krisyuk et al., in: Proceedings of the Third International Congress IRPA, Washington, IRPA (1974), p. 370.

CHANGE OF MECHANICAL PROPERTIES OF LOADED STEEL SPECIMENS SUBJECTED TO HYDROGEN ION DISCHARGE

G. Biggiero and A. Borruto

UDC 669.018.2

It was established earlier (G. Biggiero, A. Borutto, and F. Marafini, At. Energ., 49, No. 1, 22 (1980)) that under tensile stresses exceeding the static fatigue limit, the time to fracture and the form of the fracture surface depend on the intensity of hydrogen discharge in specimens of heat-treated 38 NiCrMo with the bainitic structure. Upon continuation of the experiments it was found that when the load on the specimens is far below the static fatigue limit under hydrogen discharge conditions, premature fracture occurs, which can be considered as the limiting case of fracture due to aging; in the case of the specimens which did not fracture we found that with increasing discharge time the volume of discharged hydrogen decreased and the reverse process of recovery of mechanical properties occurred. In view of this it seemed advisable to establish what stresses and hydrogen discharge regime could affect the reduction of mechanical properties as well as the initiation time and course of the process of recovery of the original properties of the steel.

Tensile tests of the specimens under hydrogen discharge conditions were performed in accordance with the procedure described earlier on an Instron machine at a constant strain rate of 0.5 mm/min. These tests were carried out at a constant current density (8 mA/cm^2) while the stress was varied (50.0, 50.5, and 57.5 kg/mm^2), as well as at constant stress (50.0 kg/mm^2) while the current density was varied (6, 8, 12, and 14 mA/cm^2). The fracture surface was examined under the scanning electron microscope and the presence of inclusions was determined with the aid of an optical microscope.

The tests at constant current density (Fig. 1) revealed:

a lowering of the reduction in area as the stress grew;

a decrease in the reduction in area, starting after 60-100 min and reaching a minimum after roughly 1600 min;

no fracturing of some specimens, even when the duration of the hydrogen discharge was prolonged 100-fold, at a load of 57.5 kg/mm^2;

coincidence of the minima on the "load—time to fracture" curve and on the curve of the reduction in area.

The tests under a constant load (Fig. 2) showed that when the current density was varied the minimum reduction in area is observed after 2100 min at 6 mA/cm^2, after 1600 min at 8 mA/cm^2, after 600 min at 12 mA/cm^2, and after 110 min at 14 mA/cm^2; the rapture stress of the specimens remains constant.

Figure 3 presents the linear dependence characterizing the relation between the current density and the time corresponding to the appearance of the minimum on the "load—time to fracture" curve.

Phase and fractographic analyses point to the important role of inclusions in the fracture of specimens at stresses below the static fatigue limit. Since the specimens were prepared from the same melt and did not differ significantly as to phase composition, we can assume that the appearance of the fracture surface is due to the hydrogen effect. Intergranular fracture was found to occur in specimens fractured during hydrogen discharge, whereas specimens characterized by a minimum on the "load—time to fracture" had a predominantly fibrous structure in the form of horizontal open canals, which indicates a loss of strength in regions with active segregation of hydrogen.

Institute of Metallurgy, University of Rome, Rome, Italy. Translated from Atomnaya Energiya, Vol. 57, No. 1, pp. 49-50, July, 1984. Original article submitted January 27, 1983.

0038-531X/84/5701-0483$08.50

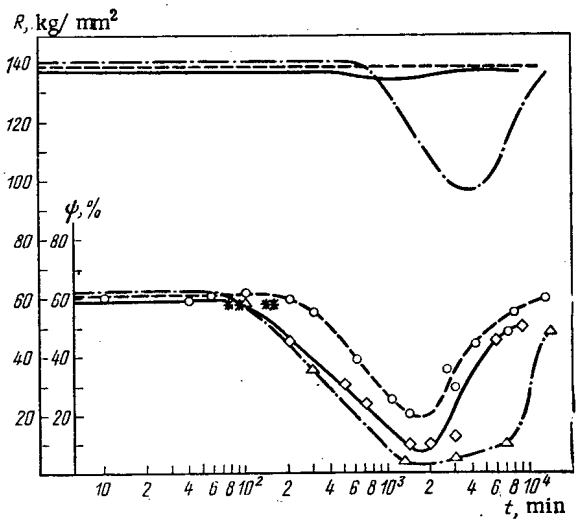

Fig. 1

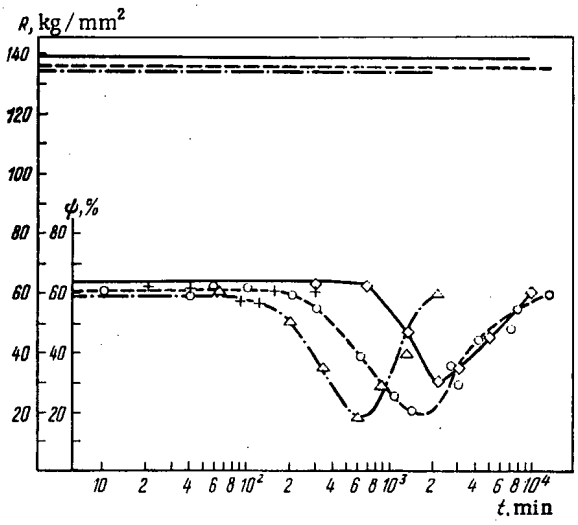

Fig. 2

Fig. 1. Variation of rapture stress and reduction in area during testing of specimens under hydrogen discharge at current density 8 mA/cm² and stress 53.5 (◇), 50 (○), and 57.5 kg/mm² (Δ);* denote specimens which raptured during the hydrogen discharge.

Fig. 2. Variation of rapture stress and reduction in area during testing of specimens under hydrogen discharge at stress 50 kg/mm² and current density 6 (◇), 8 (○), 12 (Δ), and 14 mA/cm² (+).

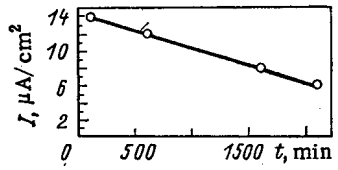

Fig. 3. Effect of current density on time required to reach minimum on "load–time to fracture" curve.

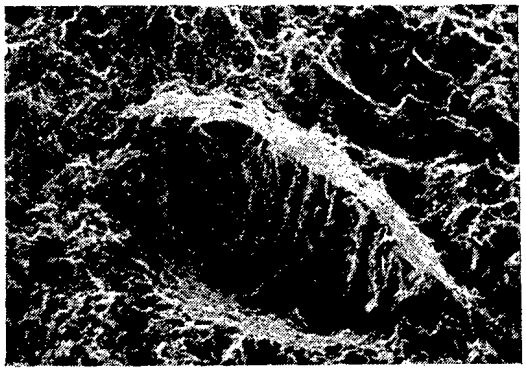

Fig. 4

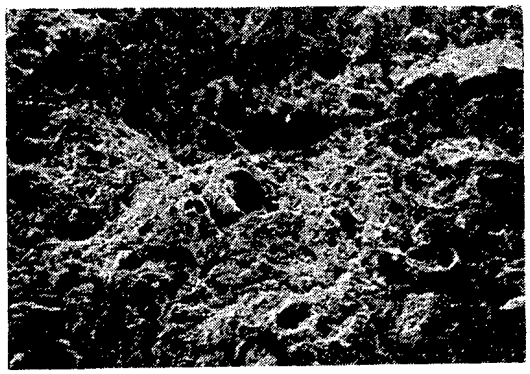

Fig. 5

Fig. 4. Fracture surface of a specimen in initial stage of hydrogen embrittlement (× 500).

Fig. 5. Fracture surface of specimen corresponding to the minimum on the "load–time to fracture" curve (× 200).

Figure 4 shows the fracture surface of a specimen, corresponding to the initial segment of the curve in Fig. 2 when pores are just beginning to appear. Specimens corresponding to the minimum on the "load–time to fracture" curve (Fig. 5) are characterized by slight radial cracks and very deep canals, formed by elongated pores; this is undoubtedly associated with the action of the hydrogen.

Thus, the results of tests at stresses below the static fracture limit, which are in agreement with data from similar tests, permit the following conclusions to be made:

1. At constant current density and constant stress the values of the reduction in area and the rupture stress change. These changes persist for a more or less long time during hydrogen discharge, and the mechanical properties then begin to recover their initial values.

2. Investigation of the specimens after practically complete recovery of the mechanical properties revealed irreversible changes in the structure of internal regions; the particular, we detected a large number of slight cracks and pores which coalesce into clearly visible canals.

3. A distinct, inversely proportional relation is observed between the effects of stress and of discharge current density. Damage begins and reaches a maximum in different intervals of time and, hence, is caused by different amounts of incorporated hydrogen.

4. It may be assumed that at a low current density hydrogen penetrates into the steel mainly along grain boundaries. When the current density increases penetration of hydrogen begins along dislocations in regions with a strongly distorted lattice. As a result the cohesion along the grain boundaries is weakened and the local plasticity of the material diminishes. In the course of the hydrogen discharge, microcavities arise in the specimens and subsequently form canals. These canals facilitate the expulsion of the hydrogen from the metal and this in turn gives rise to a reduction in the embrittlement.

ECONOMIC ASPECTS OF THE USE OF BREMSSTRAHLUNG IN RADIATION TECHNOLOGY

V. V. Krayushkin, A. V. Larichev,
and M. E. Tulupov

UDC 537.531.9

The further development of radiation technology in our country and the introduction of many radiation processes into industry have given rise to a number of problems, the most important among them being the limited production of the isotope sources which have long been the most widespread type of source used to emit ionizing radiation, as well as the increased demand for such sources. In addition, the substantial costs incurred in connection with the transportation and storage of isotope sources and the need to replace radioactive decay, and with the burial of depleted sources, the radiation danger faced by service personnel in case of accident, and the theoretical impossibility of using isotopes in some high-temperature processes and processes in which there is danger of explosion are factors which compel researchers to devote more and more attention to charged-particle accelerators [1].

During the past decades, both in our country and abroad, there have been many more accelerators produced, the range of their characteristics has been expanded, their reliability has been greatly improved, and they have been made more compact. There is by now a considerable body of experience relating to their operation in the industrial irradiation of materials by extracted electron beams. Bresmsstrahlung beams which are obtained from accelerators by means of special targets [2] and have the same penetrating capacity as gamma rays have come into wide use both in medicine and in a number of technological processes in industry [3, 4].

Such processes include:

nondestructive testing of materials;

activation analysis for determining the amounts of various elements contained in minerals, metals, and biological materials;

radiotherapy of tumors and other illnesses by means of high-energy bremsstrahlung;

sterilization of medical specimens and food products.

The use of high-energy bremsstrahlung makes it possible to carry out technological processes with large amounts of material and in thick-walled apparatuses.

When we compare the technical possibilities of using isotope sources and electron-accelerator bremsstrahluung beams in radiochemical technology, we find that most of the arguments favor the use of electron accelerators:

1. Because a bremsstrahlung beam has a given spatial orientation, the coefficient of utilization of the radiation is high (unlike the case of 4π geometry when isotope sources are used).

2. Electron accelerators make possible a much higher absorbed-dose rate than isotope sources.

3. The high beam power attained on accelerators makes for a higher specific productivity than in the case of isotope sources.

4. In case of emergency, the danger of irradiation is automatically eliminated in the case of an accelerator by blocking and signaling systems of all kinds. In processes with explosion danger also, unlike the case of isotope sources, there is no risk of radioactive contamination of the irradiated materials and the environment.

In the present study we give a preliminary economic estimate of the cost of bremsstrahlung generated by electron accelerators.

The reduced costs per unit of bremsstrahlung energy (rubles/kWh) are determined from the formula

---

Translated from Atomnaya Énergiya, Vol. 57, No. 1, pp. 50-52, July, 1984. Original article submitted January 28, 1983.

 0038-531X/84/5701-0486$08.50

$$\Pi = (C_{ann} + \varepsilon_n K) W^{-1}, \quad (1)$$

where C_{ann} represents the annual operating costs; K, capital cost of the radiation installation; ε_n, normative coefficient of effectiveness of capital investment; W, annual production of bremsstrahlung in kWh.

As was shown in [5], the economic characteristics C_{ann} and K for existing radiation installations vary linearly with the cost of the electron accelerator. To estimate the capital cost of the actual radiation source in radiation shielding (disregarding the technological equipment and additional industrial premises),

$$K = K_{acc} + K_{rs}, \quad (2)$$

where K_{acc} and K_{rs} are the costs of the accelerator and the radiation shielding, respectively.

The cost of the accelerator depends on the energy and power of the electron beam. For high-voltage accelerators ($E \leq 3$ MeV) the cost (in thousands of rubles) was found in [5]:

$$K_{acc} = 80 (1 \pm \delta) E \sqrt{N}, \quad (3)$$

where E is the electron energy, MeV; N, power of the beam, kW; δ, cost dispersion caused by different price formation at the manufacturing enterprises ($\delta \leq 0.1$). A similar estimate of the cost was made for linear resonance accelerators developed and manufactured by Soviet enterprises:

$$K_{acc} = 22 (1 \pm \delta) E \sqrt{N} \ (3 \text{ MeV} < E \leq 40 \text{ MeV}). \quad (4)$$

As is known, the thickness of the radiation shielding, and therefore its cost as well, depends on the energy of the accelerated electrons and the power of the accelerator beam. We propose estimating the cost of the radiation shielding as part of the cost of the electron accelerator:

$$K_{rs} \approx 0.2 K_{acc}. \quad (5)$$

Then the capital cost of the radiation source and the radiation shielding will be

$$K \approx 1.2 K_{acc} \quad (6)$$

Among the annual operating expenses the largest contribution is made by the amortization deductions and the cost of spare elements and assemblies for the accelerator. Therefore, in our opinion, it is legitimate to express C_{ann} in terms of K_{acc}. Operating experience at Soviet electron accelerators shows that in most cases

$$C_{ann} \approx 0.35 K_{acc}. \quad (7)$$

The annual bremsstrahlung production (in kWh) is determined from the formula

$$W = \eta \eta_{br} N T_{acc}. \quad (8)$$

Here T_{acc} is the annual operating time of the accelerator (for simplicity, we assume "pure" time, i.e., taking account of the load coefficients and the use of working time), h; η, efficiency of the irradiator [6]; η_{br}, coefficient of total bremsstrahlung output.

The coefficient of conversion of electron radiation into bremsstrahlung depends on the electron energy, the atomic number of the target, and the thickness of the target (in a thick target made of heavy-atom material there is intensive self-absorption of the bremsstrahlung). In addition, the bremsstrahlung output depends on the angle of incidence of the electron beam onto the target and the reflection (backscattering), which increases with the angle of incidence [7].

Taking account of the self-absorption of the bremsstrahlung and the backscattering, in the case of normal incidence of the electron beam onto a plane tungsten target which provides maximum bremsstrahlung output in a forward direction (into the half-space in front of the beam) [8] we found the coefficient of total bremsstrahlung output from the target:

$$\eta_{br} = 0.02 E (1 \pm \Delta), \quad \Delta \leq 0.1 \quad (1 \leq E \leq 10 \text{ MeV}). \quad (9)$$

Substituting the expressions (3), (4), (8), and (9) into formula (1) and setting $\eta = 0.8$ and $\varepsilon_n = 0.15$, we find

$$\Pi \approx \frac{\sigma}{T_{cr}\sqrt{N}} \begin{cases} \sigma = 2.65 \cdot 10^6 \text{ for } 1 \leqslant E \leqslant 3 \text{ MeV}; \\ \sigma = 7.3 \cdot 10^5 \text{ for } 3 < E \leqslant 10 \text{ MeV}. \end{cases} \quad (10)$$

Thus, knowing the established power N (kW) of the electron accelerator and the working time T_{est} [4], we can obtain from formula (10) an idea of the expected value of the reduced costs per unit of bremsstrahlung energy produced (rubles/kWh). From the expression (10) we can draw the important conclusion that the reduced costs for bremsstrahlung are not explicitly dependent on the energy (disregarding the transition from high-voltage to linear accelerators) and decrease as the power of the electron beam increases.

In the calculations we did not take account of the coefficient of utilization of the bremsstrahlung in the reaction volume (in the energy spectrum of the bremsstrahlung a large proportion is represented by low-energy photons), which, in our opinion, makes it more difficult to compare the cost of bremsstrahlung directly with the cost of γ rays from isotope sources. Taking account of the fact that the reduced costs for γ rays from ^{60}Co isotope sources amount to 6-8 rubles/kWh [9], we must admit that the cost of bremsstrahlung at existing Soviet electron accelerators remains higher today than the cost of isotope γ radiation. Thus, according to our calculations, the cost of bremsstrahlung obtained from a radiation-technological installation with the ÉLV-8 accelerator developed by the Nuclear Physics Institute of the Siberian Branch of the Academy of Sciences of the USSR (1.8 MeV, 80 kW) is about 50 rubles/kWh.

However, the present trend of steadily increasing power and decreasing cost per kilowatt of installed power at accelerators gives reason to expect a substantial decrease in the cost of bremsstrahlung and to hope that it will be capable of competing economically with radiation from isotope sources.

In conclusion, it should be noted that it evidently is not always legitimate to use in our estimate calculations the technical and economic characteristics of "pure" electron accelerators. If the bremsstrahlung source is properly designed, we can expect it to be simpler and more reliable, and therefore cheaper and more economical, than an electron accelerator used as a source of primary radiation.

LITERATURE CITED

1. R. V. Dzhagatspanyan, V. I. Kosorotov, and M. T. Filippov, Introduction to Radiochemical Technology [in Russian], Atomizdat, Moscow (1979).
2. I. A. Prudnikov et al., in: Reports of the Third All-Union Conference on the Use of Charged-Particle Accelerators in the National Economy [in Russian], Vol. IV, NIIEFA, Leningrad (1979), p. 274.
3. Yu. S. Ryabukhin and A. V. Shal'nov, Accelerated Beams and Their Utilization [in Russian], Atomizdat, Moscow (1980).
4. J. Farrel, IEEE Trans. Nucl. Sci., NS-28, No. 2, 1786 (1981).
5. V. V. Krayushkin, At. Énerg., 48, No. 2, 94 (1980).
6. Yu. S. Titkov, A. Kh. Breger, and Yu. E. Samsonov, in: Radiation Chemistry [in Russian], Atomizdat, Moscow (1972), p. 446.
7. V. F. Baranov, Dosimetry of Electron Radiation [in Russian], Atomizdat, Moscow (1974).
8. M. Berger and S. Seltzer, Phys. Rev., 2C(2), 621 (1970).
9. A. Kh. Breger, Radiochemical Technology. Its Tasks and Methods [in Russian], Atomizdat, Moscow (1979).

EFFECT OF LITHIUM ON HOT-PRESSED BORON-CARBIDE PARTS

P. D. Kervalishvili and Sh. Sh. Shavelashvili

UDC 531.21:546.34

The behavior of lithium that evolves as a result of the nuclear reaction occurring during neutron irradiation of boron carbide largely determines the variation in the characteristics of parts in a neutron field [1]. We shall present here the results obtained in investigating the effect of lithium on the dimensional and phase stability and the thermal conductivity of hot-pressed boron–carbide parts.

Cylindrical specimens of boron carbide with a density of 1.8 to 2.45 g•cm^{-3} were obtained by hot pressing in air and in a vacuum of ~1•10^{-2} Pa. In order to investigate the effect of lithium on the dimensional stability, specimens of boron carbide with a density of 1.9–2.4 g•cm^{-3} were heated together with a batch of metallic lithium with a purity of 99.9 mass % in a medium of dry high-purity argon. After isothermal annealing at 700 ± 2°C over a period of 24 h, the specimens in fact disintegrated. The degree to which the investigated specimens disintegrated depended essentially on their density. Moreover, boron carbide specimens obtained by hot pressing in air disintegrated more thoroughly than specimens prepared in a vacuum. X-ray phase analysis of the destroyed specimens showed the presence of other phases: LiB_6, $Li_2B_2O_4$, Li_2O, LiC and LiB_7C_2, which does not contradict the data published earlier [1–5].

Thus, as a result of heating, lithium atoms penetrate through pores and intergranular boundaries the interior of a boron–carbide specimen, which weakens the bonds between grains, leading to the specimen's disintegration. Moreover, in a heated specimen, there is intensive interaction between lithium on the one hand, and the impurities and the matrix components on the other, which produces new phases affecting the stability of parts. Since the percentages of oxygen, nitrogen, and carbon in specimens pressed in air amount on the average to 0.9, 0.8, and 1.5 mass %, respectively, while they amount to 0.2, 0.1, and 0.4 mass % in vacuum-pressed specimens, the percentages of additional phases in these two cases naturally amount to 3.4 and 0.9 mass percent. This explains one of the causes of the virtual destruction of boron–carbide specimens pressed in air when up to ~15 mass % lithium is introduced in them at 700°C. Another cause of this is the higher (by a factor of 10–100) percentage of structural flaws in such specimens, which promotes the penetration of lithium and segregations along the boundaries of these defects. At lower temperatures, the disintegration of specimens is negligible, while, at more elevated temperatures, the boron carbide percentage diminishes.

Determination of the parameters of lithium and boron carbide is of practical interest. In order to introduce the lithium impurity diffusively in boron carbide, metallic lithium was deposited by spray-coating on one end-face of cylindrical specimens in a vacuum of ~1•10^{-3} Pa. The boron–carbide specimens were heated to 150°C to ensure wetting. After isothermic annealing in a quartz vial in an ambient of dry high-purity argon, the diffusion specimens were cut along the axial plane. The depth and front of lithium penetration into boron carbide were then observed by means of a Nanolab-7 scanning electron microscope, manufactured by the OPTON company. Isothermic annealing at 450 ± 2°C over periods of 0.5, 1, 2.5, 7.5, and 10 h has shown that the mean depth of lithium penetration in boron–carbide specimens obeys the well-known relationship [6]:

$$l = \sqrt{Dt}, \qquad (1)$$

where l is the diffusion length, D is the diffusion coefficient, and t is the process duration.

In order to estimate the diffusion transport of lithium in the investigated boron carbide specimens, we performed annealing over a period of 5 h at 150, 250, 350, 450, 600, 800, and 1100°C. Figure 1 shows the diffusion coefficient as a function of temperature D(T) for the lithium impurity in boron carbide specimens with a density of 2.35 g•cm^{-3}, produced by hot

Translated from Atomnaya Énergiya, Vol. 57, No. 7, pp. 52–53, July, 1984. Original article submitted May 26, 1983.

0038-531X/84/5701-0489$08.50

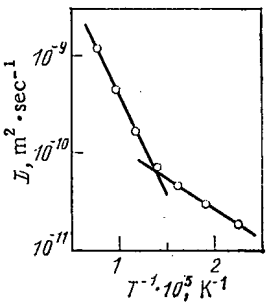

Fig. 1. Temperature dependence of the diffusion coefficient D(T) for the lithium impurity in boron carbide specimens: ○) experimental data.

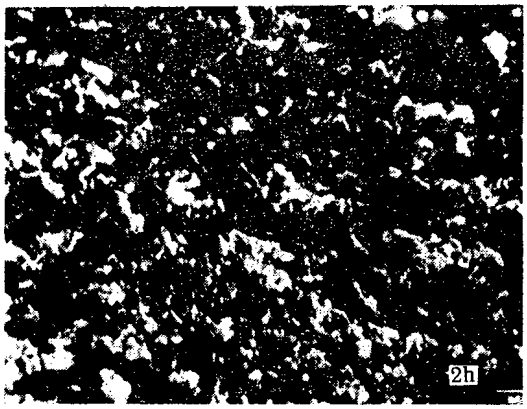

Fig. 2. Photomicrograph of the surface of a vacuum-pressed boron carbide specimen with a density of 2.35 g•cm^{-3} where lithium was introduced at 450°C over a period of 5 h. The photomicrograph was obtained by means of a Nanolab-7 scanning electron microscope, manufactured by the OPTON company, using an accelerating voltage of 15 kV.

pressing in a vacuum. As is known [7], the presence of two straight segments is a consequence of volume diffusion at 550-1100°C and boundary diffusion at temperatures of up to 350°C. In the 350-550°C range, these two mechanisms compete with each other.

Figure 2 shows the photomicrograph of the surface of a vacuum-pressed boron-carbide specimen with a density of 2.35 g•cm^{-3} after diffusion annealing at 450°C over a period of 5 h. It is evident that lithium has penetrated not only along the pores and intergranular boundaries, but also directly through polycrystalline grains.

Processing of the experimental data yielded $D_0 \approx 3\cdot10^{-8}$ m^2•sec^{-1} and $E_D \approx 0.37$ eV for the high-temperature range. In the low-temperature range of the curve, these values are equal to $D'_0 \approx 5\cdot10^{-10}$ m^2•sec^{-1} and $E_D' \approx 0.13$ eV. It should be mentioned that the maximum relative error in determining the value of D_0 is equal to ~16%, while the error in determining E_D amounts to ~32%; the confidence coefficient of the results obtained is equal to 0.86 and 0.65, respectively.

The temperature dependence of the diffusion coefficients for lithium in boron carbide with a density of 2.35 g•cm^{-3}, obtained by hot pressing in a vacuum, can be expressed by means of the equation

$$D(T) = 3\cdot10^{-8}\exp\{-0.37/kT\} + 5\cdot10^{-10}\exp\{-0.13/kT\}, \quad (2)$$

where k is the Boltzmann constant, and T is the temperature (°K).

As lithium is introduced diffusively in boron carbide, the thermal conductivity coefficient of cylindrical specimens first increases considerably. For instance, with low-temperature diffusive introduction of lithium into hot-pressed boron carbide specimens of elevated purity (with a total impurity content of ~1 mass %), the thermal conductivity coefficient

measured by means of the steady-state flux method increases on the average by a factor of 1.2-1.7. However, the thermal conductivity coefficient decreases with a further increase in the lithium percentage. Lithium probably improves the heat transfer between crsytalline grains when the lithium percentage is negligible (up to 3 mass %), while, with a further increase in the lithium percentage, the thermal conductivity diminishes as the dimensional stability is disturbed.

In conclusion, we extend our thanks to I. A. Bairamashvili for his assistance in this investigation.

LITERATURE CITED

1. P. D. Kervalishvili, At. Énerg., 51, No. 2, 123 (1981).
2. V. I. Mikheev, F. I. Shamrai, and K. Ya. Krylov, Zh. Neorg. Khim., 2, No. 6, 1223 (1957).
3. D. Secrist and W. Childs, "Investigation of lithium-boron system," US Atom. Energy Comp., TID 17149 (1962).
4. D. R. Secrist, Am. Ceram. Soc., 50, No. 10, 520 (1967).
5. R. Naslain, "Preparation de bor pur sous les formes rhomboedriques α et β des borures alcalins," Doctures Sciences Physiques Thesis, No. 188, Paris (1967).
6. B. S. Bokshtein, S. Z. Bokshtein, and A. A. Zhukhovitskii, Thermodynamics and Kinetics of Diffusion in Solids [in Russian], Metallurgiya, Moscow (1974).
7. B. I. Boltaks, Diffusion and Point Defects in Semiconductors [in Russian], Nauka, Leningrad (1972).

DIFFUSION OF ^{103}Ru AND ^{95}Zr FISSION PRODUCTS IN MONOCRYSTALLINE TUNGSTEN

D. K. Daukeev, Zh. R. Zhotabaev, R. T. Musurmankulov, and N. A. Reutova

UDC 539:219.3-173.8

An investigation of the diffusion of fission products in monocrystalline tungsten is of certain interest in connection with the development of thermoemissive converters with nuclear fuel [1]. A knowledge of the diffusion parameters of fission products, including ruthenium and zirconium, will allow the buildup of the corresponding fission products on the surface of the emitter to be calculated. A similar investigation was conducted for tungsten, deposited by the decomposition of the fluoride [2]. The calculated values of the activation energy Q were calculated for the diffusion of zirconium in tungsten [3]. The calculation of Q for both elements was carried out using the generalized correlation relation [4], connecting the diffusion parameters with the thermodynamic properties of metals, and for its derivation it was postulated that diffusion is accomplished by monovacancies and that the entropy of migration during diffusion of impurity substitution atoms is much less than the entropy of formation of vacancies. The energy of diffusion activation, determined experimentally [2], was found to be significantly less than the calculated value [3, 4]. Because of this, the coefficients of diffusion D of the fission products ^{103}Ru and ^{95}Zr in monocrystalline tungsten were measured.

Samples for the investigation were prepared by the well-known procedure [5]. Diffusion annealing was carried out in a vacuum of $4 \cdot 10^{-5}$ Pa at a temperature of 1900-2200°K during 30-100 h. The distribution of the implanted fission products before and after diffusion annealing was determined by taking thin layers from the samples by electropolishing and measuring the relative number of fission products by the γ-spectrometric method. The integrated distribution curves of the diffusing elements before and after annealing, determined in this way, are shown in Fig. 1.

The diffusion coefficients were determined by achieving the best coincidence between the experimental and calculated [6] distributions (Table 1). The values of the energy of activation Q, obtained by the method of least squares, are given in Table 2. From their comparison with the data published in [2], it was established that for tungsten deposited from the gas-

Translated from Atomnaya Énergiya, Vol. 57, No. 1, pp. 53-54, July, 1984. Original article submitted July 11, 1983.

0038-531X/84/5701-0491$08.50

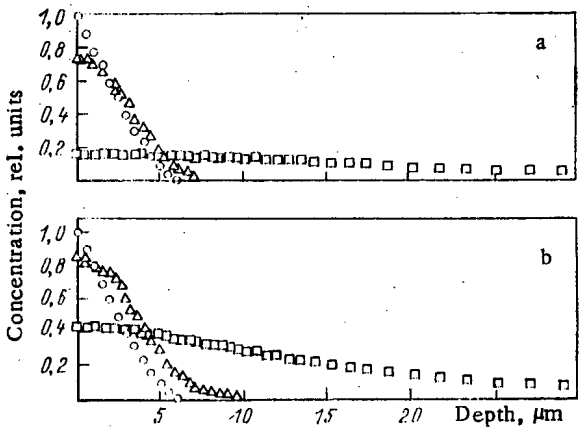

Fig. 1. Integrated distribution of ^{95}Zr (a) and ^{103}Ru (b) in monocrystalline tungsten: ○) original; △, □) after annealing at 1913 and 2118°K, respectively.

TABLE 1. Experimentally Determined Coefficients of Diffusion D, cm^2/sec

T, K	D_{Ru}	D_{Zr}
2178	$(7,14\pm4,28)\cdot10^{-12}$	$(7,06\pm4,24)\cdot10^{-12}$
2118	$(7,39\pm4,43)\cdot10^{-12}$	$(7,09\pm4,25)\cdot10^{-12}$
2118	$(8,34\pm5,00)\cdot10^{-12}$	$(6,34\pm3,80)\cdot10^{-12}$
2098	$(4,89\pm2,93)\cdot10^{-12}$	$(4,66\pm2,80)\cdot10^{-12}$
2098	$(4,81\pm2,89)\cdot10^{-12}$	$(4,33\pm2,60)\cdot10^{-12}$
1983	$(4,70\pm2,82)\cdot10^{-13}$	$(5,85\pm3,51)\cdot10^{-13}$
1953	$(1,09\pm0,65)\cdot10^{-12}$	$(6,71\pm4,03)\cdot1^{-13}$
1953	$(7,25\pm4,35)\cdot10^{-13}$	$(4,7\pm2,82)\cdot10^{-13}$
1913	$(8,29\pm4,97)\cdot10^{-14}$	$(8,08\pm4,85)\cdot10^{-14}$
1913	$(1,77\pm1,06)\cdot10^{-13}$	$(1,07\pm0,64)\cdot10^{-13}$
1873	$(6,05\pm3,02)\cdot10^{-13}$	$(4,92\pm2,95)\cdot10^{-13}$

TABLE 2. Values of the Energy of Activation Q

Element	Q, kJ/(g·atom)	Source
Ru	171,7	Expt. [2]
	464,4	Calc. [4]
	451,2±106,1	Expt. (present paper)
Zr	165	Expt. [2]
	427,1	Calc. [3]
	430,9	Calc. [4]
	501±91,7	Expt. (present paper)

eous phase, predominant diffusion is observed apparently around the boundaries of the columnar grains. At the same time, there is poor coincidence between the data obtained and the calculated values of the energy of activation of [3, 4], which indicates a vacancy mechanism of diffusion of ruthenium and zirconium in monocrystalline tungsten.

LITERATURE CITED

1. E. M. Savitskii, K. B. Povarova, and P. V. Makarov, Metallurgy of Tungsten [in Russian], Metallurgiya, Moscow (1978).
2. L. Young and R. Hudson, Penetration of Fuel and Fission Products through Tungsten, Deposited from the Gaseous Phase. Direct Conversion of Thermal Energy into Electrical Energy and Fuel Elements [Russian translation], Inf. Byul., 6(83), 173 (1969).

3. K. B. Povarova, Izv. Akad. Nauk SSSR, Met., No. 2, 163 (1981).
4. V. N. Zagryazkin, At. Énerg., 48, No. 3, 177 (1980).
5. E. S. Bekmukhambetov et al., At. Énerg., 53, No. 4, 265 (1982).
6. E. S. Bekmukhambetov et al., Fiz. Met. Metalloved., 46, No. 1, 192 (1978).

OPTIMIZING REACTOR POWER DISTRIBUTION WITH A RESTRICTED NUMBER OF SIMULTANEOUSLY DISPLACED CONTROL RODS

A. M. Afanas'ev

UDC 621.039.56

Algorithms have been given [1-4] for calculating the positions of control rods (CR) such that the energy distribution (ED) is optimal. As a rule, the transition to the optimal state requires many CR to be displaced. Even if the ED distribution is small, the number of these rods is equal to the number of working ones (those not at the end stops), which usually constitute more than half of the CR. As it is impossible to set a large number of CR in the required positions simultaneously with the reactor running, and no information is given on the displacement sequence in [1-4], it may prove difficult to attain the optimum. On the other hand, arbitrary displacement of the CR without reducing the reactor power may lead to the limiting power being exceeded in some of the channels. Here we consider an ED optimization algorithm subject to a constraint on the number of simultaneously displaced CR. The calculation amounts to successive solution of a series of problems, in each of which not more than L of the CR will be involved in the optimization. The number of these CR is selected from the total number M. The selection is made by examining the effects of changing the CR position on the optimum. When each problem has been solved, one determines the sequence in displacing the selected CR. On transferring from problem m to problem m + 1, the influence functions used in the optimization are modified. The new functions are calculated from the known ones and the values of the controls obtained from the solution for job m.

Formulation and Method of Solution. We use the symbols of [3] and [4] to formulate the problem as follows: We assume that for the operator given h(r) we know the stationary ED $N_0(\mathbf{r})$, the influence functions $\Psi_j(\mathbf{r})$, and the values of ν_j, from which we have to find the controls ρ_j characterizing the CR displacement to satisfy

$$\hat{H}N + \sum_{j=1}^{M} \rho_j F_j N = 0; \quad \int N\,d\mathbf{r} = Q; \tag{1}$$

$$\alpha_j \leqslant \rho_j \leqslant \beta_j; \quad j = 1, 2, \ldots, M \tag{2}$$

which provide a maximum in the function of

$$Z[N] = \min_i \left[\left(1 - \frac{N(\mathbf{r}_i)}{\Pi_i}\right) \frac{1}{\sigma_i} \right]. \tag{3}$$

In (1)-(3), $F_j(\mathbf{r})$ is the function for the spatial localization of control j and $F_j(\mathbf{r}) = \delta(\mathbf{r} - \mathbf{r}_j)$, while Q, α_j, and β_j are given values, with Π_i the threshold value at which the channel with coordinate r_i will be damaged, and σ_i is the error with which the damage margin is known.

In addition to (1)-(3) we introduce the requirement that not more than L rods may participate simultaneously in the optmization.

The problem is solved by steps. First we use the constraint on the number of CR to determine $\rho_j^{(1)}$ and $N^{(1)}(\mathbf{r})$. Then only the $\rho_{j_1}^{(1)}$ will differ from zero, where $j1 \in \varnothing_{j_1}$. By $\varnothing_{JS}$ we denote certain sets consisting of JS numbers of CR, with JS $\leqslant$ L. In the general case, $N^1(\mathbf{r})$ does not correspond to the optimum ED, since the optimization is performed with less than M CR. In the new state of the reactor obtained by changing the controls by $\rho_j^{(1)}$, we use the known $\Psi_j(\mathbf{r})$ and $\rho_{j_1}^{(1)}$ to calculate the new functions $\Psi_j^{(1)}(\mathbf{r})$. The latter are used to solve the next optimization and determine $N^{(2)}(\mathbf{r})$ and $\rho_{j_2}^{(2)}$, where $j2 \in \varnothing_{J2}$, and so on. We note that

Translated from Atomnaya Énergiya, Vol. 57, No. 1, pp. 54-56, July, 1984. Original article submitted December 12, 1983.

0038-531X/84/5701-0493$08.50

the sets $\varnothing_{J1}$ and $\varnothing_{J2}$ may contain identical numbers of CR. The optimization is continued until the solution in case n for a given number ε_p obeys the inequality

$$|\rho_{jn}^{(n)}| \leqslant \varepsilon_p (\beta_{jn} - \alpha_{jn}), \quad jn \in \varnothing_{Jn}. \tag{4}$$

After each problem is solved, the sequence of CR displacement is determined. Priority is given to that control whose change does not displace the automatic regulator AR beyond the given constraints and has the best effect on the ED. The following problem is solved at step m:

$$\max Z^{(m)}; \tag{5}$$

$$\hat{H}^{(m-1)} N^{(m)} + \sum_{j=1}^{M} \rho_j^{(m)} F_j N^{(m)} = 0; \quad \int N^{(m)}\, d\mathbf{r} = Q; \tag{6}$$

$$\alpha_j^{(m-1)} \leqslant \rho_j^{(m)} \leqslant \beta_j^{(m-1)}, \tag{7}$$

subject to the constraint that the number $\rho_j^{(m)} \neq 0$ is not more than L, where

$$Z^{(m)} = Z[N^{(m)}]; \quad \hat{H}^{(m-1)}(\mathbf{r}) = \hat{H}^{(m-2)}(\mathbf{r}) + \sum_{j=1}^{M} \rho_j^{(m-1)} F_j(\mathbf{r}); \tag{8}$$

$$\hat{H}^{0}(\mathbf{r}) = \hat{H}(\mathbf{r});$$

$$\alpha_j^{(m-1)} = \alpha_j^{(m-2)} + \rho_j^{(m-1)}; \quad \alpha_j^{(0)} = \alpha_j;$$

$$\beta_j^{(m-1)} = \beta_j^{(m-2)} - \rho_j^{(m-1)}; \quad \beta_j^{(0)} = \beta_j.$$

We represent the solution of (6) in the form

$$N^{(m)}(\mathbf{r}) = N^{(m-1)}(\mathbf{r}) + \sum_{j=1}^{M} \rho_j^{(m)} G_j(N^{(m)})\, \Psi_j^{(m-1)}(\mathbf{r}), \tag{9}$$

where $N^{(m-1)}$ and $\Psi_j^{(m-1)}$ are calculated at stage $m-1$ and satisfy the equations

$$\hat{H}^{(m-1)} N^{(m-1)} = 0; \quad \int N^{(m-1)}\, d\mathbf{r} = Q \quad \text{and} \quad N^{(0)}(\mathbf{r}) = N_0(\mathbf{r}); \tag{10}$$

$$\hat{H}^{(m-1)} \Psi_j^{(m-1)} = -F_j N_0 + \nu_j^{(m-1)} \mathcal{F} N_0; \quad \int \Psi_j^{(m-1)}\, d\mathbf{r} = 0$$

$$\text{and } \Psi_j^{(0)}(\mathbf{r}) = \Psi_j(\mathbf{r}), \quad \nu_j^{(0)} = \nu_j. \tag{11}$$

From (10) and (11) we have that (9) causes (6) to become zero if

$$G_j(N^{(m)}) = G_j^{(m)} = \frac{N^{(m)}(\mathbf{r}_j)}{N_0(\mathbf{r}_j)}; \tag{12}$$

$$\sum_{j=1}^{M} \rho_j^{(m)} G_j^{(m)} \nu_j^{(m-1)} = 0. \tag{13}$$

On substituting (9) into (6), the task amounts to maximizing $Z^{(m)}$ subject to the constraint of (8) and the following inequalities:

$$Z^{(m)} + \frac{1}{\Pi_i \sigma_i} \sum_{j=1}^{M} \tilde{\rho}_j^{(m)} \Psi_{ji}^{(m-1)} \leqslant Z_{0,i}^{(m-1)}, \quad i = 1, 2, \ldots, K; \tag{14}$$

$$\sum_{j=1}^{M} \tilde{\rho}_j^{(m)} \nu_j^{(m-1)} = 0; \tag{15}$$

$$\alpha_j^{(m-1)} G_j^{(m)} \leqslant \tilde{\rho}_j^{(m)} \leqslant \beta_j^{(m-1)} G_j^{(m)}, \tag{16}$$

where

$$\tilde{\rho}_j^{(m)} = \rho_j^{(m)} G_j^{(m)}; \quad N_i^{(m)} = N_i^{(m-1)} + \sum_{j=1}^{M} \tilde{\rho}_j^{(m)} \Psi_{ji}^{(m-1)};$$

$$Z_{0,i}^{(m-1)} = \left(1 - \frac{N_i^{(m-1)}}{\Pi_i}\right)\frac{1}{\sigma_i}; \quad N_i = N(\mathbf{r}_i);$$
$$\Psi_{ij} = \Psi_j(\mathbf{r}_i).$$

The values of $Z^{(m)}$, $\rho_j^{(m)}$, and $N_j^{(m)}$ are calculated by iteration using the scheme given in (4). The number of displaced CR is reduced after the first iteration, in accordance with the requirement of (8). One eliminates each CR by analyzing the effects on $Z^{(m)}$ from changes in $\rho_j^{(m)}$ to zero, where j = 1, 2, ..., M. Here, one initially uses dual estimators to determine the approximate values of $\Delta Z_j^{(m)}$ for $\rho_j^{(m)} \to 0$. Subsequently, these values are refined if necessary from the solution to the optimization problems subject to the additional condition $\rho_j^{(m)} = 0$. When the number of CR has been reduced by one, there are changes in the controls, the dual estimators, and the functional, so in the next stage all the operations to eliminate a new CR are repeated. The other iterations are performed on the basis of the CR selected for the control. After determining $\rho_{jm}^{(m)}$, where $jm \in \varnothing_{Jm}$, one calculates the new influence functions $\psi_j^{(m)}(\mathbf{r})$ and the values of $\nu_j^{(m)}$ satisfying the following equations:

$$\hat{H}^{(m-1)}\psi_j^{(m)} + \sum_{l \in \varnothing_{Jm}} \rho_l^{(m)} F_l \psi_j^{(m)} = F_j N_0 + \nu_j^{(m)} \mathcal{F} N_0; \quad \int \psi_j^{(m)} d\mathbf{r} = 0; \quad j = 1, 2, \ldots, M. \tag{17}$$

We put $\gamma_{jl}^{(m)} = \psi_j^{(m)}(\mathbf{r}_l)/N_0(\mathbf{r}_l)$ to write $\psi_j^{(m)}(\mathbf{r})$ in the form

$$\psi_j^{(m)}(\mathbf{r}) = \psi_j^{(m-1)}(\mathbf{r}) + \sum_{l \in \varnothing_{Jm}} \rho_l^{(m)} \gamma_{jl}^{(m)} \psi_l^{(m-1)}(\mathbf{r}). \tag{18}$$

After substituting this expression into (17) and using (11) we get

$$\nu_j^{(m)} = \nu_j^{(m-1)} + \sum_{l \in \varnothing_{Jm}} \rho_l^{(m)} \gamma_{jl}^{(m)} \nu_l^{(m-1)}. \tag{19}$$

From (18) we calculate $\psi_{jjm}^{(m)} = \psi_j^{(m)}(\mathbf{r}_{jm})$, where $j_m \in \varnothing_{Jm}$, and get the system of equations

$$\gamma_{jj_m}^{(m)}[N_{0,j_m} - \rho_{j_m}^{(m)}\psi_{j_m j_m}^{(m-1)}] - \sum_{l \in \varnothing_{Jm},\, l \neq j_m} \rho_l^{(m)} \psi_{lj_m}^{(m)} \gamma_{jl}^{(m)} = \psi_{jj_m}^{(m-1)}. \tag{20}$$

From (20) for each j = 1, 2, ..., M we determine the set of values of γ_{jj_m}, where $j_m \in \varnothing_{Jm}$. Then from (18) and (19) we derive $\psi_j^{(m)}(\mathbf{r})$ and $\nu_j^{(m)}$, which are used in solving problem m + 1. We note that to calculate $\psi_j^{(m)}(\mathbf{r})$ and $\nu_j^{(m)}$, where j = 1, 2, ..., M, it is necessary to invert the Jm × Jm matrix once, where $Jm \leq L$.

After each optimization step, one determines the displacement sequence for the selected CR. The reactor criticality is perturbed by displacing one CR, so we introduce the AR and solve the following equations:*

$$\hat{H}^{(m-1)}N^{(m)(j)} + \sum_{i \in \varnothing_{Jm}^{(n)}} \rho_i^{(m)} F_i N^{(m)(j)} + \rho_j^{(m)} F_j N^{(m)(j)} + \rho_{AR}^{(j)} F_{AR} N^{(m)(j)} = 0; \quad j \in \varnothing_{Jm}^{(k)}, \tag{21}$$

where $\varnothing_{Jm}^{(n)}$ and $\varnothing_{Jm}^{(k)}$ are sets of n and k CR for which correspondingly the sequence has been established and will be determined, with n + k = Jm, $\varnothing_{Jm}^{(n)} \cup \varnothing_{Jm}^{(k)} = \varnothing_{Jm}$. We introduce the new variables $\tilde{\rho}_l^{(m)(j)} = \rho_l^{(m)} N_{(\mathbf{r}l)}^{m(j)}/N_0(\mathbf{r}l)$, where l = i, j, and the AR, and write $N^{(m)(j)}(\mathbf{r})$ in the form

$$N^{(m)(j)}(\mathbf{r}) = N^{(m-1)}(\mathbf{r}) + \sum_{i \in \varnothing_{Jm}^{(n)}} \tilde{\rho}_i^{(m)(j)} \psi_i^{(m-1)}(\mathbf{r}) + \tilde{\rho}_j^{(m)(j)} \psi_j^{(m-1)}(\mathbf{r}) + \tilde{\rho}_{AR}^{(m)(j)} \psi_{AR}^{(m-1)}(\mathbf{r}), \tag{22}$$

where ψ_{AR}^{m-1} is the inverse function for the AR, which satisfies (11) with $F_j = F_{AR} = \delta(\mathbf{r} - \mathbf{r}_{AR})$. After substituting (22) into (21) we get the criticality condition

*The automatic regulator occupies the initial position after the displacement of all the CR selected at a given optimization step.

$$\sum_{i \in \mathcal{J}_{Jm}^{(n)}} \nu_i^{(m-1)} \tilde{\rho}_i^{(m)(j)} + \tilde{\rho}_j^{(m)(j)} \nu_j^{(m-1)} + \tilde{\rho}_{AR}^{(m)(j)} \nu_{AR}^{(m-1)} = 0. \qquad (23)$$

In accordance with (22) we write down the values of $N^{m(j)}(\mathbf{r})$ at the points $\mathbf{r}_j$ and $\mathbf{r}_{j_n}$, where $f_n \in \mathcal{J}_{Jm}^{(n)}$, to get a system composed of n + 1 equations. We solve this together with (23) and determine for each $j \in \mathcal{J}_{Jm}^{(k)}$ the sets of n + 2 values $\tilde{\rho}_{AR}^{(m)(j)}$, $\tilde{\rho}_j^{(m)(j)}$, and $\tilde{\rho}_{jn}^{(m)(j)}$. Then from (22) we recover $N^{(m)(j)}(\mathbf{r})$ and calculate $\rho_{AR}^{(j)}$. In accordance with the resulting $\rho_{AR}^{(j)}$, we select the number of the controls whose change by $\rho_j^{(m)}$ does not displace the AR beyond the limit.* For the latter from $N^{(m)(j)}(\mathbf{r})$ we calculate $Z^{(m)(j)}$ and assign to sequence n + 1 that CR for which the functional is largest.

This algorithm shows that to solve the problem one needs, as in [1-4], information on the initial ED $N_0(\mathbf{r})$ and the corresponding influence functions $\Psi_j(\mathbf{r})$ together with the values of ν_j, where j = 1, 2, ..., M as well as on the influence function for the AR.

The algorithms given here have been used with the OPTIMA program [4] written in FORTRAN for the BÉSM-6 as the OPTIMA-2 program. To solve the problem with this program requires virtually the same volume of executive store as for the OPTIMA one. The OPTIMA-2 program handles the same problem as in [4].

LITERATURE CITED

1. I. Ya. Emel'yanov et al., At. Énerg., 44, No. 4, 310 (1978).
2. O. L. Bozhenkov et al., ibid., 51, No. 2, 91 (1981).
3. A. A. Anikin and Ya. V. Shevelev, Nuclear Science and Engineering, Series Reactor Physics and Engineering [in Russian], Issue 3(12), 35 (1980).
4. A. M. Afanas'ev, At. Énerg., 54, No. 5, 368 (1982).

*If necessary, one can calculate $\rho_{AR}^{(j)}$ and $N^{(m)(j)}(\mathbf{r})$ initially as corresponding to the partial change in control j.

ANOMALOUS EFFECTS OF SMALL DOSES OF IONIZING RADIATION IN METALS AND ALLOYS

I. P. Chernov, A. P. Mamontov,
A. A. Botaki, P. A. Cherdantsev,
B. V. Chakhlov, and S. R. Sharov

UDC 621.039.83

Systematic studies have been made on the effects of small ionizing-radiation doses on defective semiconductor crystals, which have revealed an interesting feature: γ-ray doses of 10^4-10^6 R (1 R = $2.58 \cdot 10^{-4}$ Ci/kg) or an electron flux of 10^{12}-10^{14} cm^{-2} does not increase the number of defects but instead reduces it and produces structure ordering [1]. The number of defects eliminated can be determined from the backscattering of channeled charged particles, and this exceeds the number of electron–hole pairs produced by a factor 10. This indicates that the ordering is produced by chain reactions between defects initiated by the ionization [2, 3]. One naturally seeks to establish whether a similar ordering occurs in metals and alloys. For this purpose we have examined the effects of ^{60}Co γ rays on copper, tungsten and VK alloys.

Copper is a good model material, and extensive evidence has been published on the effects of large ionizing-radiation doses on its physical properties. To avoid possible effects from the semiconducting compounds CuO and WO, the specimens were analyzed for oxygen by an activation method. We used copper foil of thickness $1.4 \cdot 10^{-5}$ m and wire of diameter $2 \cdot 10^{-5}$ m, as well as sheet tungsten of thickness $1 \cdot 10^{-3}$ m of grade V-ML, in which the atomic proportion of oxygen did not exceed 10^{-2}%. To introduce additional defects, the copper specimens were quenched by heating them in argon to 600°C and cooling them in water at 3-4°C. The tungsten specimens were cut with a diamond disk. The VK-6 and VK-8 alloys had branched WC–Co interfaces with elevated defect contents. We used standard rods and also parallelepipeds of size 0.25 × 0.25 × 3.5 cm with a diamond wheel from tools for working materials. The faces of the parallelepiped were then ground with diamond paste.

The changes in defectiveness produced by the ionizing radiation were monitored by measuring the specific resistance ρ at a known temperature. In that case, the change in specific resistance $\Delta\rho$ is directly related to the change in defect concentration ΔC [4]:

$$\Delta\rho = 2\pi m v \Delta C r^2 / n e^2,$$

where n is the number of electrons in unit volume; e, v, and m, electron charge, velocity, and mass; and r, effective radius of the scattering centers.

The specimens were irradiated with a cobalt source giving a dose rate of 278 R/sec. When the set dose had been reached at room temperature, the specimens were placed in a thermostat maintained at 295°K. At this temperature we measured $\Delta\rho$ by a two-probe method with an R363 dc potentiometer. The difference $\Delta\rho$ was determined by comparing the ρ for the irradiated and unirradiated specimens. The error in determining $\Delta\rho$ was estimated from the repeated measurements on a single specimen as not more than 0.2%. The $\Delta\rho = f(D)$ relation for copper was also measured at liquid-nitrogen temperature. The results obtained at 295 and 78°K agreed within the errors of the measurements.

Two interesting facts were observed: firstly, low doses reduced the specific resistance (Fig. 1 and Table 1), and secondly, the defects continued to alter after the irradiation. Figure 2 indicates that the relaxation time was 60-80 h. The $\Delta\rho$ measurements enabled us to determine the number of defects eliminated. The averaged data indicated that 1% of point defects (8.45×10^{20} cm^{-3}) raised the specific resistance of copper by 1.7-7 $\mu\Omega \cdot cm$, or by 100-400% relative to ρ at 25°C. Then ΔC for quenched copper is $(5 \pm 3) \times 10^{18}$ cm^{-3}, while for tungsten it is ~10^{19} cm^{-3}.

Translated from Atomnaya Énergiya, Vol. 57, No. 1, pp. 56-58, July, 1984. Original article submitted January 9, 1984.

0038-531X/84/5701-0497$08.50

TABLE 1. Reduction in Specific Resistance

Specimen	Dose, R	ρ, %
Quenched copper	$5 \cdot 10^5$	1,0—1,5
Tungsten 0,3×0,1×3,5 cm	$2 \cdot 10^5$	5,0
VK-8 0,25×0,25×3,5 cm	$4 \cdot 10^5$	10—13
VK-8, rods 0.25 × 0.25 × 3.0 cm	$4 \cdot 10^5$	6—8

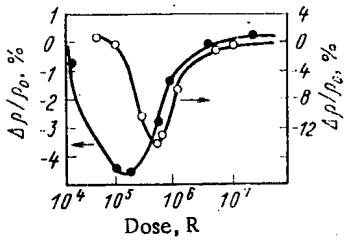

Fig. 1

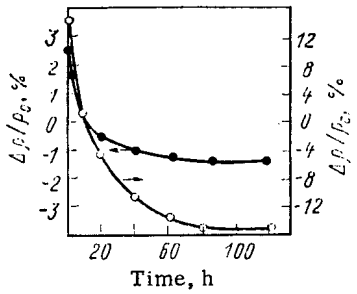

Fig. 2

Fig. 1. Dependence of the change in specific resistance on dose for tungsten (●) and VK-8 alloy (○).

Fig. 2. Relaxation in specific resistance after irradiation to $5 \cdot 10^5$ R for VK-8 (○) and $5 \cdot 10^4$ R for (●).

There was found to be a complete analogy between the effects of γ rays on semiconductors and metals with defect structures. In both cases, the largest number of defects was eliminated for γ doses in the range 10^4-10^6 R (10^5 R for AsGa, $2 \cdot 10^5$ R for W, $5 \cdot 10^4$ R for quenched copper, and $5 \cdot 10^5$ R for VK-8); there were also relaxation processes that continued for several days after the end of the irradiation. The Frenkel' defects formed on irradiation were few in number (10^{12}-10^{14} cm^{-3}) and could not have an appreciable effect on the structure rearrangement.

Less than a thousandth of the atoms would be ionized at these doses, so only a minute number of defects would be eliminated by the annihilation of the primary-ionization defects (5×10^{14} cm^{-3} in copper and 10^{16} cm^{-3} in tungsten). However, experiment shows that the number of defects eliminated is 1000 times larger. This means that there are conditions favorable to accentuating the effects of ionization on defect annihilation in metals.

The lifetimes of particle—hole pairs in metals are very short (10^{-16} sec), so recombination occurs essentially at the point where the pair is produced, and weak ionization does not affect the properties. However, if the structure is highly defective, the point defects may group together and produce a perturbation potential W(r) for electrons in the conduction band. If one represents the perturbation potential as a one-dimensional periodic function $W(x) = \lambda \cos(2qx/\hbar)$, there are two periodicities acting on the electron: one related to the lattice period and the other caused by the quasiperiodic disposition of the defect groups. In accordance with perturbation theory [5], energy gaps of width $\Delta \sim \lambda$ appear in the continuous spectrum (or in the conduction band of the metal) at energy $E_n = n^2q^2/2m$ ($n = 1, 2, \ldots$). The occurrence of a gap in the spectrum should reduce the conductivity, as is observed. Also, one can calculate the particle—hole lifetime τ by the method of Van Roosbrooch and Shockley [6], which gives

$$\tau = \exp \lambda/T,$$

where T is the temperature in energy units. Consequently, the particle–hole pair lifetime increases considerably in a metal with a defective structure, and a pair has time to interact with defect groups and be captured. In that case, as in a semiconductor, the charge is localized at the defect groups, which prevent annihilation. Therefore, low ionizing-radiation doses (10^4-10^7 R) acting on metals and alloys with highly defective structures initiate reduction in the number of defects and produce ordering.

LITERATURE CITED

1. I. P. Chernov et al., Fiz. Tekh. Poluprovodn., 14, 2271 (1980).
2. P. A. Cherdantsev, I. P. Chernov, and A. P. Mamontov, ibid., 16, 480 (1982).
3. P. Cherdansev, I. Chernov, and A. Mamontov, Rad. Effects, 60, 67 (1982).
4. M. S. Koval'chenko et al., Radiation Damage to Refractory Compounds [in Russian], Atomizdat, Moscow (1979).
5. D. I. Blokhintsev, The Principles of Quantum Mechanics [in Russian], Nauka, Moscow (1976).
6. W. Van Roosbrooch and W. Shockley, Phys. Rev., 94, 1558 (1954).

CHANGES IN THE STRUCTURE OF VK ALLOY PRODUCED BY LOW γ-RAY DOSES

I. P. Chernov, Yu. A. Timoshnikov,
A. P. Mamontov, V. A. Korotchenko,
I. A. Lapsker, and B. S. Semukhin

UDC 621.039.83

It has been found [1, 2] that defects are eliminated and the structure is ordered in a defective semiconductor or metal by low γ-ray doses (10^4-10^7 R, 1 R = $2.58 \cdot 10^{-4}$ Ci/kg) when less than a hundredth of the atoms are ionized, which is evidently possible only by the release of stored energy, for example, by chain defect annihilation [3, 4] initiated by the ionization.

We have examined the heat production and structural changes occurring on irradiating VK-8 alloy with low γ-ray doses. The REM-200 scanning electron microscope showed that the specimens of VK-8 contained tungsten carbide particles in the form of polyhedral prisms or cylinders with transverse dimensions of 1-10 μm. According to published data [5], the defective regions in this alloy are localized at the WC–Co boundaries.

If the number of defects is reduced by ionizing radiation as a result of defect annihilation or rearrangement, there should be some accompanying heat release. Therefore, one expects that the temperature of the specimen in the first cycle will be different from those in subsequent ones, since in each successive irradiation cycle there will be only heating by the radiation. The specimens were irradiated with ^{60}Co γ rays at a dose rate of 278 R/sec. A VK-8 specimen of size 1 × 1.5 × 8 cm was placed in a thermally insulated cell taking the form of two foam-plastic vessels of different sizes inserted one in the other. The free space between them was filled with insulating material. The cover was also made of foam plastic and had two holes for inserting a thermocouple.

The specimen temperature was measured with a differential Chromel–Copel thermocouple. The temperature of the reference junction was kept at the melting point of ice, and this was outside the irradiation zone. Reliable thermal contact between the working junction and the specimen was provided by indium–gallium alloy. A PP-63 potentiometer recorded the thermocouple. The error in temperature measurement was not more than ±0.5°C.

Check experiments were performed with silicon and gallium arsenide as well as with annealed copper, whose temperatures should be affected only by the radiation heating, and the differences between the heating curves in successive irradiation cycles of duration ~20 h each did not exceed 0.5°C. For the VK-8 specimens, the temperature varied from 28 to 61°C in the first cycle and from 28 to 58°C in the subsequent ones, i.e., the differences in the final

Translated from Atomnaya Énergiya, Vol. 57, No. 1, pp. 58-59, July, 1984. Original article submitted January 9, 1984.

0038-531X/84/5701-0499$08.50

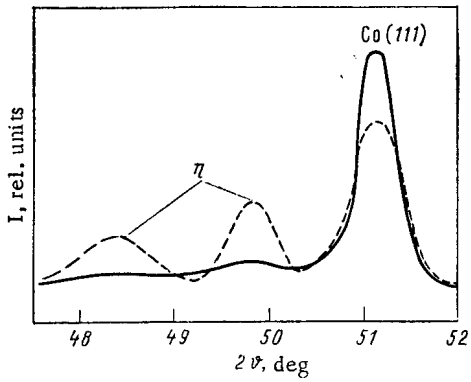

Fig. 1. Parts of the x-ray patterns from VK-8 alloy before irradiation ———) and after irradiation -----).

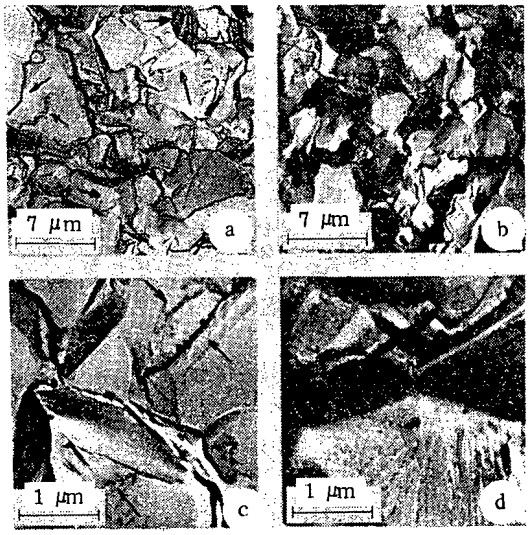

Fig. 2. Failure surfaces of VK-8 alloy in the initial state (a and c) and the irradiated state (b and d), carbon replica, platinum shadowing, arrows indicating chains of pores.

temperature were ~3°C. In such an experiment, one measures the average temperature, and this does not rule out local heating to a higher temperature, for example as a result of chain reactions between defects [3, 4] in regions with high defect concentrations (here at the WC–Co boundaries), where the structure of the material may change.

We examined the structure of specimens in the form of plates 1.5 × 1.0 × 0.1 cm cut by electrospark working using DRON 1.5 and DRON 0.5 diffractometers with filter Cu K_α and monoenergetic Fe K_α radiations. An SM-1 computer calculated the lattice parameters and performed the indexing.

As would be expected, the specimens consisted in the main of tungsten carbide and cobalt. The tungsten carbide had a hexagonal lattice whose parameters varied between specimens within the following limits: a = 2.905–2.907 Å, c = 2.837–2.838 Å (1 Å = 10^{-10} m). The cobalt had a cubic AI lattice with unit-cell parameter a = 3.565–3.562 Å.

After γ-ray irradiation to $2 \cdot 10^7$ R, reflections from a new phase appeared (Fig. 1). The published data and the computer indexing demonstrate that these reflections correspond to a ternary compound, the η_2 phase of variable composition having the chemical formula Co_xW_yC. This phase has a cubic O_h lattice with parameter a = 10.8–10.9 Å [6].

To identify the compound, the initial and irradiated specimens were examined by secondary-ion mass spectrometry. The primary beam was provided by nitrogen ions of energy 3.2 keV, and the current density at the target was $5 \cdot 10^{-7}$ A/cm^2. The secondary ions were filtered for energy by a cylindrical analyzer with a resolution of $\Delta E/E$ = 0.01 and were then analyzed by a

mass separator with a resolution of 200. The mass spectra of the irradiated specimens showed peaks corresponding to CoWC ions, which were absent from those for the initial specimens.

The production of the new phase and the change in defectiveness altered the cracked surfaces. This was confirmed by examining the surfaces by replica methods with a ÉVM-100L transmission electron microscope with a resolution of 20 Å.

Figure 2 shows planar surfaces for an initial specimen (a and c) and one irradiated with γ rays to a dose of 10^7 R (b and d). There are the following characteristic features in the surfaces of the initial specimens:

1) pores in the tungsten carbide particles along the curved edges of the cleavage planes and also at the WC-Co boundaries;

2) brittle failure in the tungsten carbide particles (failure surface smooth without ridges or signs of stream patterns); and

3) viscous failure in the cobalt bonding. Regions of stretching around the tungsten carbide particles are seen, which indicates that the material was in a compound state of strain and that cracks propagated, so the failure occurred along the most effective WC—Co boundaries.

Irradiation substantially altered the characteristics of the fracture: firstly, the pores along the edges of the cleavage planes vanished, and they diminished in number at the WC—Co boundaries; second, elements of viscous fracture appeared at the surfaces of the tungsten carbide: ridges and stream patterns; and thirdly, the stretching of the cobalt bonding around the tungsten carbide particles was reduced.

Therefore, the ordering in VK alloy at low doses is accompanied by a rise in temperature and considerable structural changes. The most marked changes are pore healing and the production of the new phase η_2 CoWC, which occurred in regions of high defect concentrations such as WC—Co boundaries. It seems that these structural changes are due to local heating caused by chain reactions between defects.

LITERATURE CITED

1. I. P. Chernov et al., Fiz. Tekh. Poluprovodn., 14, 2271 (1980).
2. I. P. Chernov et al., At. Énerg., 57, No. 1 (1984) (This issue).
3. P. A. Cherdantsev, I. P. Chernov, and A. P. Mamontov, Fiz. Tekh. Poluprovodn., 16, 480 (1982).
4. P. Cherdansev, I. Chernov, and A. Mamontov, Rad. Effects, 60, 67 (1982).
5. I. N. Chaporova and K. S. Chernyavskaya, The Structures of Sintered Hard Alloys [in Russian], Metallurgiya, Moscow (1975).
6. V. I. Tret'yakov, Principles of the Metallorgraphy and Production Technology of Sintered Hard Alloys [in Russian], Metallurgiya, Moscow (1976).

PARAMETERS OF NEUTRON RESONANCES OF ^{108}Cd

V. A. Anufriev, S. I. Babich,
V. N. Nefedov, and N. G. Kocherygin

UDC 621.039.556

The results of an investigation of the total neutron cross section of ^{108}Cd in the 0.3-400-eV range of neutron energy are presented in this paper. Study of the energy dependence of the cross section of ^{108}Cd is of undoubted practical interest due to the need to select the optimal conditions for reactor accumulation of ^{109}Cd ($T_{1/2}$ = 453 days), which is used for the fabrication of x-radiation sources. The published data on the neutron cross section of ^{108}Cd are limited only to values of σ_γ (E_0 = 0.025 eV) and I_γ obtained from integrated measurements [1, 2]. For the present the only measurements of the energy dependence of the ^{108}Cd cross section have been carried out by the authors of [3], in which most of the attention was devoted only to the cross section in the thermal range of neutron energies.

The neutron resonances of ^{108}Cd have been investigated by measurement of the transmission of a cadmium sample enriched in ^{108}Cd (57.5%). The energy dependence of the transmission was measured with the neutron spectrometer of an SM-2 reactor using the time-of-flight method [4]. The best resolution of the spectrometer for a time-of-flight baseline of 92 m was 58 nsec/m. The value of the background neutrons did not exceed 5%. Metallic cadmium (mass of 79 mg) mounted in a quartz tube with an inner diameter of 1.12 mm was used as the sample. Detailed information on the composition of the sample being investigated is given in Table 1.

It is shown in Fig. 1 how the transmission T of the cadmium sample in the 50-400-eV range depends on energy. Four levels of ^{108}Cd have been determined in the investigated range of neutron energies. The resonant levels were identified using the data on impurity cadmium isotopes recommended in [5]. The parameters of the levels calculated by the "shape" method are given in Table 2 in comparison with the data of [3].

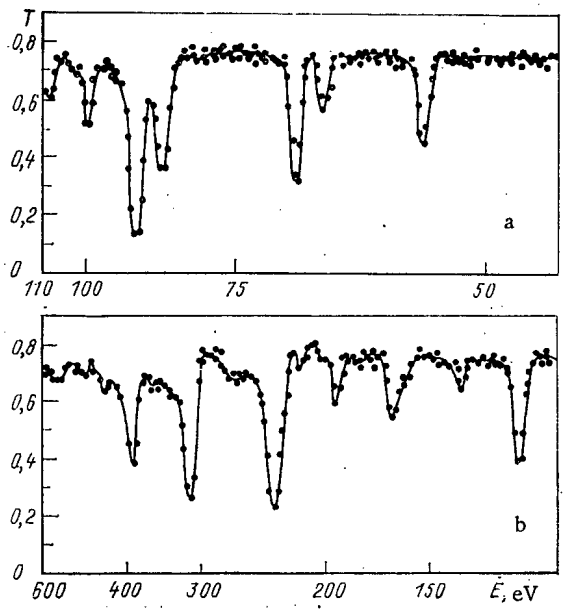

Fig. 1. Energy dependence of the transmission of the cadmium sample at an energy of (a) 50-110 and (b) 110-400 eV; ———) fitting result using the resonance parameters given in Table 2; ●) experimental values of the transmission as a function of energy.

Translated from Atomnaya Énergiya, Vol. 57, No. 1, pp. 59-60, July, 1984. Original article submitted January 13, 1984.

 0038-531X/84/5701-0502$08.50

TABLE 1. Characteristics of Cadmium

Isotope	Isotopic composition, %	Content of isotope, 10^4 atoms/b*
^{106}Cd	0,35	1,58
^{108}Cd	57,5±1,8	255±7
^{110}Cd	6,72	29,3
^{111}Cd	5,74	24,8
^{112}Cd	12,46	53,3
^{113}Cd	4,33	18,4
^{114}Cd	11,14	46,8
^{116}Cd	1,76	7,3

*1 b = 10^{-28} m^2.

TABLE 2. Parameters of the Neutron Resonance of ^{108}Cd

Data of this paper			Data of [3]		
E_0, eV	Γ, meV	$2g\Gamma_n$, meV	E_0, eV	Γ, meV	$2g\Gamma_n$, meV
54,2±0,4	115±45	0,63±0,03	54,3	100	0,7
233,6±3,5	345±48	384±50	234	100	490±60
312±5	500±128	710±60	314	100	1070±150
337±5	110*	4,3±0,5	—	—	—

*Assumed value of Γ.

As follows from Table 2, a discrepancy with the data of [3] is observed in the values of Γ_n for the level with E_0 = 312 eV. A possible cause of the overestimation of the value of Γ_n in [3] can be assumed to be insufficient resolution of the spectrometer used in this range of neutron energies. In addition we were the first to detect the level with E_0 = 337 eV, which we assign to ^{108}Cd.

Using the resonance parameters, the two-group constants of ^{108}Cd were calculated: the resonance capture integral I_γ = 12 ± 2 b, and the capture cross section for E_0 = 0.025 eV is σ_γ = 0.20 ± 0.03 b. The calculated value of the capture cross section differs from the experimental values σ_γ = 1.3 ± 0.3 and 2.7 ± 0.9 b given in [1] and [2], respectively.

LITERATURE CITED

1. S. Mangal et al., Nucl. Phys., 36, 542 (1962).
2. A. G. Beda, L. N. Kondrat'ev, and E. F. Tret'yakov, At. Énerg., 16, No. 2, 145 (1964).
3. V. F. Razbudei, V. P. Vertebnyi, and A. V. Muravitskii, in: Neutron Physics [in Russian], Part 2, TsNIIatominform, Moscow (1977), p. 276.
4. N. G. Kocherygin et al., Preprint NINAR 28(387), Dimitrovgrad (1979).
5. BNL-325, 3rd ed. (1973).

MEASUREMENT OF THE FISSION CROSS SECTION OF ^{244}Cm WITH FAST NEUTRONS, USING A NANOGRAM QUANTITY OF ISOTOPE

P. E. Vorotnikov, L. D. Kozlov, and Yu. D. Molchanov

UDC 539.173

The conditions of reprocessing, storage, and transportion of cooled spent nuclear fuel are determined to a considerable degree by the buildup in it, during irradiation, of ^{244}Cm. In enriched ^{239}Pu-fuel, two-thirds of the energy release of the actinides and ~90% of the neutron yield is due to ^{244} Cm [1]. According to IAEA documents [1], the necessity for nuclear data requires measurements of the fission cross section of ^{244}Cm by fast neutrons with an accuracy of 20%. At the present time, measurements of this cross section by monoenergetic neutrons are known at individual points in the superthreshold range of neutron energies E_n [2, 3], and more systematic measurements over a wide range of E_n on neutrons from an underground nuclear explosion [4, 5], the accuracy of which is estimated as approximately 50% [1].

For the determination of $\sigma_f(E_n)^{244}$Cm, we have used the metnod of measuring the fission cross section of the transuranic elements in a pulsed electrostatic accelerator (ESA), developed in the I. V. Kurchatov Institute of Atomic Energy, with a nanogram quantity of isotope [6] (a factor of 10^3-10^4 less than was required previously [4, 5]). A solid TiT-target, bombarded with protons from the pulsed ESA, served as the neutron source [7]. The diameter of the beam of ions at the target amounted to ~1 mm, the frequency of the current pulses was 2 MHz, their duration 5 nsec, and the average current at the target was 6 μA. The layer of fissile material with a diameter of ~1.5 mm and containing 5 ng of ^{244}Cm, was positioned at an angle of 0° relative to the beam of protons. The distance between the centers of the layer and target amounted to ~3 mm for the relative measurements of $\sigma_f(E_n)$ and ~6 mm for the absolute measurement of the cross section, carried out for an average energy E_n = 1100 keV. The neutron flux was measured with flat-response counters [8], calibrated with standard neutron sources. The fission fragments were detected with a gas scintillation chamber with a diameter of 2 cm and a thickness of 1 cm, filled with xenon to a pressure of 1.5 atm (1 atm = 101.325 kPa) and connected with a FÉU-30 photomultiplier. In order to record the time spectra, a time-of-flight spectrometer [9], developed previously, was used.

Part of the instrumental spectra obtained are shown in Fig. 1, from which it can be seen that the fission events caused by the neutrons, are well distinguished on the background of uniformly distributed spontaneous fissions, although the number of induced fissions N_{ind} is much less than the number of spontaneous fissions N_{sp}:

$$N_{sp} = 2.2 \cdot 10^{-8} N_{at} \varepsilon t_m / T_f;$$
$$N_{ind} = 10^{-24} N_{at} N_n \varepsilon \sigma_f,$$

where N_{at} is the number of atoms of ^{244}Cm in the layer; N_n, number of neutrons passing through 1 cm^2 of the layer; ε, recording efficiency of the fission fragments; σ_f and $T_f = 1.3 \cdot 10^7$ [10], fission cross section (b) and the period of spontaneous fission of ^{244}Cm, yr; t_m, measurement time, sec. From these relations we obtain

$$\sigma_f = \frac{2.2 \cdot 10^{16} N_{ind}\, t_m}{N_{sp}\, T_f N_n} \text{ (b)}.$$

Thus, N_{at} and ε, which usually carry large errors in the results, do not enter into the expression for σ_f.

When processing the data obtained, the experimentally measured corrections for neutrons scattered by the chamber material were taken into account, and also the calculated corrections

Translated from Atomnaya Énergiya, Vol. 57, No. 1, pp. 61-62, July, 1984. Original article submitted January 13, 1984.

0038-531X/84/5701-0504$08.50

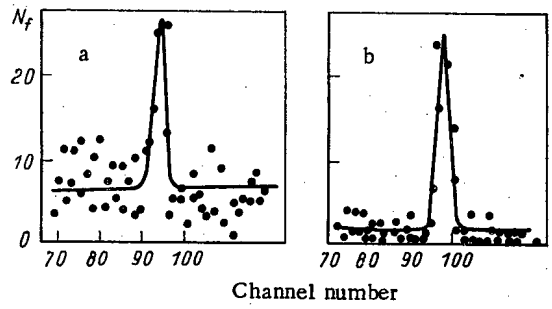

Fig. 1. Time spectra, obtained with E_n = 480 keV after 10 h (a) and with E_n = 950 keV after 2 h of measurements (b).

TABLE 1. Measurement Results of the Fission Cross Section of ^{244}Cm by Neutrons

E_n, keV	σ_f, b	Error of rel. measurements of σ_f, σ_f, %		
		statistical	isotopic composition	total
390±70	0,18	22	15	28
480±90	0,44	14	8	18
580±90	0,65	14	5,3	17
690±90	1,06	15	3,2	17
790±100	1,72	11	2,7	13
950±95	1,77	9	2,2	12
1080±90	1,63	10	1,8	12
1280±80	1,58	15	1,7	17

Note. The absolute accuracy of σ_f is 9%.

due to the angular distribution T_d of the neutrons and their scattering by the material of the accelerator target, the commensurability of the distances between the target and the layer with their diameters, the possible nonuniformity of the layer and isotopic composition. The layer was prepared from the curium fraction of the chemically separated products of irradiation of ^{241}Am in a reactor. The fraction of the different isotopes was calculated from their buildup curve [10], correlated with the yields of ^{243}Am, $^{244+246}$Cm, and ^{245}Cm, measured on a Ge(Li) γ-spectrometer. Thus, the following composition of the layer was obtained, %: ^{241}Am < 0.2; ^{243}Am = 4.1 ± 1.0; ^{242,243}Cm < 0.15; ^{244}Cm = 78 ± 3.5; ^{245}Cm = 1.3 ± 0.4; ^{246}Cm = 16 ± 3; ^{247}Cm = 0.4 ± 0.1; ^{248}Cm = 0.4 ± 0.1.

The results of the measurements are given in Table 1. They coincide well with the data of [4], obtained by using an underground nuclear explosion and also, like the latter, for $E_n \leq 800$ keV exceed the data published in [5] by approximately 40%. The accuracy of the relative values of σ_f obtained by us is determined mainly by the statistical count of the fission fragments, the absolute accuracy of the $\sigma_f(E_n)$ curve — the error of the neutron flux calibration (±6%). We did not measure and we did not take account of the anisotropy of the angular distribution of the ^{244}Cm fission fragments by neutrons, as with the thickness of the layer used by us, this could not appreciably increase the error.

Based on the analysis of the results, taking account of the increase of the effective number of channels of competing processes [first and foremost the neutron emission $N_n(E_n) = 2\pi\rho_{comp}(E^*) \times \Gamma_n(E_n)$] and the binding energy of the neutron B_n = 5.52 MeV [11], values are obtained for the height of the fission barrier of ^{245}Cm of B_f = 6.17 ± 0.05 MeV and its curvature $\hbar\omega_f = 2\pi dE^*/d \times \ln N_f$ ($E^* < B_f$) = 0.70 ± 0.05 MeV.

LITERATURE CITED

1. Transactinium Isotope Nuclear Data (TND), IAEA-186, Vol. 1, Vienna, p. 3 (1976).
2. P. Koontz and D. Barton, in: Proceedings of the Conference on Neutron Cross Sections and Technology, Washington (1968), p. 527.
3. É. F. Fomushkin et al., Yad. Fiz., 17, 24 (1973).
4. M. Moore and G. Keyworth, Phys. Rev., C3, 1956 (1971).

5. É. F. Fomushkin, G. F. Novoselov, and Yu. I. Vinogradov, Yad. Fiz., 31, 39 (1980).
6. P. E. Vorotnikov et al., Problems of Nuclear Science and Technology. Series Nuclear Constants [in Russian], No. 1(40) (1981), p. 77.
7. P. E. Vorotnikov et al., in: Applied Nuclear Spectroscopy [in Russian], Atomizdat, Moscow (1970), p. 305.
8. V. Allen, in: Fast Neutron Physics [in Russian], Vol. 1, Gosatomizdat, Moscow (1963), p. 253.
9. P. E. Vorotnikov et al., in: Neutron Physics. Data of the Fourth All-Union Conference on Neutron Physics [in Russian], TsNIIatominform, Moscow, Part 4 (1977), p. 238.
10. V. M. Gorbachev, Yu. S. Zamyatnin, and A. A. Lbov, Principal Characteristics of the Heavy Element Isotopes [in Russian], Atomizdat, Moscow (1975).
11. Neutron Cross Sections, BNL-325, Vol. 1 (1973).

MEASUREMENT TECHNIQUES
Izmeritel'naya Tekhnika
Vol. 27, 1984 (12 issues) $520

MECHANICS OF COMPOSITE MATERIALS
Mekhanika Kompozitnykh Materialov
Vol. 20, 1984 (6 issues) $430

METAL SCIENCE AND HEAT TREATMENT
Metallovedenie i Termicheskaya Obrabotka Metallov
Vol. 26, 1984 (12 issues) $540

METALLURGIST
Metallurg
Vol. 28, 1984 (12 issues) $555

PROBLEMS OF INFORMATION TRANSMISSION
Problemy Peredachi Informatsii
Vol. 20, 1984 (4 issues) $420

PROGRAMMING AND COMPUTER SOFTWARE
Programmirovanie
Vol. 10, 1984 (6 issues) $175

PROTECTION OF METALS
Zashchita Metallov
Vol. 20, 1984 (6 issues) $480

RADIOPHYSICS AND QUANTUM ELECTRONICS
Izvestiya Vysshikh Uchebnykh Zavedenii, Radiofizika
Vol. 27, 1984 (12 issues) $520

REFRACTORIES
Ogneupory
Vol. 25, 1984 (12 issues) $480

SIBERIAN MATHEMATICAL JOURNAL
Sibirskii Matematicheskii Zhurnal
Vol. 25, 1984 (6 issues) $625

SOIL MECHANICS AND FOUNDATION ENGINEERING
Osnovaniya, Fundamenty i Mekhanika Gruntov
Vol. 21, 1984 (6 issues) $500

SOLAR SYSTEM RESEARCH
Astronomicheskii Vestnik
Vol. 18, 1984 (6 issues) $365

SOVIET APPLIED MECHANICS
Prikladnaya Mekhanika
Vol. 20, 1984 (12 issues) $520

SOVIET ATOMIC ENERGY
Atomnaya Énergiya
Vols. 56-57, 1984 (12 issues) $560

SOVIET JOURNAL OF GLASS PHYSICS AND CHEMISTRY
Fizika i Khimiya Stekla
Vol. 10, 1984 (6 issues) $235

SOVIET JOURNAL OF NONDESTRUCTIVE TESTING
Defektoskopiya
Vol. 20, 1984 (12 issues) $615

SOVIET MATERIALS SCIENCE
Fiziko-khimicheskaya Mekhanika Materialov
Vol. 20, 1984 (6 issues) $445

SOVIET MICROELECTRONICS
Mikroėlektronika
Vol. 13, 1984 (6 issues) $255

SOVIET MINING SCIENCE
Fiziko-tekhnicheskie Problemy Razrabotki Poleznykh Iskopaemykh
Vol. 20, 1984 (6 issues) $540

SOVIET PHYSICS JOURNAL
Izvestiya Vysshikh Uchebnykh Zavedenii, Fizika
Vol. 27, 1984 (12 issues) $520

SOVIET POWDER METALLURGY AND METAL CERAMICS
Poroshkovaya Metallurgiya
Vol. 23, 1984 (12 issues) $555

STRENGTH OF MATERIALS
Problemy Prochnosti
Vol. 16, 1984 (12 issues) $625

THEORETICAL AND MATHEMATICAL PHYSICS
Teoreticheskaya i Matematicheskaya Fizika
Vol. 58-61, 1984 (12 issues) $500

UKRAINIAN MATHEMATICAL JOURNAL
Ukrainskii Matematicheskii Zhurnal
Vol. 36, 1984 (6 issues) $500

Send for Your Free Examination Copy

Plenum Publishing Corporation, 233 Spring St., New York, N.Y. 10013
In United Kingdom: 88/90 Middlesex St., London E1 7EZ, England
Prices slightly higher outside the U.S. Prices subject to change without notice.

RUSSIAN JOURNALS IN THE PHYSICAL AND MATHEMATICAL SCIENCES

AVAILABLE IN ENGLISH TRANSLATION

ALGEBRA AND LOGIC
Algebra i Logika
Vol. 23, 1984 (6 issues) $360

ASTROPHYSICS
Astrofizika
Vol. 20, 1984 (4 issues) $420

AUTOMATION AND REMOTE CONTROL
Avtomatika i Telemekhanika
Vol. 45, 1984 (24 issues) $625

COMBUSTION, EXPLOSION, AND SHOCK WAVES
Fizika Goreniya i Vzryva
Vol. 20, 1984 (6 issues) $445

COSMIC RESEARCH
Kosmicheskie Issledovaniya
Vol. 22, 1984 (6 issues) $545

CYBERNETICS
Kibernetika
Vol. 20, 1984 (6 issues) $445

DIFFERENTIAL EQUATIONS
Differentsial'nye Uravneniya
Vol. 20, 1984 (12 issues) $505

DOKLADY BIOPHYSICS
Doklady Akademii Nauk SSSR
Vols. 274-279, 1984 (2 issues) $145

FLUID DYNAMICS
Izvestiya Akademii Nauk SSSR, Mekhanika Zhidkosti i Gaza
Vol. 19, 1984 (6 issues) $500

FUNCTIONAL ANALYSIS AND ITS APPLICATIONS
Funktsional'nyi Analiz i Ego Prilozheniya
Vol. 18, 1984 (4 issues) $410

GLASS AND CERAMICS
Steklo i Keramika
Vol. 41, 1984 (6 issues) $590

HIGH TEMPERATURE
Teplofizika Vysokikh Temperatur
Vol. 22, 1984 (6 issues) $520

HYDROTECHNICAL CONSTRUCTION
Gidrotekhnicheskoe Stroitel'stvo
Vol. 18, 1984 (12 issues) $385

INDUSTRIAL LABORATORY
Zavodskaya Laboratoriya
Vol. 50, 1984 (12 issues) $520

INSTRUMENTS AND EXPERIMENTAL TECHNIQUES
Pribory i Tekhnika Éksperimenta
Vol. 27, 1984 (12 issues) $590

JOURNAL OF APPLIED MECHANICS AND TECHNICAL PHYSICS
Zhurnal Prikladnoi Mekhaniki i Tekhnicheskoi Fiziki
Vol. 25, 1984 (6 issues) $540

JOURNAL OF APPLIED SPECTROSCOPY
Zhurnal Prikladnoi Spektroskopii
Vols. 40-41, 1984 (12 issues) $540

JOURNAL OF ENGINEERING PHYSICS
Inzhenerno-fizicheskii Zhurnal
Vols. 46-47, 1984 (12 issues) $540

JOURNAL OF SOVIET LASER RESEARCH
A translation of articles based on the best Soviet research in the field of lasers
Vol. 5, 1984 (6 issues) $180

JOURNAL OF SOVIET MATHEMATICS
A translation of Itogi Nauki i Tekhniki and *Zapiski Nauchnykh Seminarov Leningradskogo Otdeleniya Matematicheskogo Instituta im. V. A. Steklova AN SSSR*
Vols. 24-27, 1984 (24 issues) $1035

LITHOLOGY AND MINERAL RESOURCES
Litologiya i Poleznye Iskopaemye
Vol. 19, 1984 (6 issues) $540

LITHUANIAN MATHEMATICAL JOURNAL
Litovskii Matematicheskii Sbornik
Vol. 24, 1984 (4 issues) $255

MAGNETOHYDRODYNAMICS
Magnitnaya Gidrodinamika
Vol. 20, 1984 (4 issues) $415

MATHEMATICAL NOTES
Matematicheskie Zametki
Vols. 35-36, 1984 (12 issues) $520

continued on inside back cover